

Rochester Institute of Technology

RIT Digital Institutional Repository

Theses

5-2-2017

Ferromagnetic Resonance to Investigate Spin Pumping in Permalloy Multilayers

Thomas White
tjw4183@rit.edu

Follow this and additional works at: <https://repository.rit.edu/theses>

Recommended Citation

White, Thomas, "Ferromagnetic Resonance to Investigate Spin Pumping in Permalloy Multilayers" (2017). Thesis. Rochester Institute of Technology. Accessed from

This Thesis is brought to you for free and open access by the RIT Libraries. For more information, please contact repository@rit.edu.

Ferromagnetic Resonance to Investigate Spin Pumping in Permalloy Multilayers

Thomas White

Thesis

Submitted in Partial Fulfillment of the Requirements for the Degree of

Masters of Science

in

Materials Science and Engineering

Rochester Institute of Technology

College of Science

School of Chemistry and Materials Science

Rochester, NY

May 2, 2017

Committee Approval:

Dr. Casey Miller, Advisor Director of Materials Science and Engineering	Date
--	------

Dr. Linda Barton Associate Professor of Physics	Date
--	------

Dr. Joseph Hornak Professor of Chemistry and Imaging Science	Date
---	------

Dr. Steve Weinstein Department Head of Chemical Engineering	Date
--	------

Abstract

Coplanar Waveguide Ferromagnetic Resonance Spectroscopy (CPW-FMR) was used to investigate the spin dynamics of the thin film multilayers Py/Ir vs. Py/Cu/Ir. The properties of both sample sets were evaluated as a function of the Ir thickness. The gyromagnetic ratio, γ , is found to be independent of the Ir thickness and determined to be approximately 29.4 GHz/T for all samples. The magnetization, M , is found to be 7249 G for the Py/Cu/Ir samples compared to 7630 G for the Py standard. For the Py/Ir bilayer, M decreases as Ir thickness increases, ranging from 7641 G to 7293 G. The thickness dependence on M for Py/Ir is believed to be caused by induced perpendicular anisotropy. The inhomogeneous broadening (ΔH_0) is nearly double for Py/Ir compared to Py/Cu/Ir. There is a strong enhancement of the Gilbert damping parameter when the Ir layer has a direct interface with magnetic layer ($\alpha = 0.023$) compared to when the interfaces are interrupted with a Cu layer ($\alpha = 0.013$). The control sample Py demonstrated a damping parameter consistent with other investigations ($\alpha = 0.0084$). This indicates the presence of spin memory loss at the interface of Py and Ir. Effective Spin mixing conductance, g_{eff} , was found to be $8.8 \pm 0.3 \text{ nm}^{-2}$ for Py/Cu/Ir, and $25.2 \pm 0.5 \text{ nm}^{-2}$ for the Py/Ir samples. There is a thickness dependence on the damping for the Py/Ir samples that was not observed Py/Cu/Ir samples. This is believed to be related to a proximity effect for the Py-Ir interface. The thickness dependence on the damping for Py/Ir was found to be approximately $\lambda = 0.5 \pm 0.1 \text{ nm}$.

Table of Contents

Abstract.....	iii
List of Tables	vi
List of Figures	vii
Introduction and Overview.....	1
Section 1: Spintronics and Spin Pumping.....	2
Spintronics	2
Spin Currents and Spin Pumping.....	4
Section 2: Tools & Techniques	6
FMR	6
FMR Theory.....	6
Equipment.....	9
Absorption Spectrum	11
FMR Noise and Errors	13
XRR	16
XRR Introduction	16
Basic Theory	17
Sheet Resistance	18
Section 3: Py/Ir vs. Py/Cu/Ir: Observations of Spin Memory Loss	21
Abstract.....	21
Experimental Details	21
Samples.....	21
FMR Measurements.....	25
Results.....	29
Resonance Field and Linewidths.....	29
Gyromagnetic Ratio	31
Effective Magnetization	31
Kittel Fits for all Py/Ir samples	33
Kittel fits for all Py/Cu/Ir samples	36
Inhomogeneous Broadening.....	38
Gilbert Damping.....	39
Plots of ΔH vs. f for Py/Ir	41

Plots of ΔH vs. f for Py/Cu/Ir	44
Thickness Dependence of the Damping.....	46
Spin Mixing Conductance.....	49
Conclusion.....	50
Interpretation and Future Work	51
Section 4: Acknowledgments.....	54
Section 5: Appendix	55
FMR Measurements: A Guide for Future Users.....	55
Matlab Tools for Processing FMR Data.....	57
Quick Start Guide	57
Detailed Overview & Guide.....	61
Source Code	66
Bibliography	73

List of Tables

Table 1: Thickness results for Py and Py/Cu layers from XRR analysis. The column Uncertainty refers to the uncertainty of the fit. Py and Cu are not distinguished by the XRR so a net thickness of the two layers is given. To find the Cu thickness, the average Py thickness from the Py/Ir samples was subtracted from the net thickness of Py-Cu. In this table, sample names are formed from their sputtering time for Ir (ex. Py/Ir 15s means Ir was sputtered for 15 seconds). Once the thicknesses were determined, and in all in rest of this thesis, samples are always identified by Ir thickness.	23
Table 2: Final residuals for ΔH vs. for Py/Cu/Ir. Conditional formatting was used to identify the largest residuals. This was used to track down outlying data.	28
Table 3: Final residuals for ΔH vs. for Py/Ir. This was used to track down outlying data.	28
Table 4: H_{res}, for all Py/Cu/Ir samples and Py standard in Oe. Columns are organized by the frequency. Rows are the Ir thickness in nm. For example, the H_{res} at 3GHz for the sample $t_{Ir}=0nm$ is 136 Oe.	30
Table 5: Resonance field, H_{res}, for all Py/Ir samples in Oe. Columns are organized by the frequency. Rows are the Ir thickness in nm. For example, the H_{res} at 3GHz for the sample $t_{Ir}=4nm$ is 140 Oe.	30
Table 6: Py/Cu/Ir spectrum linewidths in Oe. For example, the linewidth at $f=3GHz$ at thickness $t_{Ir}=0$ nm is 20 Oe with a standard deviation near 0 Oe.	30
Table 7: Py/Ir spectrum linewidths in Oe. For example, the linewidth at $f=3GHz$ at thickness $t_{Ir}=4nm$ is 49 Oe with a standard deviation of 5Oe.	31

List of Figures

- Figure 1: Giant Magnetoresistance (GMR) is an effect where there is a remarkable increase in electrical resistance when ferromagnetic layers (in blue) are in antiparallel alignment (right) as opposed to parallel alignment (left). The black arrows indicate the magnetization orientation of the ferromagnetic layers. GMR is an example of spin dependent transport and was the discovery that kicked off significant interest in spintronics..... 2**
- Figure 2: (a) In normal metals there is an equivalent density of states of spin up and spin down electrons, resulting in no net magnetization (magnetization is indicated by the arrows). In a magnetized ferromagnetic material there is a higher population of one spin orientation. The splitting of the density of states for when layered ferromagnets have anti-parallel alignment (b) causes a higher resistance and a lower resistance for parallel alignment (c). 3**
- Figure 3: The Landau-Lifshitz-Gilbert equation describes the precession of a sample's magnetization around an applied field, H . In red is the precession vector and the damping vector is shown in green. The dotted blue line show the path that the magnetization will take to reach equilibrium with H 6**
- Figure 4: An alternating field, h_{rf} , can perturb the magnetization out of equilibrium. At the resonance condition, the magnetization will precess around H forming what is called the precession cone..... 8**
- Figure 5: The RF transmission passes an RF diode before reaching the lock-in amplifier. The block “AC source” provides an AC current to the two Helmholtz coils that are situated over the poles. The Helmholtz coil, H_{ac} , provide a 490 Hz AC field parallel to the DC field. This field is used as a reference for lock-in amplification of the FMR absorption. The block “lock-in” receives the AC reference signal and the absorption signal to create. 9**
- Figure 6: A cross section view of the CPW (gold) with a sample on top (grey). The insulator (blue) is Scotch[®] tape. This shows how the perturbing field is applied to the sample transverse to the DC field. In this diagram, the DC field is oriented into the page. 10**
- Figure 7: The FMR setup where a) is the NanOsc PhaseFMR tool b) is the DC power supply and c) is the electromagnet. The Helmholtz coils are the copper rings sitting on the pole face. 11**
- Figure 8: The coplanar waveguide, CPW, (gold) with a sample (black). The Hall Probe (blue) is seen and reports**

DC field strength. Plastic screws secure the CPW to an aluminum framing held in place between the pole faces. Scotch tape can be seen on the CPW. The tape reduces an induced damping caused by eddy currents in the sample..... 11

Figure 9: Example FMR spectrum. This spectrum is from a permalloy sample (Py) at $f=3$ GHz. 12

Figure 10: Example of data cut off by a narrow sweep. This can be prevented by taking broader sweeps. If time is not an issue, take very broad sweeps. Large differences in resonance fields between samples require adjustments to the measurement settings. 13

Figure 11: Some sweeps will give results that don't appear as obvious outliers but give incorrect data 14

Figure 12: An example of saturated data for the three maximum data points. The maximum value for our detector is 15. It is important to review the plots to ensure accurate fits and data are created. This plot is included because it is a less obvious example of a bad fit. 15

Figure 13: A diagram for x-ray reflectivity (XRR) showing how interference changes with the incident angle, α_i , for a single thin film. Note that the angles are not to scale and exaggerated. λ is the wavelength of the x-ray and t is the thickness of the thin film. The red and blue lines are two different incident rays that experience destructive interference and would result in a "valley" in the intensity counts (Figure 14). XRR will produce fringe patterns caused by the interference of beams reflecting off of parallel film surfaces. Thickness, roughness, and electron density all influence the XRR patterns (Figure 14). 17

Figure 14: This graph shows a representative XRR fit and the influences each parameter can have on the shape. [27]..... 18

Figure 15: Sheet resistance measurements are made by passing a current along one edge of a sample and measuring the voltage drop on the parallel edge. This process is repeated in the perpendicular direction and the equality in Eqn. 7 is used to 20

Figure 16: Diagram of sample structures, not to scale. There are 11 samples of each Py/Ir and Py/Cu/Ir. Not shown in the figure is the Si substrate nor the Al capping layer..... 22

Figure 17: X-ray reflectivity scans for Py/Cu/Ir and Py/Ir. Iridium thickness $t_{Ir}=4.5$ nm. 22

Figure 18: Deposition thickness of iridium as a function of deposition time. There was no significant difference in iridium thicknesses between samples with and without Cu for the same deposition time. The XRR was

performed on 8 samples and the thicknesses were interpolated and extrapolated for all samples..... 24

Figure 19: Sheet conductance (inverse sheet resistance) vs. Ir thickness. Between the two sample sets there is a shift in the sheet conductance due to the Cu layer increasing the conductance a constant amount, but the trend is uniform for both sample sets, showing that the Cu layer does not impact the Ir layer quality. 24

Figure 20: Example FMR absorption spectrums for standard permalloy sample at $f=3$ and 18 GHz. Lines are fits points are data. Red points are for all data measured. Blue points are the data that are used in the fit as determined by the Matlab code (See Matlab code description in Appendix). Notice the width of the spectrum is much larger for higher frequencies..... 25

Figure 21: Field sweeps for control sample, Py/Cu/Ir , and Py/Ir where $t_{Ir}=15$ nm. $f=3$ GHz for all three sweeps. These sweeps are shown without the portioning ability of the Matlab code so all points are the same color and are included in the fit. 26

Figure 22. An example spectrum fit that gave unrepresentative ΔH value. There is uncharacteristically high noise for this measurement. See the discussion on errors in the section “FMR measurement Procedure.” 29

Figure 23: Effective magnetization, M_{eff} , vs. iridium thickness. No thickness dependence is observed for Py/Cu/Ir, but a dependence is observed for Py/Ir..... 32

Figure 24: The ΔH vs. f for Py/Ir (blue), Py.Cu/Ir (copper), and the control (black); $t_{Ir}=15$ nm for both. A large increase in the slope for Py/Ir samples can be seen..... 38

Figure 25: ΔH_0 vs. t_{Ir} , error bars come from the fit confidence. The ΔH_0 for Py/Cu/Ir is in copper and Py/Ir is in blue. The black line shows ΔH_0 for the Py standard. The x axis is on a log scale to make the data easier to see..... 39

Figure 26: Gilbert damping parameter vs iridium thickness. As the iridium thickness increases alpha quickly saturates. The grey line is α for Py, 0.0084. The lines are fit using the characteristic length determined in the following section “Thickness Dependence of the Damping” 41

Figure 27: The ΔH vs. iridium thickness. Each color is a different frequency. The frequencies range from 18 (dark blue diamonds on top) down to 2 GHz (light blue, lowest points) in 1 GHz steps. A trend can be observed for all frequencies..... 46

Figure 28: The ΔH were normalized and averaged across frequencies. A clear trend is now seen for ΔH vs. t_{Ir} 47

Figure 29: For ΔH vs. t_{ir} for Py/Cu/Ir no thickness dependence is observed. This data were created by normalizing the linewidths as was done for Py/Ir in Figure 28. 48

Figure 30: The damping enhancement is used to determine the effective spin mixing conductance, g_{eff} . Note that the fit lines are showing the characteristic length found for the linewidth dependency on thickness shown in Figure 28. 50

Introduction and Overview

The core of this research was investigating permalloy ($\text{Ni}_{80}\text{Fe}_{20}$) and iridium thin film structures, in a study called “Py/Ir vs. Py/Cu/Ir: Observations of Spin Memory Loss.” (Py/Ir indicates a permalloy layer adjacent to an iridium layer and Py/Cu/Ir indicates there is a copper layer between the permalloy and iridium). The first two sections of this thesis are intended to serve as introductions to relevant topics, so that by the third section, the core investigation of the Py/Ir films can be understood.

This research is in the new field of spintronics, the research and application of an electron’s spin. In Section 1, a qualitative explanation is given on background of spintronics. It attempts to answer why researchers care about this topic, before moving on to the background concepts that are relevant.

In Section 2 the theory and practice of the measurement methods are described for ferromagnetic resonance spectroscopy (FMR), x-ray reflectivity (XRR), and sheet resistance measurement. Special focus is given to FMR, as it is the primary tool used in this research and a considerable amount of lab time was spent installing and establishing protocols for the FMR. When discussing the theory for FMR, more details about the concepts from Section 1 are naturally discussed.

Section 3 presents the research project “Py/Ir vs. Py/Cu/Ir: Observations of Spin Memory Loss” an investigation of the effects caused by a direct Py-Ir interface and an investigation of the thickness dependencies on the Ir layer. This type study has been done for permalloy thin films with other adjacent metals, but no observations have been made for pure iridium layers. This investigation contributes to science by measuring multilayers systems never before examined. In addition, many phenomenon in spintronics are poorly understood, so by providing measurements of a new system, this study will provide more data on which to develop theories.

Section 1: Spintronics and Spin Pumping

Spintronics

Aside from its charge, an electron that is deployed in all modern electronics has another important intrinsic property: spin or *the intrinsic angular momentum* [1, 2, 3]. In non-ferromagnetic materials electron spins are randomly oriented by thermal vibrations. In ferromagnetic materials exchange coupling overcomes the thermal disordering and causes long range ordering of the spins. Ferromagnetic materials, colloquially called magnets, are when there is a net alignment of electrons [4]. When ferromagnetic materials are incorporated into electronic devices, the polarization of the spins can play an important role in device functions. This is referred to as spintronics. Spintronics is the study of an electron's intrinsic angular momentum and its application in devices [1, 3].

The origin of spintronics as a major technology was the discovery of giant magnetoresistance (GMR) in 1988 [1, 5]. GMR is an effect where the electric resistance in special ferromagnet multilayers has a remarkable increase when the different layers have antiparallel alignment of their magnetization, as shown in Figure 1.

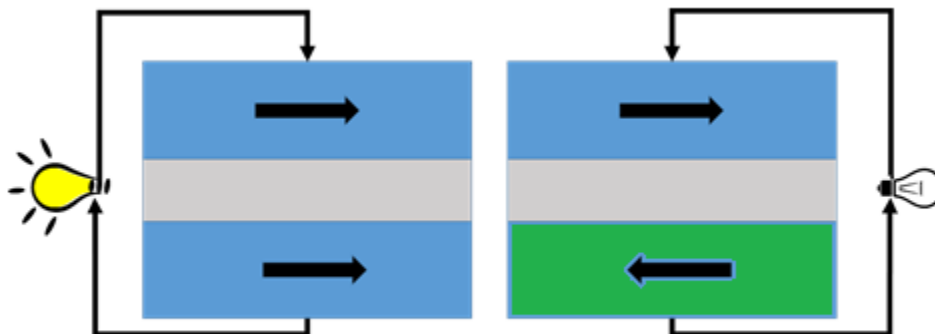


Figure 1: Giant Magnetoresistance (GMR) is an effect where there is a remarkable increase in electrical resistance when ferromagnetic layers (in blue) are in antiparallel alignment (right) as opposed to parallel alignment (left). The black arrows indicate the magnetization orientation of the ferromagnetic layers. GMR is an example of spin dependent transport and was the discovery that kicked off significant interest in spintronics.

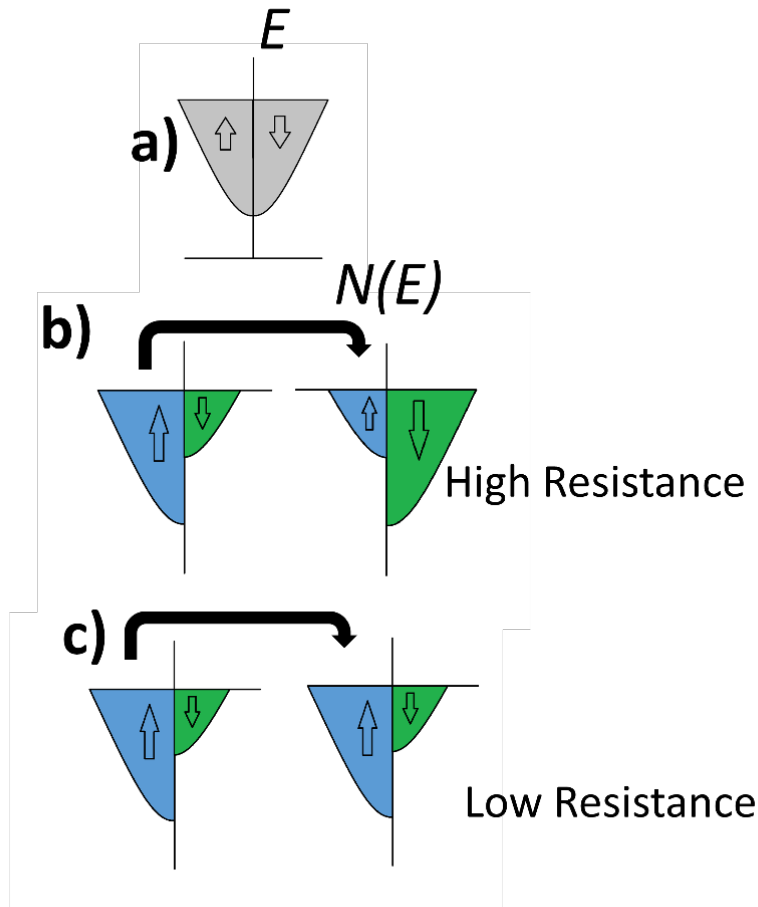


Figure 2: (a) In normal metals there is an equivalent density of states of spin up and spin down electrons, resulting in no net magnetization (magnetization is indicated by the arrows). In a magnetized ferromagnetic material there is a higher population of one spin orientation. The splitting of the density of states for when layered ferromagnets have anti-parallel alignment (b) causes a higher resistance and a lower resistance for parallel alignment (c).

GMR is based on the dependence of electron scattering on the spin orientation. For a ferromagnetic material, the density of states at the Fermi level (the electrons responsible for a current) is dependent on the spin orientation. When a current passes through a ferromagnet, electrons with a spin orientation of the minority density of states experience scattering and have shorter mean free path. When a current passes two ferromagnetic layers with anti-parallel magnetizations, both spin orientations will experience increased scattering. This causes an increase in resistance for the multilayers. When the magnetizations are parallel, electrons with the majority spin orientation have a much greater mean free path in both layers and the

resistance is greatly decreased. The discovery of GMR was the first time practical control of a materials properties could be manipulated via the spin.

The discovery of GMR quickly revolutionized data storage [6]. The key example for the application and impact of spintronics is the massive increase in data density on modern hard drives. The advantages of spin based devices include reducing the power consumption and overcoming the velocity limit of electric charge [2]. In the 1990s the introduction of the GMR head in mainstream devices allowed for massive compound growth in the data density in hard drives. In 1990, the data density on a hard drive was around 0.01 Gb/in². By 2010 the density increased to over 300 Gb/in², in line with Moore's law [6]. The fast impact of the discovery of GMR led to the 2007 Nobel Prize for physicists Albert Fert and Peter Grünberg [1, 5]. Further spintronics research transformed information technologies with the development of high-density magnetic recording and new types of non-volatile solid state memory approaches.

A common focus in modern spintronics research is to improve current devices and create novel spin-based solid state memory devices. Solid state devices have the substantial benefit of no moving parts. Magnetoresistive random access memory MRAM is an example of a solid state device that has huge potential [1]. This currently holds a niche market but it is likely that MRAM will become a dominant form of memory: in contrast to other RAM varieties, the permanent magnetic materials used in MRAM offer the possibility of "instant boot" for computers [7, 8].

In order for new useful technologies to be developed from spintronics, more research needs to be done on the fundamental underlying physics. A key topic that needs to be understood is how the spin of electrons influence the transport properties in materials.

Spin Currents and Spin Pumping

At the core of spintronics is spin-dependent transport. Spin dependent transport refers to transport of spin angular momentum by simple charge currents [9]. In GMR, this spin-dependent transport originates from the ferromagnets, which have more spin up than spin down electrons. These materials serve as sources of spin current. Despite many years of studies there are still many unanswered question in spin transport. For example the well-known GMR effect is still actively researched [3]. A type of spin transport that is relevant in this

research is called spin current.

A spin current is a flow or transfer of spin angular momentum. Spin currents carry spin from one place to another. Just as electronic devices require a charge current to operate, spin based devices require spin currents. Spin current is associated with a flow of angular momentum, which allows quantum information to transport across different structures, analogous to quantum optics that distribute information across optical networks [10]. Spin currents can occur in the absence of a charge current [3].

Spin currents can be generated by creating an imbalance of spin-up and spin-down electrons [11]. There are two categories for the way this is done: 1) generated via electrical injection (passing an electric current) through ferromagnetic conductors, as is the case in GMR; or 2) via spin pumping from magnetization dynamics in an adjacent ferromagnet [1]. Most methods used to generate spin currents require strong magnetic fields and interfaces between ferromagnets and semiconductors. These methods have obvious limitations in applications. A method that bypasses these limitations is spin pumping [10].

Spin pumping occurs when a non-magnetic conductor is in contact with a ferromagnet. When the magnetic moment of a ferromagnet is placed in an external magnetic field, the moment precesses in what is called Larmor precession. When the ferromagnetic layer's magnetization is driven into precession, i.e., when ferromagnetic resonance is excited (this can be done via microwave excitation as is done in this research), a spin current is generated that can flow into adjacent materials [3, 12, 13, 14]. The precession of magnetization in a ferromagnet will "pump" the spins into an adjacent nonmagnetic (NM) layer (this is essentially the spins diffusing into the adjacent material). This spin transfer into the NM can dampen the precessing moment in the ferromagnet [1, 3, 14]. Another source of dampening is spin memory loss, where interfacial effects cause an increase in damping. The enhanced damping is a key interest in this research.

In this research, spin currents were generated using spin pumping via ferromagnetic resonance (FMR) in order to investigate the spin dynamics of samples. In FMR a spin current is "pumped" by inducing a precession of the magnetization in a ferromagnetic (FM) layer [15]. This precession will cause a transfer of spin angular momentum into a non-magnetic normal

layer. The precession of the magnetization in a FM layer acts like a peristaltic pump, causing spin currents to cross the interface. The spin current flows perpendicular to the interface and shares the average spin-orientation of the precessing of the FM layer [3]. The details of FMR are given next.

Section 2: Tools & Techniques

FMR

FMR Theory

Magnetic phenomena are often investigated through their dynamic behavior. This can be done by perturbing or driving the magnetization at resonance and measuring the response. This is what is done with ferromagnetic resonance (FMR), the primary tool of this thesis. FMR is a standard tool to probe the dynamic properties of ferromagnetic thin films [15].

To explain FMR simply, imagine a ferromagnetic sample with a magnetization M . If the sample is placed in an external magnetic field, H , the magnetization will precess towards H to minimize the energy. M will reach an equilibrium when it is parallel to H . To drive M into a precession during an FMR experiment, an RF magnetic field, h_{rf} , is applied transverse to H . The h_{rf} is applied by an electromagnetic signal that is transmitted through a coplanar waveguide (CPW). When the frequency, f , of the transverse field is at the resonance condition, M will precess around H in a precessional cone. The equation that describes the magnetization's precession is the Landau-Lifshitz-Gilbert (LLG) equation [3].

Landau Lifshitz Gilbert Equation

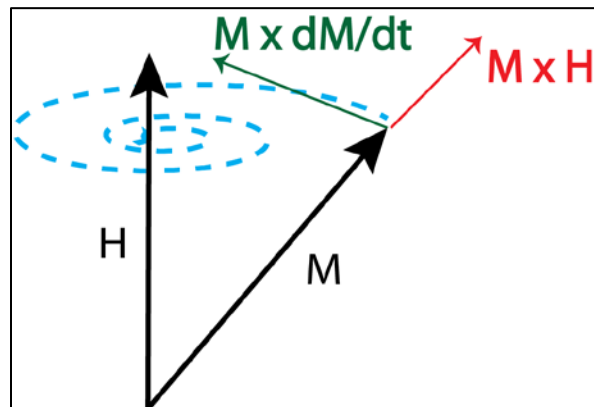


Figure 3: The Landau-Lifshitz-Gilbert equation describes the precession of a sample's magnetization around an applied field, H . In red is the precession vector and the damping vector is shown in green. The dotted blue line show the path that the magnetization will take to reach equilibrium with H .

The dynamics of the magnetization's precession involves two torques (Figure 3): the first pulls M towards H (damping torque, green) and the second points orthogonally to M and H (the precessional torque, red) [3, 16]. These vectors are described in the LLG:

Eqn. 1

$$\frac{d\mathbf{M}}{dt} = -\frac{\gamma}{2\pi} \mathbf{M} \times \mathbf{H}_{eff} - \frac{\alpha}{M_s} \mathbf{M} \times \frac{d\mathbf{M}}{dt}$$

In the LLG equation, $\gamma/2\pi$, is the gyromagnetic ratio, α is the Gilbert damping parameter, M is the magnetization of the sample, M_s is the magnetization (a scalar value), and H_{eff} is the effective field. The first term is a field-like torque and the second is a damping torque [3], see Figure 3. \mathbf{M}/M_s is the unit vector for the orientation of the magnetization. The gyromagnetic ratio, γ , is the ratio of a particle's magnetic moment to its angular momentum. The damping torque moves the local magnetization vector toward the local effective field direction. The Gilbert damping parameter, α , is a dimensionless scaling term for the damping vector. This phenomenological term is related to the magnetization relaxation rate, which is of high interest for applications. The underlying mechanisms behind the Gilbert damping are still poorly understood and are important for future applications [3, 6, 17].

It can be seen in the LLG equation and in Figure 4 that the magnitude of α has an impact on the size of the precession cone angle. One major activity of this thesis is to use spins pumped from a ferromagnet into a neighboring normal metal via FMR; the efficiency of this process directly depends on the cone angle.

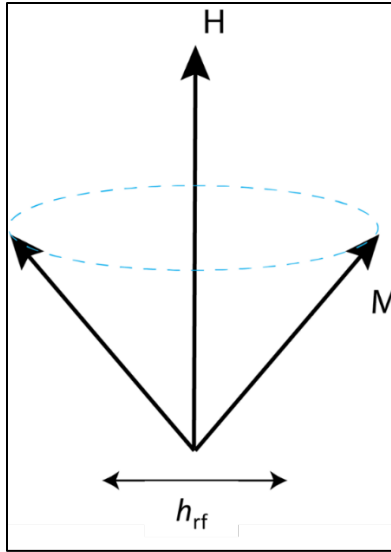


Figure 4: An alternating field, h_{rf} , can perturb the magnetization out of equilibrium. At the resonance condition, the magnetization will precess around H forming what is called the precession cone.

When spin pumping occurs, an enhanced Gilbert damping can arise if the normal metal destroys the state of the spins that enter it (i.e., the normal metal offers a new loss mechanism for angular momentum) [3, 14]. Interestingly, the only properties of the ferromagnet layer (FM) that influence spin pumping are magnetization, the intrinsic anisotropies, and magnetization damping. These determine the precession cone angle for the ferromagnetic resonance. Beyond these, the properties of the FM have only weak effect on the observed FMR signals [1, 18].

The LLG equation is part of a common simplification that is taken to describe ferromagnetic thin films called the macrospin approximation, where the magnetization is assumed to be spatially uniform. The macrospin is usually acceptable for single domain samples with a mostly uniform magnetization [3, 17, 19]. This way the LLG simplifies to two coupled differential equations and makes analytical progress possible [3]. Thin film samples in this thesis, while not true single domains, are describable by the macrospin approach because they are uniformly magnetized by the homogeneous magnetic field, and the field strengths used in this research are far above the field required to saturate the magnetization (which is always less than 20 Oe for permalloy) [3, 14, 16, 17]. Another requirement for LLG to accurately describe, the damping must be small compared to the precession, which is not an issue for the ferromagnetic alloy used [4, 20].

Comparison to other magnetic resonance techniques

FMR is similar to other resonance spectroscopy techniques like nuclear magnetic resonance (NMR) and electron paramagnetic resonance (EPR). All three techniques use RF to disturb the orientation of a magnetic moment. Where NMR operates on nuclear spins, EPR and FMR use electron spins. FMR is orders of magnitude more intense than EPR because the spins in FMR are correlated to one another, so the entire sample acts synchronously. FMR measurements typically use RF frequencies greater than 2 GHz. For contrast common frequencies used in NMR are within the range of 10 to 500 MHz [21].

Equipment

Installing, setting up, and establishing procedures for an FMR was a large focus of this research. This section will give a brief description of the equipment used for FMR measurements.

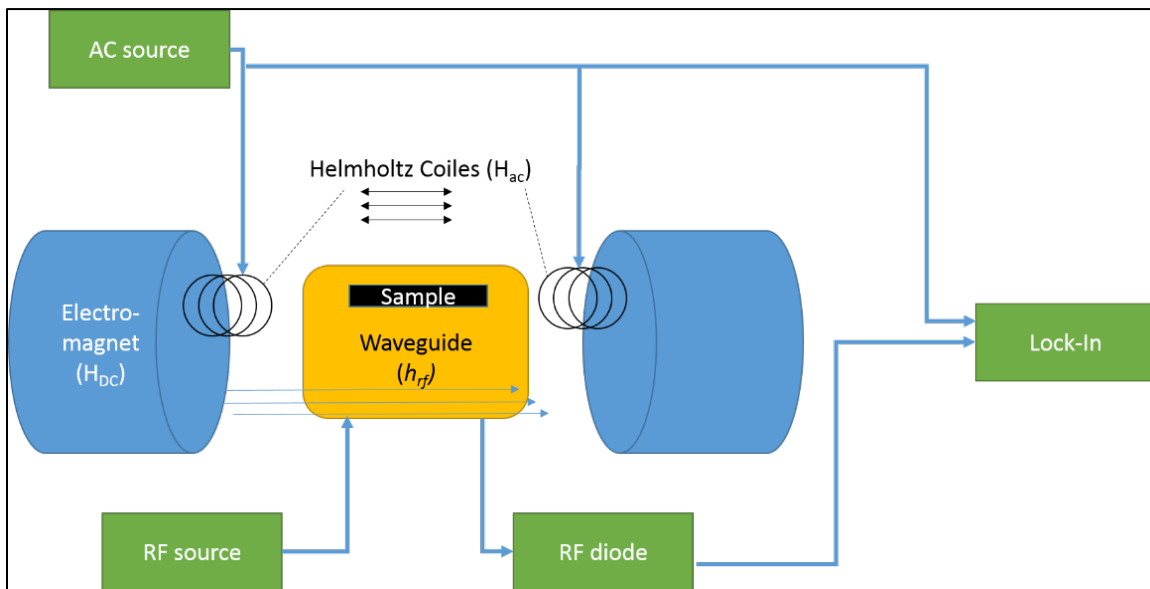


Figure 5: The RF transmission passes an RF diode before reaching the lock-in amplifier. The block “AC source” provides an AC current to the two Helmholtz coils that are situated over the poles. The Helmholtz coil, H_{ac} , provide a 490 Hz AC field parallel to the DC field. This field is used as a reference for lock-in amplification of the FMR absorption. The block “lock-in” receives the AC reference signal and the absorption signal to create.

A diagram of the FMR setup is shown in Figure 5. An RF signal is generated by a YIG resonator within the NanOsc tool (from the block “RF Source”) and then transmitted by coaxial cable through the coplanar waveguide (gold box) to provide the perturbing magnetic field, h_{rf} , transverse to the applied DC magnetic field, H_{DC} . The sample is placed film down (substrate up) on the CPW in what is referred to as the *flip-chip geometry*. The CPW and the sample are fixed

between the electromagnet pole faces parallel to the applied DC magnetic field, Figure 7. A DC current is provided to control the external magnetic field. The sample is positioned in the center of the pole faces where the magnetic flux is approximately constant over the entire sample, Figure 8. Helmholtz coils provide an AC field that is used for lock-in detection. This added AC field modulates the FMR response. An RF diode then eliminates the RF portion of the signal and the modulated response is recovered using a lock-in amplifier that uses the same AC source as the reference signal. The lock-in operates at 490Hz as the band pass filter is centered at this frequency. Two lock-in receivers are used; clocking two lock-ins at a 90 degree phase shift removes phase sensitivity on the measured spectrum. It was found that changing the modulation amplitude does not affect the spectrum linewidth. More details on how measurements are made are discussed in the appendix.

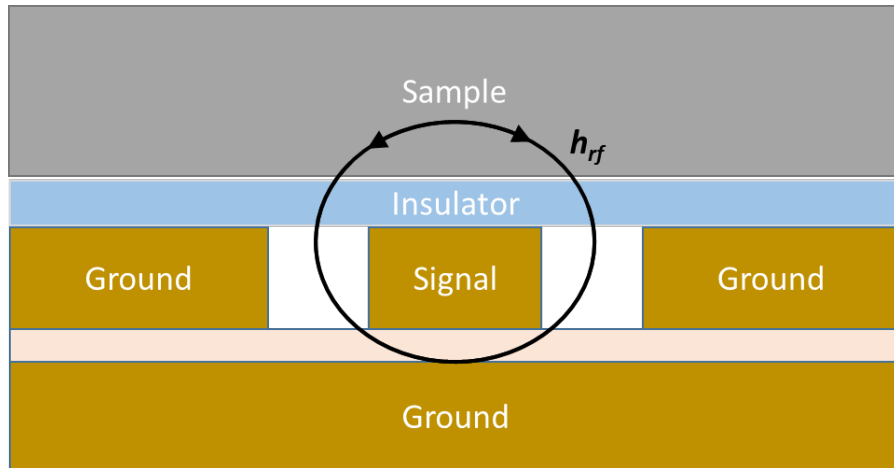


Figure 6: A cross section view of the CPW (gold) with a sample on top (grey). The insulator (blue) is Scotch® tape. This shows how the perturbing field is applied to the sample transverse to the DC field. In this diagram, the DC field is oriented into the page.

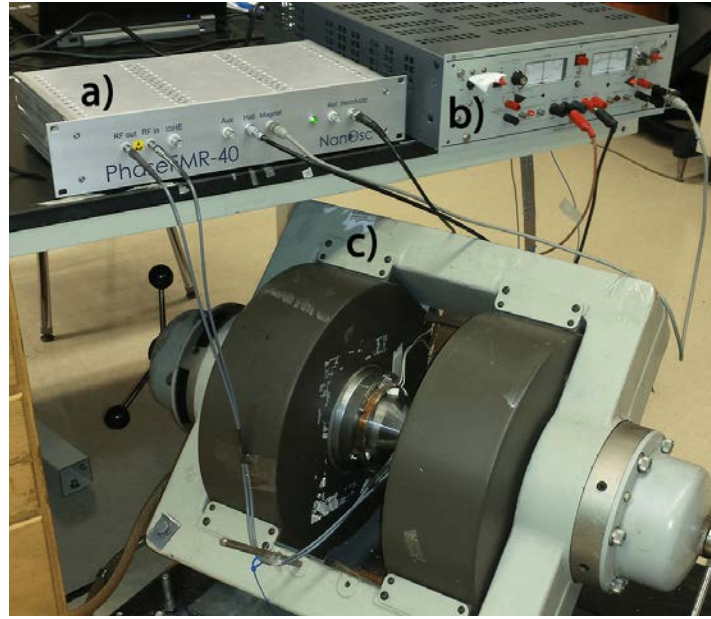


Figure 7: The FMR setup where a) is the NanOsc PhaseFMR tool b) is the DC power supply and c) is the electromagnet. The Helmholtz coils are the copper rings sitting on the pole face.

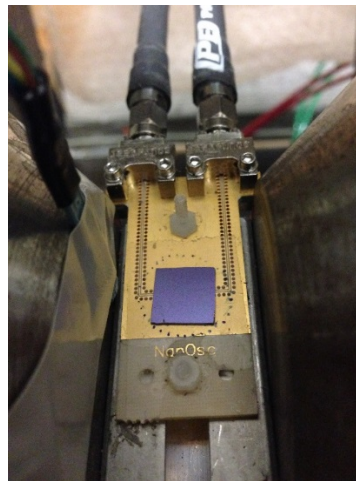


Figure 8: The coplanar waveguide, CPW, (gold) with a sample (black). The Hall Probe (blue) is seen and reports DC field strength. Plastic screws secure the CPW to an aluminum framing held in place between the pole faces. Scotch tape can be seen on the CPW. The tape reduces an induced damping caused by eddy currents in the sample.

Absorption Spectrum

To obtain a single FMR spectrum, the RF field is held at constant frequency and the DC magnetic field is swept from a high magnetic field (approximately 4000 Oe) down past the resonance condition. This produces a single absorption spectrum. An example spectrum is shown in Figure 9:

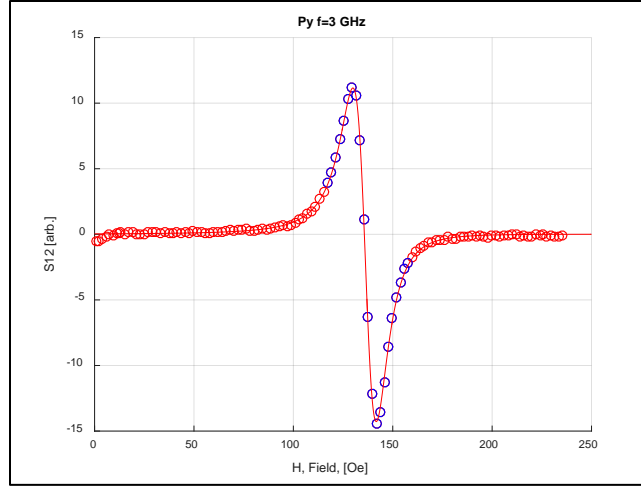


Figure 9: Example FMR spectrum. This spectrum is from a permalloy sample (Py) at $f=3$ GHz.

This single spectrum provides two relevant pieces of information, the resonance field H_{res} and the spectrum linewidth, ΔH . The H_{res} and ΔH are extracted by fitting the absorption signal to the derivative of an asymmetrical Lorentzian (lock-in detection gives the derivative of the absorption signal).

The resonance condition is dependent on the strength of an external DC magnetic field and the frequency of the RF magnetic field. At the FMR resonance condition, there is an absorption of the RF field. The absorption causes a measurable loss in the transmission coefficient of the CPW, S_{21} . The change in S_{21} (the FMR spectrum) is fit to find the resonance field, H_{res} , and the spectrum's linewidth, ΔH , using the following equation:

Eqn. 2

$$S_{21} = k_1 \frac{4\Delta H(H - H_{res})}{(\Delta H^2 + 4(H - H_{res})^2)^2} + k_2 \frac{\Delta H^2 - 4(H - H_{res})^2}{(\Delta H^2 + 4(H - H_{res})^2)^2}$$

The resonance field H_{res} is the strength of the DC magnetic field where the signal crosses the axis (i.e., the peak of the absorption). The ΔH is the full width at half maximum of the absorption, which is approximately the peak fields in the derivative signal. The first term is called the symmetric term and the second term is the antisymmetric term. k_1 and k_2 are the symmetric and antisymmetric coefficients respectively.

This procedure of holding a constant RF frequency while sweeping the magnetic field from high-to-low is repeated to obtain the H_{res} and ΔH at a range of RF frequencies. The samples are saturated in the same maximum field so that the system starts from the same

configuration for every measurement. In the next step, the frequency dependences of H_{res} and ΔH are fit to extract the main dynamical parameters of interest: the gyromagnetic ratio (γ), the effective magnetization (M_{eff}), the Gilbert damping parameter, (α), and the inhomogeneous broadening (ΔH_0).

The H_{res} and the resonance frequency, f_{FMR} , are plotted and fit with the Kittel equation [22, 23, 24]:

Eqn. 3

$$f = \frac{\gamma}{2\pi} \sqrt{H_{res}(H_{res} + 4\pi M_{eff})}$$

By fitting to the Kittel equation γ and M_{eff} are extracted. The extracted γ is then used in the fit ΔH vs. f to extract α and ΔH_0 [15, 24, 25].

Eqn. 4

$$\Delta H = \frac{2\alpha}{\gamma} f + \Delta H_0$$

FMR Noise and Errors

There are multiple ways outlier data can arise. A common way is if the sweep field is too narrow. Examples of narrow sweep fields are shown in Figure 10:

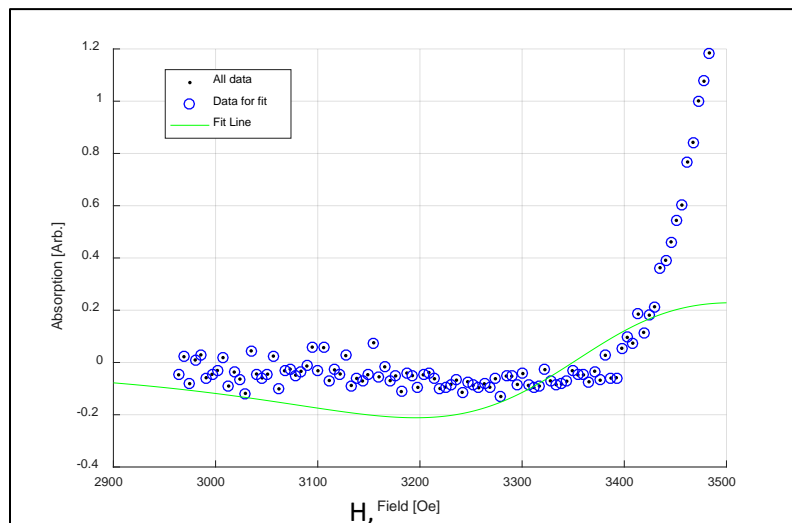


Figure 10: Example of data cut off by a narrow sweep. This can be prevented by taking broader sweeps. If time is not an issue, take very broad sweeps. Large differences in resonance fields between samples require adjustments to the measurement settings.

A more insidious result is when a sweep that is too narrow gives results that are close to

correct. In these cases an obvious outlier may not arise. An example is in Figure 11.

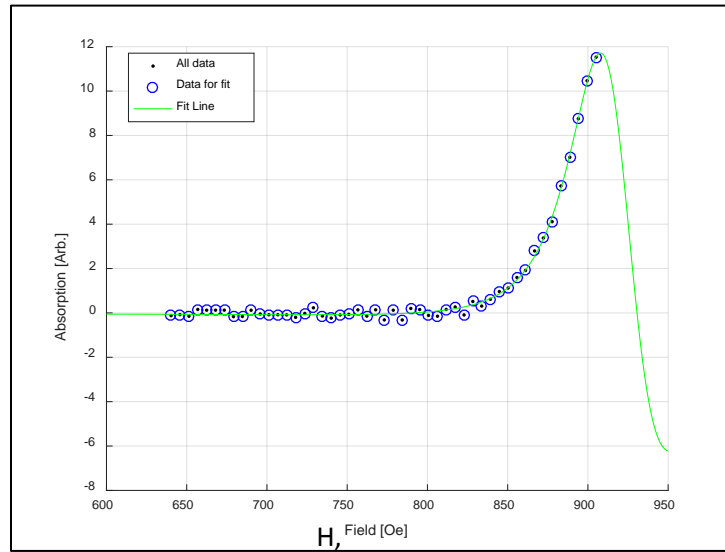


Figure 11: Some sweeps will give results that don't appear as obvious outliers but give incorrect data

This occurs when the resonance field shifts near the edge of swept range. For example if a sweep table is set up based on Permalloy standard, a sample with thick layer of a heavy metal will have a resonance that is less than the “Stop Field”. In this case the sweep table will need to be adjusted and the sample should be re-measured at this frequency.

Another source of insidious data is saturated spectrums, meaning the full-scale maximum of the detector is reached (Figure 12). These situations can be difficult to detect because the fitting algorithm still appears to fit the data well with respect to goodness of fit, but the inferred linewidth is enhanced in order to compensate for the saturated signal. In these cases, the estimated resonance field is usually still pretty accurate. If this occurs lower the gain.

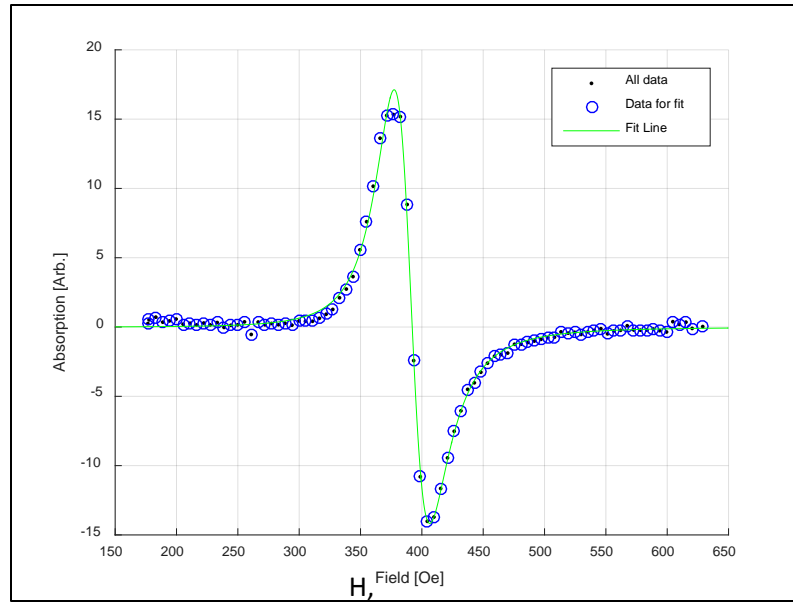


Figure 12: An example of saturated data for the three maximum data points. The maximum value for our detector is 15. It is important to review the plots to ensure accurate fits and data are created. This plot is included because it is a less obvious example of a bad fit.

There are many sources of possible error. While the vast majority of measurements are “good” once a sweep table is set up, noise or mismeasurements can occur for various reasons:

Possible sources of errors in the data:

- Mechanical vibrations can be felt in the laboratory at unpredictable times. When in the lab you can feel the floor vibrate at seemingly random times (the building air handlers are directly below the FMR).
- Temperature differences between sample measurement days. There is no climate control in the building. As side note, take care in the summer when humidity can cause the electromagnet and cooling water lines to sweat. This can damage components and rust the magnetic poles.
- Rf background noise may introduce noise. (As you read this there are probably multiple wavelengths of RF passing around or through you. Wi-Fi for example commonly uses 5.9 GHz.
- The vents in the room are extremely variable and can cause significant changes in the air flow in the room. Keep the CPW sheltered from drafts during measurements.
- Dirt and dust can contaminate the surface of samples. Some of the dust could even be ferromagnetic. This likely does not have an impact for FMR but is definitely a

concern with sensitive measurements like the VSM.

- Sign flipping introduced by NanoOsc software. “Sign flipping” is when the software incorrectly calculates the sign of the signal when correcting the phase of the quadrature data. The sign flipping has not been observed in the latest release of NanoOsc software. If the issue is seen again, the Matlab code can be modified to correct the phase by including the following function:

```
function [I_mod,Q_mod]=phase_correct(I,Q,phi);  
[th,R]=cart2pol(I,Q);  
I_mod=R.*sin(th+phi);  
Q_mod=R.*cos(th+phi);  
end
```

This code can be placed within an optimization loop that maximizes the in phase signal (I_{mod}) by altering ϕ . This could be placed within the Matlab function `FMR_spectrum.m` (see Appendix for description of this code) to correct the phase each time data is processed but it is believed this would be unnecessary, unless the code is needed as general case for any FMR system; unless modifications are made to the system, the phase shift should stay constant.

XRR

XRR Introduction

X-ray reflectivity (XRR) is an extremely useful analytical technique used to characterize thin films and multilayers. XRR measures intensity of reflected monochromatic x-rays that graze a sample at a small angle. The measurements are done with constant x-ray wavelength and sweeping angle. The angle of reflection and intensity of the reflected x-rays are the data used to determine the sample characteristics. The intensity of reflection is dependent on three structural parameters of the thin films: the difference in electron density at interfaces, the roughness of the interfaces (if there is a sharp change in electron density or more gradient-like change), and the thickness of the thin films. In this thesis, the primary concern is multilayer thicknesses. The technique is useful for thickness determination below 200nm with a precision about 0.3 nm, depending on surface roughness (this is an average over the entire sample area, i.e., an RMS roughness). XRR thickness measurements require flat samples, good contrast in

electron density, and low sample roughness (<5nm is a common rule).

Basic Theory

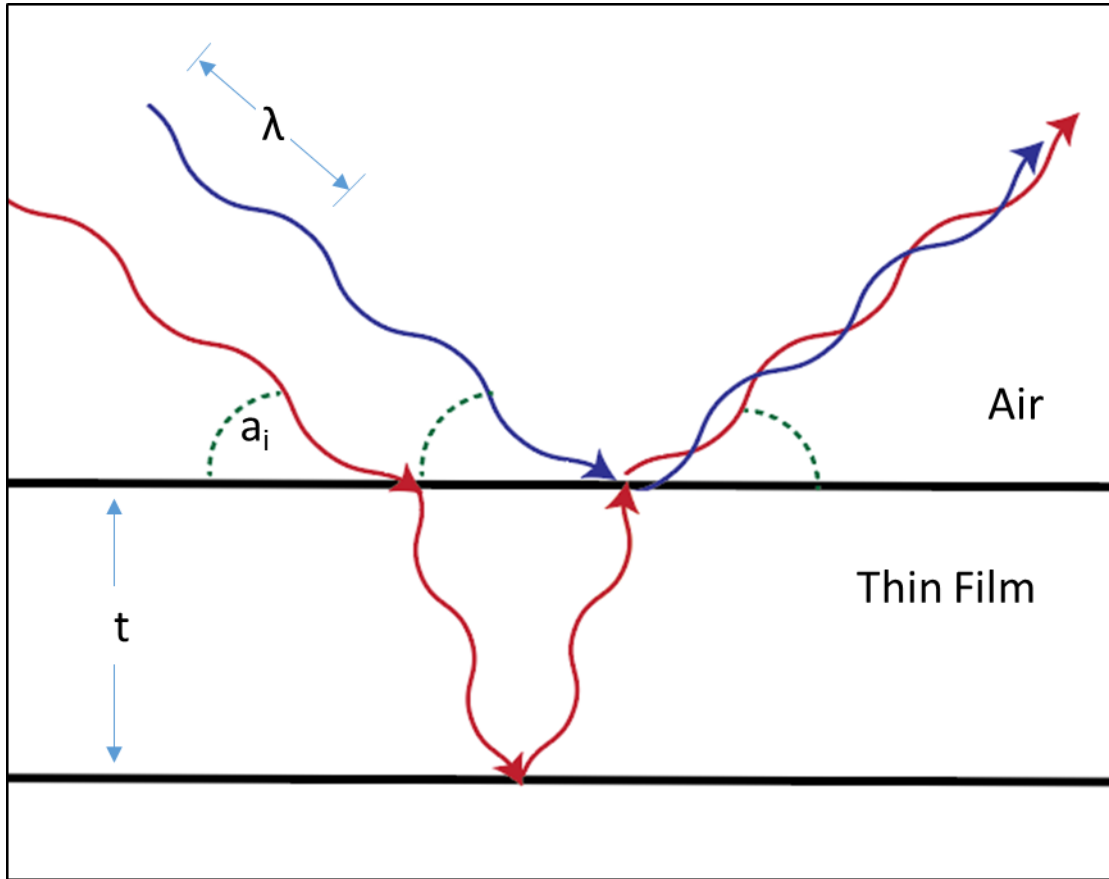


Figure 13: A diagram for x-ray reflectivity (XRR) showing how interference changes with the incident angle, a_i , for a single thin film. Note that the angles are not to scale and exaggerated. λ is the wavelength of the x-ray and t is the thickness of the thin film. The red and blue lines are two different incident rays that experience destructive interference and would result in a "valley" in the intensity counts (Figure 14). XRR will produce fringe patterns caused by the interference of beams reflecting off of parallel film surfaces. Thickness, roughness, and electron density all influence the XRR patterns (Figure 14).

XRR peaks are observed due to the interference of the incident waves from the separate interfaces causing oscillations in the reflected intensity. A more detailed explanation follows; when a beam of x-rays encounters a sharp change in electron density (layer surface or interface of two layers), an amount of the x-rays are reflected and many at the same angle as incidence in what is called specular reflection. Each interface will reflect a characteristic amount of x-rays. The reflections from different interfaces will then show wave interference patterns. The phase difference is dependent on the distance of the reflecting interfaces, i.e. the thickness of the thin film layers. So when x-rays in constructive interference are collected simultaneously by a detector there are noticeable "peaks" in the intensity. The separation of the peaks

corresponds to layer thickness. Amplitude of peaks increases with increasing density contrast of the thin film layers. X-rays mainly reflect from electrons, and the materials in the thin films must have sufficient electron density to be observed. For example, aluminum layers are practically invisible in this research experiments, because this is dependent on the incident angle and the photon wavelength which is controlled by x-ray source. In Dr. Michael Pierce's lab at RIT, x-rays are generated with copper and the wavelength is approximately $\lambda = 0.154$ nm.

To determine the thin film properties, a fitting procedure is done to the XRR data. A modified Bragg equation can be used to find the film thickness by positions of the fringes:

Eqn. 5

$$m\lambda = 2t\sqrt{\sin^2(a_i) - \sin^2(a_c)}$$

Where t is the thickness of the thin film layer, a_i is the angle of an observed fringe, a_c is the critical angle, m is the integer number of fringe, and λ is the wavelength of the incident x-ray [26].

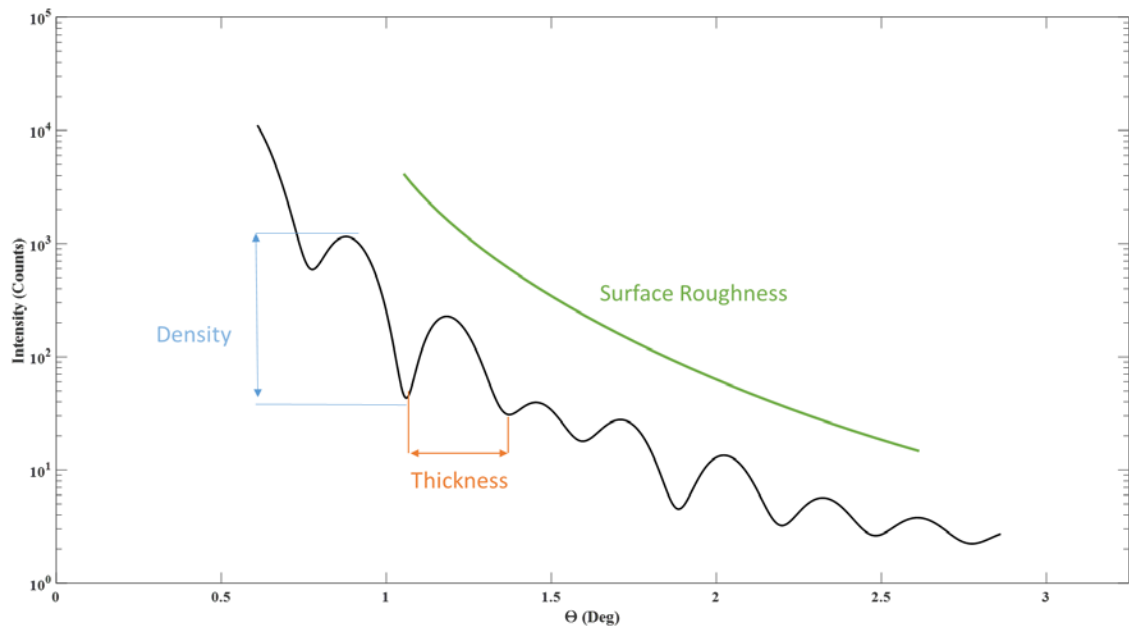


Figure 14: This graph shows a representative XRR fit and the influences each parameter can have on the shape. [27]

Sheet Resistance

A protocol was developed for measuring the sheet resistance of thin film samples using the Van der Pauw method. The Van der Pauw Method was developed to measure sheet

resistance of two dimensional samples with arbitrary shapes. In this research measuring the sheet resistance is used to verify layer quality.

Sheet resistance is the resistance to current running parallel to the surface of a sample. The sheet resistance is a function of thickness. The resistance can be written in terms of the sheet resistance by incorporating the thickness and resistivity into a single factor in the standard resistance formula:

Eqn. 6

$$R = \frac{\rho L}{W t} = R_s \left(\frac{L}{W} \right)$$

Where R is the resistance, R_s is the sheet resistance, t is the depth of the thin film, ρ is the resistivity, and L and W are the length and width dimension. The units for sheet resistance simplify to Ω , the same units as resistivity. The sheet resistance is then often denoted as “Ohms per Square”, Ω/\square . Sheet resistance is independent of the area of a sample (a square meter and a square centimeter of the same thin film are expected to have the same sheet resistance). The factor (L/W) can be viewed as the aspect ratio of a sample. So a sample that is 20 units long and 1 unit wide would show a different resistance as a square sample. This property has particular utility for thin films as it can be measured directly with a four point probe. The common four point measurement method, where voltage drop is measured in-line between current probes, requires a correction factor for geometries. To circumvent the geometric dependence, the Van der Pauw method can be used to find sheet resistance, independent of sample shape. The method is valid with the following assumptions:

- The four contacts are small enough to be considered points.
- The contacts are positioned along the perimeter of the sample.
- The sample has homogenous thickness and isotropic resistance (use the Montgomery method for anisotropic measurements).
- The sample surface must be singly connected (meaning there are no gaps or holes).

Measurements for the van der Pauw method are made by passing a current from two adjacent points (like A and B) and measuring the voltage between the parallel points (C and D).

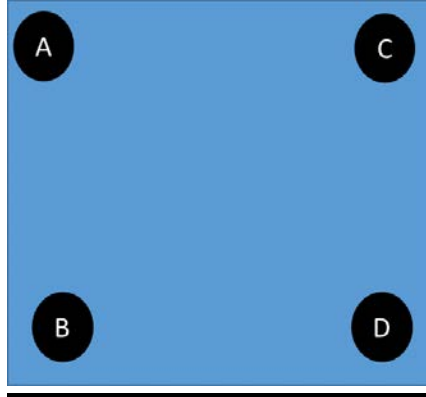


Figure 15: Sheet resistance measurements are made by passing a current along one edge of a sample and measuring the voltage drop on the parallel edge. This process is repeated in the perpendicular direction and the equality in Eqn. 7 is used to

Dividing the voltage by the current gives a resistance (in this case written as $R_{AB,CD}$). The resistance is then determined in the perpendicular orientation, with a current from point B to D and the voltage measured from A to C to give, $R_{BD,AC}$. The actual sheet resistance can then be determined from these resistances by the relation:

Eqn. 7

$$e^{-\pi R_{AB,CD}/R_s} + e^{-\pi R_{BD,AC}/R_s} = 1$$

To improve the accuracy of the measurement, the measurements can be repeated with voltage and current probes swapped to find $R_{CD,AB}$ and $R_{CA,DB}$ and averaged with the parallel measurements.

Section 3: Py/Ir vs. Py/Cu/Ir: Observations of Spin Memory Loss

Abstract

A core investigation of this research was comparing the dynamics of Py/Ir and Py/Cu/Ir samples, where Py = Ni₈₀Fe₂₀. Coplanar waveguide ferromagnetic resonance (CPW-FMR) was used to study the spin dynamics for Py/Ir and Py/Cu/Ir multilayers as a function of Ir thickness. There is a strong enhancement of the Gilbert damping parameter when the Ir layer has direct interface with magnetic layer ($\alpha=0.023$) compared to when the interfaces are interrupted with a Cu layer ($\alpha=0.013$). The control sample Py demonstrated a damping parameter consistent with other investigations ($\alpha=0.0084$) [28, 29]. This indicates the presence of “spin memory loss” at the interface of Py and Ir. There is no correlation observed between Ir thickness and the gyromagnetic ratio, γ . There was a correlation between the damping and Ir thickness for the Py/Ir samples that was not observed Py/Cu/Ir samples. This is may be related to a proximity effect (induced ferromagnetism in in non-ferromagnetic atoms due to proximity with ferromagnetic atoms) caused by the existence of a direct interface between Py and Ir. The characteristic length for this proximity effect was found to be approximately $\lambda= 0.46 \pm 0.10$ nm. Effective spin mixing conductance at saturation, g_{eff} , was found to be 8.8 ± 0.3 nm⁻² for Py/Cu/Ir, and 25.2 ± 0.5 nm⁻² for the Py/Ir samples.

Experimental Details

Samples

Samples were fabricated by Dr. Casey Miller at the University of Gothenburg in Sweden. Samples were grown onto oxidized silicon wafers by magnetron sputtering in 3 mTorr of ultra-high purity Ar using a load-locked system with a base pressure of 15 nTorr. Deposition rates for each material (Py 0.068 nm/s; Cu 0.05 nm/s; Ir 0.034 nm/s) were held constant for all samples, changing only the deposition time to achieve different thicknesses. The thickness of Py and Cu were held constant at 4.5 nm and 1.8 nm respectively, while the Ir ranged from 0.6 nm to 46 nm. The reference is a Py layer (4.5 nm) sample with a Cu layer (1.8 nm).

All samples were capped with 5nm of Al. Al serves as a barrier to oxidation. A reference Py includes a Cu layer between the Al cap and the Py, as there is evidence that direct interfacing between Py and Al causes slight increase in damping, perhaps because of the lattice mismatch between Py and Al. A basic diagram of the samples is shown in Figure 16.

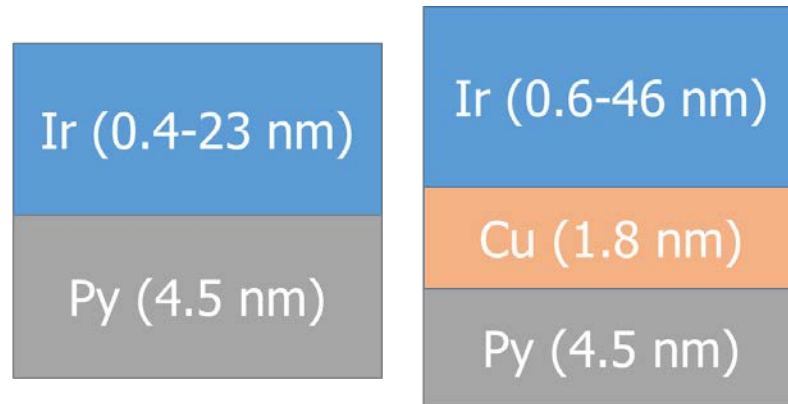


Figure 16: Diagram of sample structures, not to scale. There are 11 samples of each Py/Ir and Py/Cu/Ir. Not shown in the figure is the Si substrate nor the Al capping layer.

Verifying thicknesses with X-ray Reflectivity

Thicknesses were verified with XRR. Example XRR sweeps and fits are shown in Figure 17.

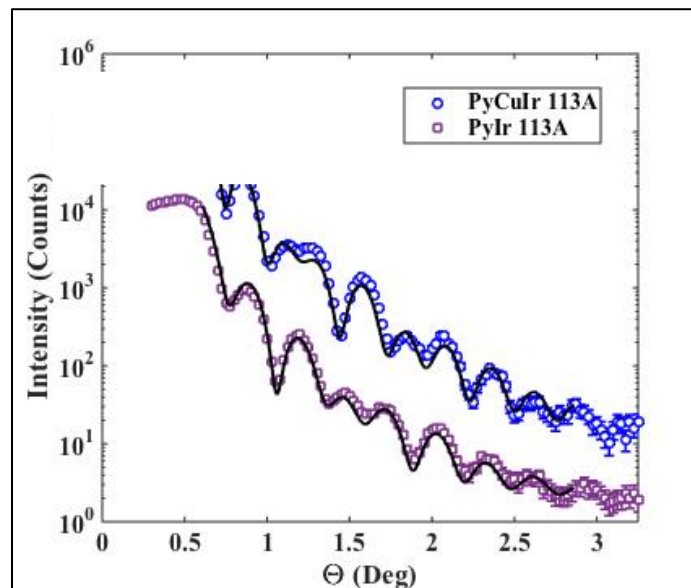


Figure 17: X-ray reflectivity scans for Py/Cu/Ir and Py/Ir. Iridium thickness $t_{Ir}=4.5$ nm.

The layer thicknesses for eight samples were determined, four of each sample set. Because the sputtering time was constant for all Py and Cu depositions, the thickness results can be averaged. For the Py/Cu/Ir samples, a net thickness of Py-Cu is reported from the fit; the x-rays were not able to distinguish between the Py and Cu layers as they have similar electron density. To determine the Py thickness for all samples, the average Py thickness from the four Py/Ir measurements were averaged. The Cu thickness is then determined by subtracting the Py

thickness from the average Py-Cu thickness. See Table 1 for the XRR results for Py and Py-Cu thicknesses.

Sample	Py Thickness [nm]	Uncertainty		
Py/Ir 15s	4.5	0.25		
Py/Ir 22s	4.4	0.30		
Py/Ir 50s	4.5	0.20		
Py/Ir 113	4.6	0.15		
Py/Ir 254	4.3	0.20		
Sample	Py/Cu net Thickness [nm]	Uncertainty	Py Thickness average [nm]	Stand. Deviation
Py/Cu/Ir 15s	6.1	0.20	4.5	0.1
Py/Cu/Ir 22s	6.1	0.10	Py/Cu Thickness average [nm]	Stand. Deviation
Py/Cu/Ir 50s	6.3	0.30	6.2	0.1
Py/Cu/Ir 113	6.3	0.15	Cu Thickness [nm]	
Py/Cu/Ir 254	6.4	0.20	1.8	0.2

Table 1: Thickness results for Py and Py/Cu layers from XRR analysis. The column Uncertainty refers to the uncertainty of the fit. Py and Cu are not distinguished by the XRR so a net thickness of the two layers is given. To find the Cu thickness, the average Py thickness from the Py/Ir samples was subtracted from the net thickness of Py-Cu. In this table, sample names are formed from their sputtering time for Ir (ex. Py/Ir 15s means Ir was sputtered for 15 seconds). Once the thicknesses were determined, and in all in rest of this thesis, samples are always identified by Ir thickness.

The Ir layer thickness vs. sputtering time was plotted for all eight samples in Figure 18. There was no significant difference in iridium thicknesses between samples with and without Cu for the same deposition time. The XRR was performed on eight samples. The slope then gives the conversion from sputtering time to Ir thickness. The sputtering rate was found to be 0.04 nm/s for iridium. The Ir thicknesses were interpolated and extrapolated for all other samples. Figure 18 shows the Ir thickness vs. deposition time.

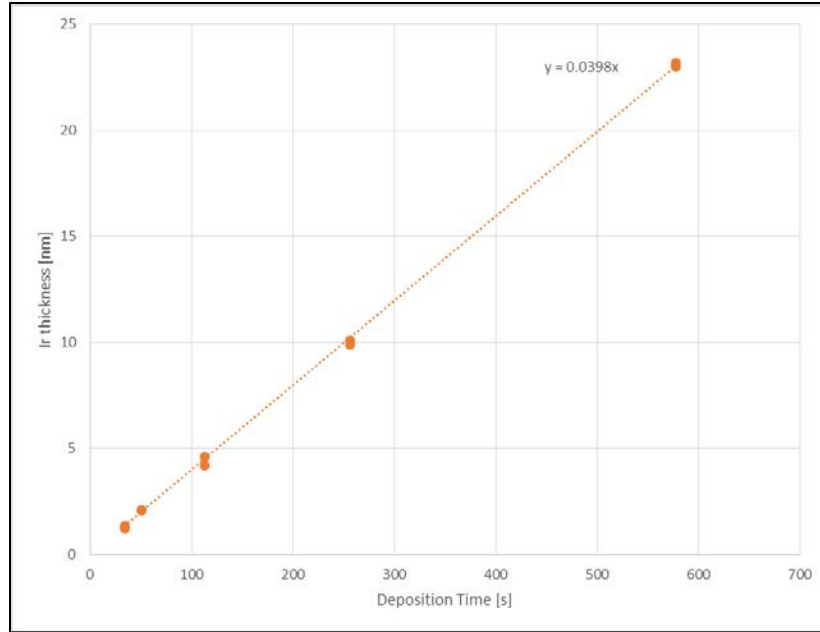


Figure 18: Deposition thickness of iridium as a function of deposition time. There was no significant difference in iridium thicknesses between samples with and without Cu for the same deposition time. The XRR was performed on 8 samples and the thicknesses were interpolated and extrapolated for all samples.

Qualifying Iridium layer quality with sheet conductance

The van der Pauw method was used to determine the sheet conductance of all samples in order to investigate the sample quality. The sheet conductance increases equivalently with increasing Ir thickness for both sample series, indicating that the Cu layer had no significant impact on the Ir layer quality [23].

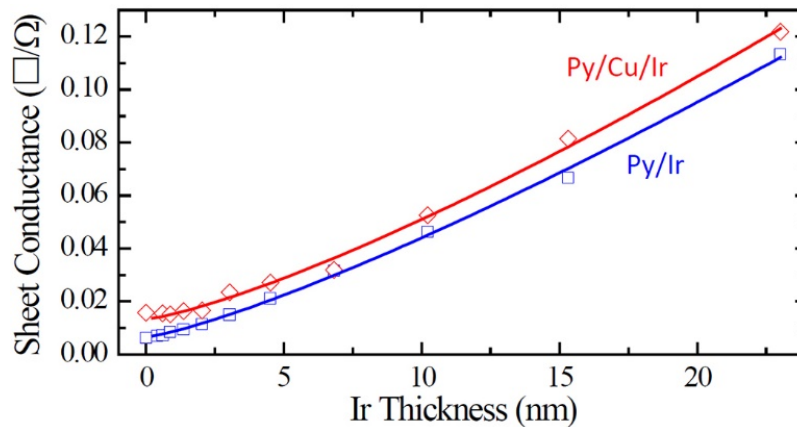


Figure 19: Sheet conductance (inverse sheet resistance) vs. Ir thickness. Between the two sample sets there is a shift in the sheet conductance due to the Cu layer increasing the conductance a constant amount, but the trend is uniform for both sample sets, showing that the Cu layer does not impact the Ir layer quality.

Measuring the sheet conductance is very important for Inverse Spin Hall Effect (ISHE) measurements. ISHE measurements are voltages, and sheet conductance is needed to convert

the measurements to current [25, 30]. This is future work for the lab, and will not be discussed in detail here.

FMR Measurements

All spectra in this study were taken at room temperature with constant RF excitation frequency and amplitude while the applied field is reduced from an initial saturation at 4 kOe below the resonance field. Two example field sweeps at different frequencies are shown in Figure 20.

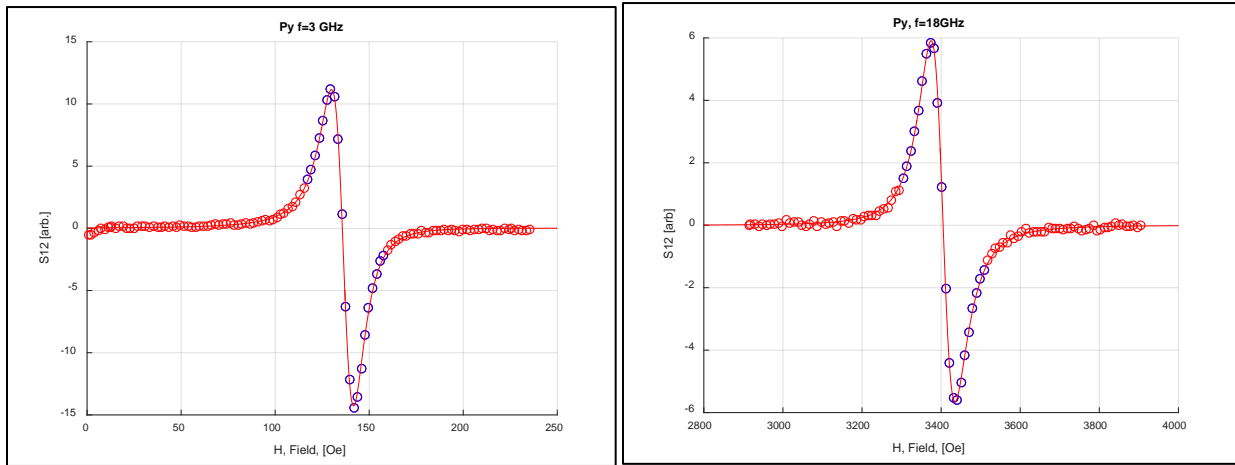


Figure 20: Example FMR absorption spectra for standard permalloy sample at $f=3$ and 18 GHz. Lines are fits points are data. Red points are for all data measured. Blue points are the data that are used in the fit as determined by the Matlab code (See Matlab code description in Appendix). Notice the width of the spectrum is much larger for higher frequencies.

It was found that the Ir layer increases the linewidth. Additionally there is a significant increase in the linewidth when the Ir layer has a direct interface with the Py. Notice in Figure 20 that data points near the spectrum are blue. These are the data points that are used for the fit and determination of H_{res} and ΔH . Only fitting data near the resonance increases the confidence in the fit parameters significantly. Partitioning the data for the fit is automatically done by the Matlab code (see appendix for more details on the fitting procedure).

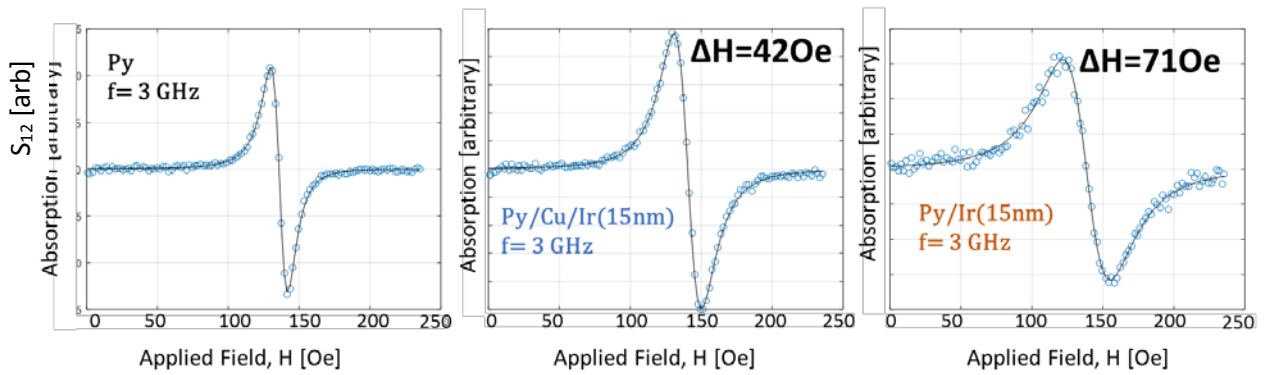


Figure 21: Field sweeps for control sample, Py/Cu/Ir, and Py/Ir where $t_{Ir}=15$ nm. $f=3$ GHz for all three sweeps. These sweeps are shown without the portioning ability of the Matlab code so all points are the same color and are included in the fit.

In general, the signal to noise ratio decreased with increased Ir thickness and was worse for the direct interface samples, Py/Ir. These trends can be seen in

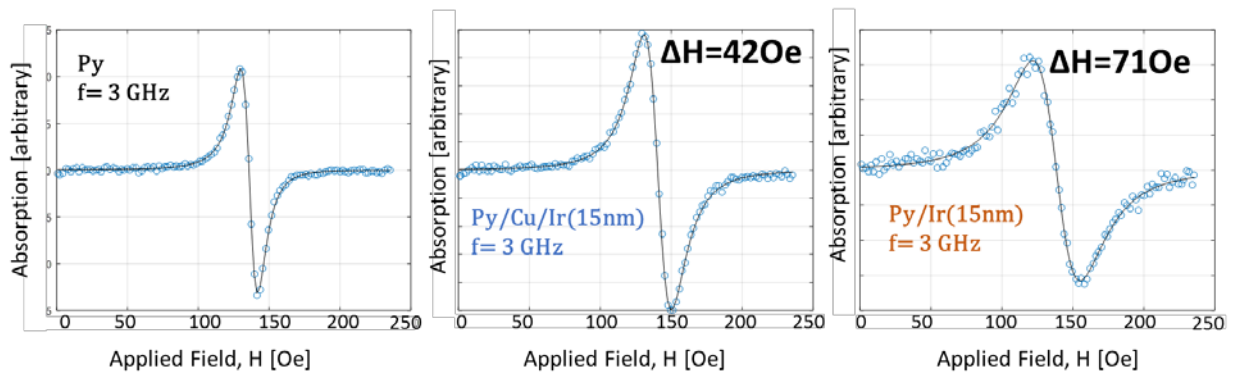


Figure 21. Notice the amplitude of the signal decreases and the noise increases when going from the standard Py to Py/Cu/Ir to Py/Ir.

On the first attempts to process the data for this experiment, the parameters were, M_{eff} and α , were calculated for each individual sweep. It was found that the parameters obtained from a single sweep had high variance. To work around this, H_{res} and ΔH were extracted from multiple sweeps and the values were averaged. This improved the confidence in the results significantly. The standard deviation of the resulting parameters was reduced by approximately 50%. When fitting the data to a model, the Kittel or to the ΔH vs. f , error will propagate from a single outlier more severely than when averaging multiple values together. Additionally, when averaging multiple data points, statistics can be applied to remove outliers.

Each sample was measured 3 to 8 times, depending on the confidence in the fits.

Measurements were spread out over multiple weeks. There were a 94 total sweeps taken. Each measurement was a sweep of 16 frequencies from 3 to 18 GHz (2 GHz was not included in final calculations; at this low frequency other effects influence the linewidth). Once all measurements were made and the spectrums were fit, H_{res} and ΔH data were cleaned.

To clean the data, data points where the confidence in ΔH was greater than 10% of the value of ΔH were removed. Chauvenet's criterion was then applied along constant frequencies to remove severe outliers. This statistical method assesses whether a datum is a statistical outlier. A Matlab code was made to apply Chauvenet's criterion to the data, and is located in the Appendix. Next a linear line was fit to ΔH vs. f (as discussed in FMR theory section this is a linear relationship). The absolute values of the residual were calculated and placed on a table. On the table, Excel's conditional formatting highlighted the largest residual values. The fits associated with the large residual values were examined to see if there were any noticeable issues with the fits. Data that clearly had bad fits was then deleted. An example of a data point removed was from the spectrum shown Figure 22. The reason a blind statistical tool was not applied at this step is that data was deleted if there were clearly problems with an individual spectrum fit. This way, since there were multiple measurements of each spectrum, a frequency for some samples would not be entirely rejected (i.e., we were able to keep 15GHz for 46nm by eliminating that bad sweep from the data set, so instead of averaging four sweeps, we only average three). The final results are seen in Table 2 and Table 3.

	Residual Linewidth (abs(Data-fitline)) [Oe]																
Py/Cu/Ir	Frequency [GHz]																
Ir thickness [nm]	2	3	4	5	6	7	8	9	10	11	12	13	14	15	16	17	18
0.0	2	1	0	1	1	1	1	1	0	2	0	0	0	0	0	0	0
0.1	1	0	1	1	1	1	1	0	1	0	4	2	5	0	2	0	0
0.1	2	1	1	1	0	2	0	5	2	1	3	0	1	0	1	4	1
0.1	1	1	0	1	1	1	1	1	0	1	0	0	3	4	4	0	0
0.2	2	1	0	1	1	2	1	1	1	1	0	1	1	0	1	0	0
0.3	3	1	1	1	2	1	0	2	1	1	2	1	2	1	1	1	3
0.5	3	1	0	1	3	0	1	1	0	2	0	5	1	4	4	1	3
0.7	2	1	0	2	1	1	1	1	1	1	1	2	1	0	3	2	2
1.0	2	1	1	1	1	1	2	4	2	2	0	1	0	2	0	4	4
1.5	3	1	1	1	1	1	2	0	1	1	4	1	2	3	0	3	1
2.3	3	1	1	1	2	0	0	2	0	1	2	2	2	0	6	3	4
4.6	3	1	1	1	1	1	1	1	3	0	0	0	2	7	5	0	2

Table 2: Final residuals for ΔH vs. for Py/Cu/Ir. Conditional formatting was used to identify the largest residuals. This was used to track down outlying data.

	Residual Linewidth (abs(Data-fitline)) [Oe],																
Py/Ir	Frequency [GHz]																
Ir thickness [nm]	2	3	4	5	6	7	8	9	10	11	12	13	14	15	16	17	18
0.4	2	1	3	2	3	1	2	0	5	4	2	4	1	0	1	2	2
0.6	5	1	1	2	1	3	2	2	2	1	1	2	1	3	1	4	0
0.9	2	1	0	1	0	2	2	3	3	3	3	1	0	1	1	1	1
1.4	2	2	0	0	1	4	0	2	1	3	1	2	1	2	5	1	1
2.0	2	0	1	2	3	0	2	0	1	2	4	3	0	2	1	0	2
3.0	2	0	3	2	1	0	0	0	2	3	1	4	5	1	2	3	2
4.5	5	1	0	1	1	0	3	2	1	5	2	3	1	6	6	1	1
6.8	3	2	1	1	1	1	1	3	2	1	1	0	3	1	8	1	2
10.2	2	3	2	1	1	3	4	1	0	1	2	5	1	3	4	3	4
15.3	5	3	2	0	4	2	6	3	2	3	2	6	3	1	0	5	3
23.0	3	1	2	1	3	0	0	3	1	3	4	1	4	6	2	2	8

Table 3: Final residuals for ΔH vs. for Py/Ir. This was used to track down outlying data.

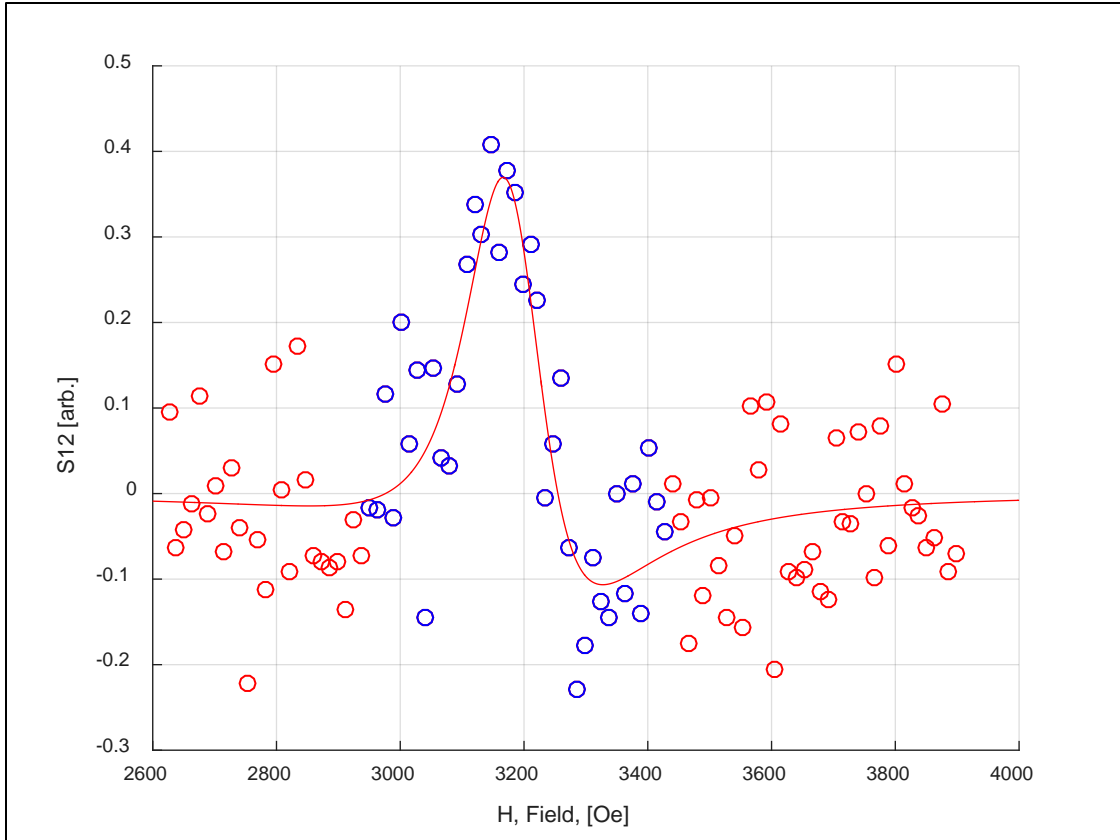


Figure 22. An example spectrum fit that gave unrepresentative ΔH value. There is uncharacteristically high noise for this measurement. See the discussion on errors in the section "FMR measurement Procedure."

Results

Resonance Field and Linewidths

Table 4 and Table 5 summarize the thickness and frequency dependence of H_{res} for the Py/Cu/Ir and Py/Ir sets, respectively. Columns are organized by the frequency and rows are the iridium thickness, t_{Ir} . The standard is included in Table 4 as a thickness of zero. Corresponding linewidth results are in Table 6 and Table 7 for Py/Cu/Ir and Py/Ir, respectively. As discussed above, each value in H_{res} and ΔH tables is the average of multiple measurements. The values shown in the tables below were used for the fits that help determine the magnetic and dynamic parameters of interest for each sample.

Py/Cu/Ir	Resonance Field [Oe]																	
	Frequency [GHz]																	
	2	3	4	5	6	7	8	9	10	11	12	13	14	15	16	17	18	
0.0	62 ± 0	136 ± 0	236 ± 0	363 ± 0	512 ± 0	682 ± 0	871 ± 0	1077 ± 0	1297 ± 0	1531 ± 3	1774 ± 2	2027 ± 0	2289 ± 1	2558 ± 0	2834 ± 1	3116 ± 0	3403 ± 1	
0.6	62 ± 1	141 ± 0	244 ± 2	375 ± 0	529 ± 1	704 ± 1	900 ± 1	1109 ± 3	1334 ± 0	1572 ± 3	1821 ± 1	2078 ± 1	2343 ± 0	2615 ± 0	2896 ± 1	3180 ± 2	3470 ± 1	
0.9	66 ± 4	145 ± 4	251 ± 3	383 ± 4	540 ± 5	716 ± 5	913 ± 5	1125 ± 4	1354 ± 5	1591 ± 6	1842 ± 7	2101 ± 4	2370 ± 6	2645 ± 7	2926 ± 6	3214 ± 6	3506 ± 4	
1.4	66 ± 1	145 ± 1	250 ± 0	382 ± 1	537 ± 1	714 ± 1	907 ± 2	1121 ± 2	1346 ± 3	1584 ± 3	1832 ± 3	2093 ± 3	2359 ± 4	2632 ± 4	2915 ± 4	3199 ± 4	3489 ± 5	
2.0	69 ± 8	147 ± 7	251 ± 8	384 ± 7	538 ± 8	715 ± 8	908 ± 8	1120 ± 8	1346 ± 8	1583 ± 9	1833 ± 9	2093 ± 9	2358 ± 10	2633 ± 9	2913 ± 9	3199 ± 9	3489 ± 10	
3.0	63 ± 4	142 ± 4	245 ± 4	378 ± 3	532 ± 3	708 ± 3	902 ± 4	1114 ± 3	1339 ± 2	1578 ± 3	1826 ± 3	2084 ± 3	2351 ± 4	2625 ± 4	2904 ± 5	3192 ± 6	3482 ± 8	
4.5	60 ± 4	139 ± 4	244 ± 4	376 ± 3	531 ± 2	707 ± 3	904 ± 3	1114 ± 1	1342 ± 1	1580 ± 3	1830 ± 1	2089 ± 0	2357 ± 4	2626 ± 3	2911 ± 7	3197 ± 6	3486 ± 7	
6.8	69 ± 0	148 ± 0	252 ± 0	385 ± 1	539 ± 1	716 ± 1	911 ± 2	1122 ± 2	1347 ± 4	1585 ± 4	1835 ± 3	2094 ± 4	2359 ± 4	2633 ± 5	2915 ± 5	3202 ± 7	3491 ± 7	
10.2	60 ± 9	139 ± 9	244 ± 9	377 ± 8	533 ± 9	710 ± 8	906 ± 8	1119 ± 8	1345 ± 8	1582 ± 8	1834 ± 8	2093 ± 8	2363 ± 5	2636 ± 5	2918 ± 6	3205 ± 6	3497 ± 2	
15.3	64 ± 2	143 ± 2	247 ± 2	380 ± 2	535 ± 2	711 ± 1	906 ± 0	1119 ± 0	1346 ± 1	1583 ± 1	1832 ± 1	2092 ± 1	2360 ± 1	2633 ± 2	2915 ± 0	3200 ± 4	3491 ± 2	
23.0	63 ± 2	143 ± 1	249 ± 1	381 ± 3	538 ± 2	716 ± 3	911 ± 5	1125 ± 4	1354 ± 4	1593 ± 4	1843 ± 5	2102 ± 6	2371 ± 4	2647 ± 6	2928 ± 8	3215 ± 5	3501 ± 7	
46.0	59 ± 0	139 ± 0	244 ± 0	377 ± 0	534 ± 0	711 ± 0	908 ± 1	1121 ± 1	1349 ± 1	1588 ± 1	1838 ± 1	2099 ± 1	2365 ± 1	2645 ± 3	2924 ± 4	3212 ± 5	3500 ± 0	

Table 4: H_{res} for all Py/Cu/Ir samples and Py standard in Oe. Columns are organized by the frequency. Rows are the Ir thickness in nm. For example, the H_{res} at 3GHz for the sample $t_{Ir}=0$ nm is 136 Oe.

Py/Ir	Resonance Field [Oe]																	
	Frequency [GHz]																	
	2	3	4	5	6	7	8	9	10	11	12	13	14	15	16	17	18	
0.4	65 ± 5	140 ± 4	239 ± 4	366 ± 4	514 ± 3	685 ± 5	871 ± 3	1074 ± 4	1296 ± 6	1525 ± 4	1768 ± 3	2019 ± 4	2282 ± 6	2555 ± 9	2827 ± 7	3104 ± 4	3394 ± 8	
0.6	51 ± 5	134 ± 9	233 ± 8	360 ± 7	509 ± 7	679 ± 7	868 ± 9	1072 ± 8	1289 ± 4	1523 ± 9	1764 ± 2	2019 ± 8	2278 ± 3	2548 ± 7	2825 ± 4	3106 ± 7	3389 ± 4	
0.9	58 ± 5	136 ± 3	239 ± 4	369 ± 5	520 ± 4	694 ± 4	886 ± 5	1094 ± 6	1316 ± 6	1551 ± 7	1796 ± 3	2054 ± 8	2316 ± 9	2585 ± 6	2868 ± 9	3148 ± 5	3440 ± 5	
1.4	63 ± 2	142 ± 2	244 ± 3	375 ± 2	530 ± 2	705 ± 2	897 ± 3	1105 ± 2	1329 ± 3	1565 ± 3	1812 ± 2	2070 ± 3	2332 ± 4	2604 ± 4	2879 ± 5	3166 ± 6	3456 ± 3	
2.0	59 ± 4	139 ± 4	241 ± 4	373 ± 2	525 ± 4	699 ± 3	892 ± 3	1100 ± 4	1324 ± 3	1559 ± 3	1806 ± 3	2058 ± 6	2325 ± 6	2596 ± 2	2876 ± 6	3156 ± 5	3445 ± 5	
3.0	63 ± 5	143 ± 5	246 ± 5	377 ± 6	529 ± 4	705 ± 7	898 ± 6	1106 ± 7	1330 ± 7	1566 ± 7	1812 ± 6	2070 ± 10	2334 ± 9	2609 ± 8	2884 ± 14	3171 ± 13	3460 ± 12	
4.5	54 ± 2	135 ± 1	239 ± 1	370 ± 4	524 ± 2	700 ± 4	891 ± 4	1103 ± 2	1327 ± 3	1560 ± 3	1809 ± 2	2067 ± 5	2331 ± 4	2607 ± 4	2883 ± 4	3169 ± 11	3460 ± 9	
6.8	60 ± 7	140 ± 5	243 ± 4	376 ± 0	528 ± 5	705 ± 0	894 ± 5	1106 ± 0	1326 ± 6	1565 ± 1	1809 ± 6	2068 ± 2	2331 ± 9	2606 ± 3	2879 ± 12	3167 ± 2	3455 ± 5	
10.2	61 ± 2	141 ± 2	244 ± 2	374 ± 2	531 ± 3	704 ± 0	899 ± 1	1107 ± 2	1333 ± 2	1569 ± 2	1816 ± 1	2075 ± 4	2340 ± 2	2609 ± 4	2892 ± 3	3176 ± 2	3460 ± 1	
15.3	61 ± 5	142 ± 4	245 ± 5	376 ± 5	531 ± 5	706 ± 6	899 ± 5	1111 ± 5	1337 ± 4	1575 ± 6	1822 ± 6	2083 ± 9	2346 ± 7	2617 ± 6	2897 ± 6	3184 ± 5	3471 ± 3	
23.0	66 ± 4	146 ± 3	251 ± 4	384 ± 3	538 ± 3	715 ± 3	910 ± 4	1121 ± 3	1349 ± 6	1588 ± 5	1831 ± 6	2094 ± 5	2361 ± 4	2630 ± 5	2908 ± 10	3199 ± 12	3498 ± 6	

Table 5: Resonance field, H_{res} for all Py/Ir samples in Oe. Columns are organized by the frequency. Rows are the Ir thickness in nm. For example, the H_{res} at 3GHz for the sample $t_{Ir}=4$ nm is 140 Oe.

Py/Cu/Ir	Linewidth [Oe]																	
	Frequency [GHz]																	
	2	3	4	5	6	7	8	9	10	11	12	13	14	15	16	17	18	
0.0	15 ± 0	20 ± 0	25 ± 0	30 ± 0	35 ± 0	41 ± 0	46 ± 0	52 ± 0	58 ± 0	67 ± 0	70 ± 5	76 ± 2	81 ± 0	87 ± 0	93 ± 0	99 ± 0	104 ± 0	
0.6	25 ± 0	32 ± 0	40 ± 0	49 ± 1	57 ± 1	67 ± 0	75 ± 3	83 ± 3	91 ± 1	100 ± 3	104 ± 7	119 ± 1	130 ± 2	134 ± 7	141 ± 2	151 ± 3	159 ± 1	
0.9	24 ± 2	32 ± 2	41 ± 1	50 ± 1	58 ± 2	65 ± 1	75 ± 2	80 ± 5	92 ± 2	103 ± 3	108 ± 5	121 ± 6	130 ± 4	138 ± 9	148 ± 10	160 ± 5	164 ± 4	
1.4	25 ± 1	34 ± 1	43 ± 2	51 ± 1	60 ± 1	71 ± 1	79 ± 2	88 ± 3	99 ± 4	108 ± 4	117 ± 5	127 ± 4	139 ± 8	150 ± 7	151 ± 6	165 ± 10	174 ± 6	
2.0	25 ± 1	32 ± 1	41 ± 1	49 ± 2	57 ± 0	66 ± 1	75 ± 4	87 ± 1	93 ± 2	104 ± 1	112 ± 1	122 ± 1	131 ± 2	139 ± 3	147 ± 3	157 ± 4	166 ± 1	
3.0	25 ± 1	33 ± 1	41 ± 1	49 ± 0	57 ± 1	67 ± 1	76 ± 2	84 ± 1	94 ± 2	103 ± 1	111 ± 2	121 ± 1	133 ± 2	141 ± 3	148 ± 2	159 ± 0	170 ± 1	
4.5	25 ± 1	32 ± 1	40 ± 1	48 ± 1	55 ± 0	66 ± 3	74 ± 1	85 ± 2	92 ± 4	104 ± 2	110 ± 7	114 ± 4	127 ± 8	141 ± 1	141 ± 7	155 ± 4	166 ± 3	
6.8	23 ± 0	31 ± 0	40 ± 0	48 ± 1	58 ± 2	68 ± 1	78 ± 3	88 ± 4	99 ± 3	109 ± 5	116 ± 7	126 ± 5	138 ± 9	147 ± 6	159 ± 10	168 ± 12	174 ± 11	
10.2	24 ± 1	32 ± 1	41 ± 1	48 ± 2	57 ± 1	68 ± 1	75 ± 3	82 ± 3	97 ± 2	102 ± 2	113 ± 3	123 ± 7	131 ± 4	142 ± 1	150 ± 4	162 ± 4	164 ± 2	
15.3	26 ± 0	33 ± 0	42 ± 0	49 ± 1	58 ± 0	66 ± 2	75 ± 1	86 ± 1	93 ± 1	104 ± 1	109 ± 2	122 ± 5	128 ± 3	142 ± 2	148 ± 2	160 ± 1	164 ± 9	
23.0	26 ± 1	34 ± 1	43 ± 0	51 ± 1	60 ± 0	71 ± 2	81 ± 1	89 ± 2	100 ± 3	109 ± 2	119 ± 4	128 ± 4	142 ± 5	149 ± 4	165 ± 7	171 ± 2	175 ± 1	
46.0	26 ± 0	33 ± 0	41 ± 0	49 ± 1	57 ± 0	66 ± 0	75 ± 1	84 ± 1	91 ± 0	103 ± 2	112 ± 2	121 ± 2	128 ± 6	145 ± 3	143 ± 6	157 ± 6	167 ± 10	

Table 6: Py/Cu/Ir spectrum linewidths in Oe. For example, the linewidth at $f=3$ GHz at thickness $t_{Ir}=0$ nm is 20 Oe with a standard deviation near 0 Oe.

Py/Ir	Linewidth [Oe]																
	Frequency [GHz]																
	2	3	4	5	6	7	8	9	10	11	12	13	14	15	16	17	18
Ir Thickness (nm)																	
0.4	36 ± 2	49 ± 5	60 ± 4	79 ± 4	89 ± 4	106 ± 3	124 ± 5	136 ± 3	146 ± 4	169 ± 6	178 ± 4	198 ± 3	209 ± 4	224 ± 6	238 ± 9	252 ± 7	270 ± 4
0.6	40 ± 1	51 ± 5	67 ± 9	79 ± 8	95 ± 7	108 ± 7	124 ± 7	139 ± 9	155 ± 8	171 ± 4	188 ± 9	204 ± 2	218 ± 8	230 ± 3	248 ± 7	266 ± 4	278 ± 7
0.9	40 ± 0	54 ± 5	69 ± 3	82 ± 4	98 ± 5	112 ± 4	126 ± 4	147 ± 5	161 ± 6	170 ± 6	186 ± 7	204 ± 3	218 ± 8	235 ± 9	249 ± 6	263 ± 9	279 ± 5
1.4	41 ± 1	56 ± 2	70 ± 2	85 ± 3	99 ± 2	111 ± 2	130 ± 2	147 ± 3	160 ± 2	173 ± 3	190 ± 3	204 ± 2	223 ± 3	239 ± 4	257 ± 4	266 ± 5	281 ± 6
2.0	43 ± 1	56 ± 4	71 ± 4	85 ± 4	100 ± 2	117 ± 4	135 ± 3	148 ± 3	163 ± 4	181 ± 3	199 ± 3	207 ± 3	225 ± 6	243 ± 6	255 ± 2	272 ± 6	285 ± 5
3.0	43 ± 3	56 ± 5	68 ± 5	84 ± 5	100 ± 6	117 ± 4	132 ± 7	147 ± 6	165 ± 7	175 ± 7	194 ± 7	213 ± 6	228 ± 10	240 ± 9	252 ± 8	266 ± 14	283 ± 13
4.5	44 ± 3	57 ± 2	71 ± 1	86 ± 1	102 ± 4	118 ± 2	130 ± 4	147 ± 4	166 ± 2	176 ± 3	195 ± 3	209 ± 2	229 ± 5	250 ± 4	265 ± 4	274 ± 4	290 ± 11
6.8	43 ± 1	57 ± 7	71 ± 5	84 ± 4	100 ± 0	115 ± 5	130 ± 0	143 ± 5	159 ± 0	176 ± 6	193 ± 1	207 ± 6	219 ± 2	239 ± 9	261 ± 3	267 ± 12	281 ± 2
10.2	42 ± 2	58 ± 2	72 ± 2	87 ± 2	101 ± 2	115 ± 3	129 ± 0	150 ± 1	164 ± 2	181 ± 2	194 ± 2	206 ± 1	228 ± 4	245 ± 2	254 ± 4	277 ± 3	293 ± 2
15.3	43 ± 2	56 ± 5	71 ± 4	84 ± 5	96 ± 5	113 ± 5	125 ± 6	144 ± 5	160 ± 5	174 ± 4	195 ± 6	214 ± 6	227 ± 9	240 ± 7	254 ± 6	266 ± 6	289 ± 5
23.0	41 ± 2	55 ± 4	72 ± 3	85 ± 4	98 ± 3	118 ± 3	132 ± 3	145 ± 4	164 ± 3	183 ± 6	192 ± 5	212 ± 6	231 ± 5	237 ± 4	256 ± 5	272 ± 10	298 ± 12

Table 7: Py/Ir spectrum linewidths in Oe. For example, the linewidth at $f=3\text{GHz}$ at thickness $t_{\text{Ir}}=4\text{nm}$ is 49 Oe with a standard deviation of 5Oe.

Gyromagnetic Ratio

The f - H_{res} response of each sample was fit to the Kittel equation to extract the gyromagnetic ratio (γ) and effective magnetization (M_{eff}). The Kittel equation was Eqn. 3 and discussed Section 2, repeated here for convenient reference:

Eqn. 3

$$f = \frac{\gamma}{2\pi} \sqrt{H_{\text{res}}(H_{\text{res}} + 4\pi M_{\text{eff}})}$$

With both γ and M_{eff} as free parameters, no evidence was found of γ changing between samples or sample types. The average value of γ when used as a fitting parameter was $29.4 \pm 0.2 \text{ GHz/T}$. This is also the value determined for γ for the Py standard. Consequently, γ was held constant at 29.4 GHz/T for all analyses presented here. Setting γ to a fixed value improves the confidence in the fitted M_{eff} values.

Using the relation:

Eqn. 8

$$\gamma = \frac{g\mu_B}{\hbar}$$

The γ found corresponds to a Landé g -factor of 2.10, where μ_B is the Bohr magnetron, and \hbar is the reduced Plank's constant. This value is consistent with other studies [23, 31].

Effective Magnetization

In-plane anisotropy evaluated using MOKE was found to be negligible in all samples (less than 1% change; this is a major advantage of using Py), and was thus excluded from our analysis. The Kittel fits were universally excellent.

M_{eff} of the control sample was found to be 7630 ± 35 G. This is comparable to Py samples of similar thickness. No appreciable dependence of M_{eff} on thickness for the Py/Cu/Ir samples was observed. However it was observed that, as shown in Figure 23, there is a trend of decreasing M_{eff} with Ir thickness for the Py/Ir samples. Neglecting the two thinnest Py/Ir samples ($t_{\text{Ir}} = 0.4$ and 0.6 nm), which had M_{eff} comparable to the Py control sample, the data are well fit to a decaying exponential that asymptotically approaches M_{eff} of the Py/Cu/Ir samples with a length scale of 18 ± 3 nm.

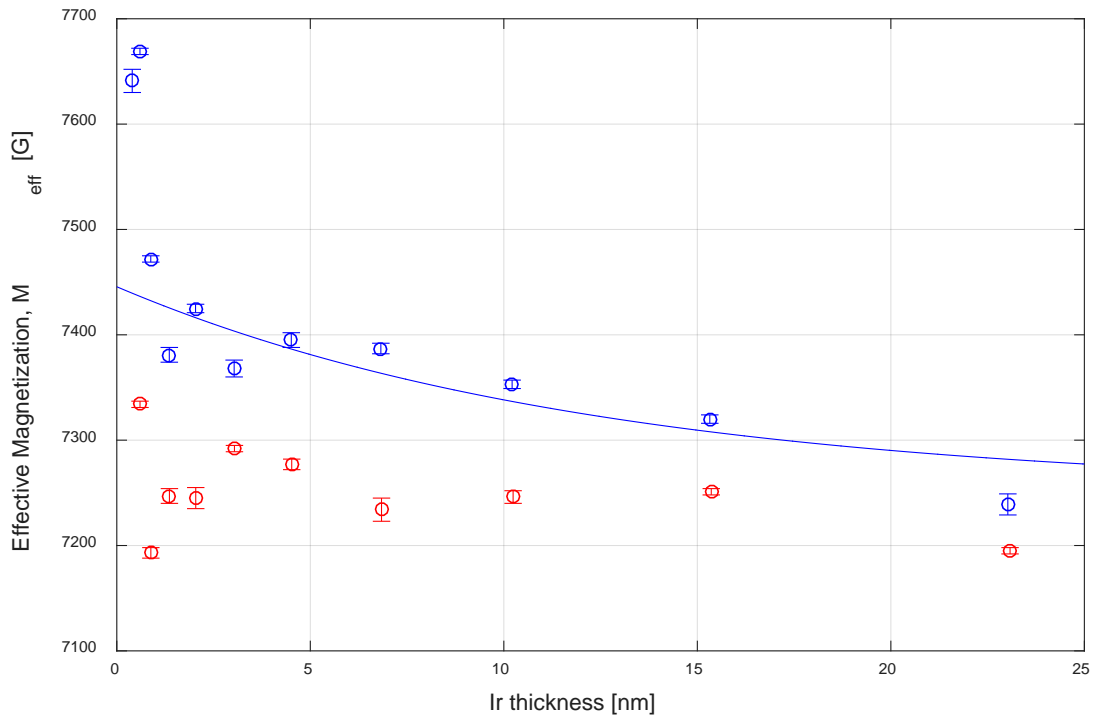


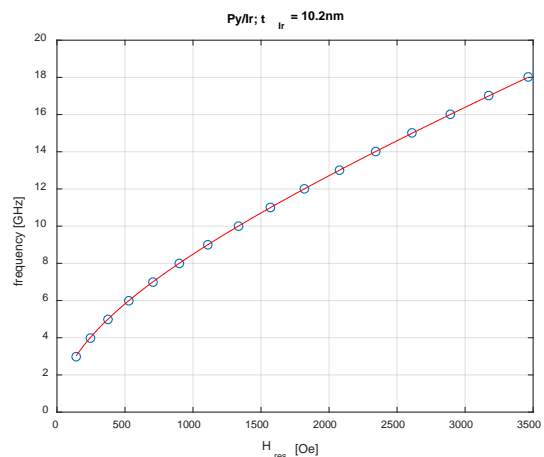
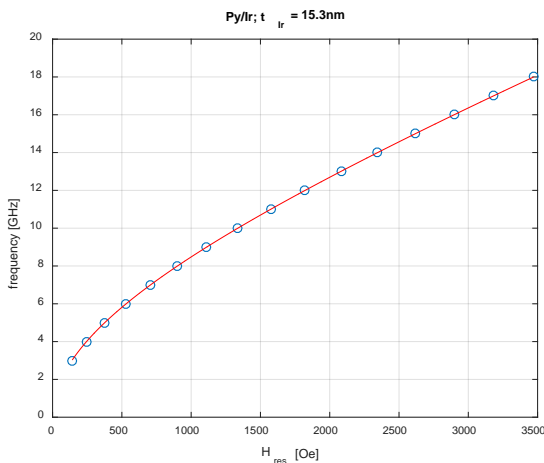
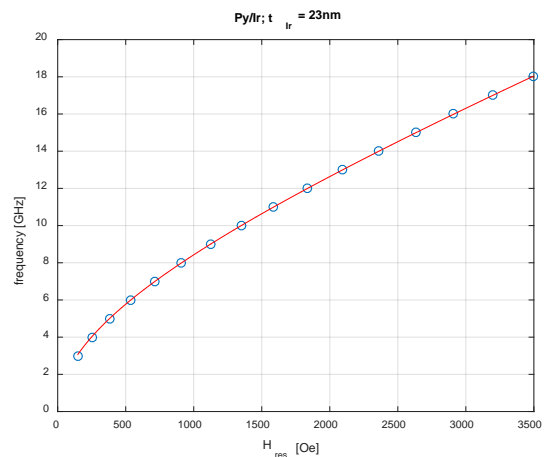
Figure 23: Effective magnetization, M_{eff} , vs. iridium thickness. No thickness dependence is observed for Py/Cu/Ir, but a dependence is observed for Py/Ir.

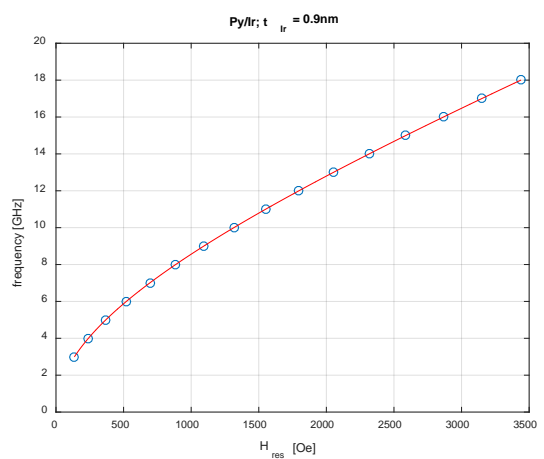
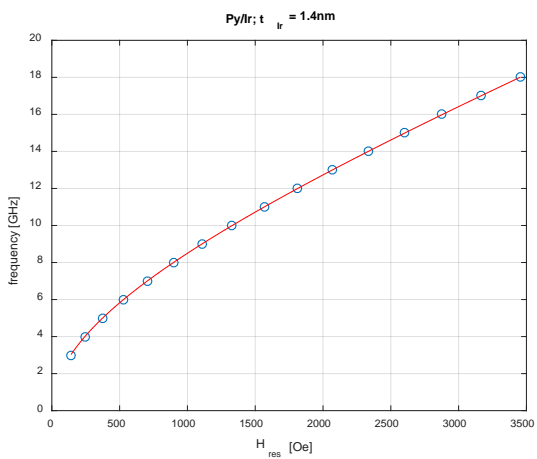
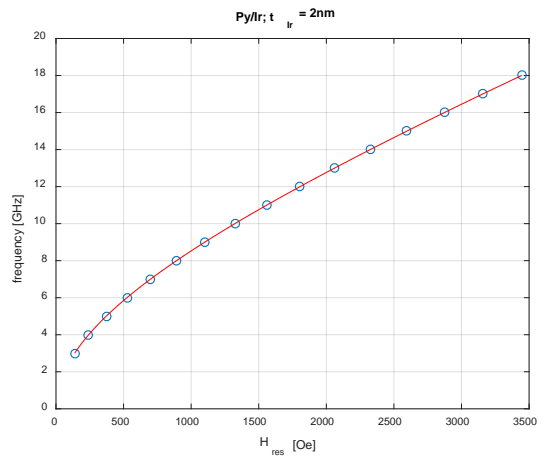
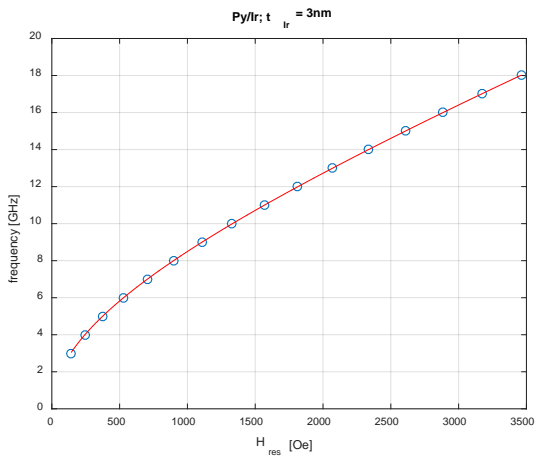
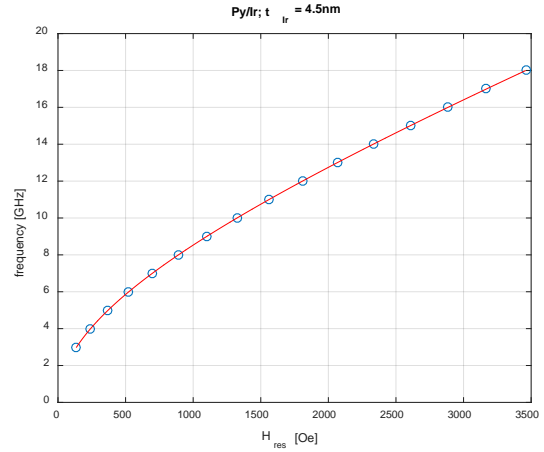
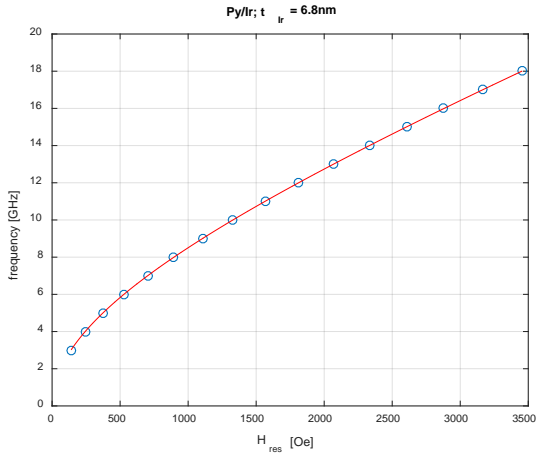
Together, these observations indicate a tunable, but minor, perpendicular magnetic anisotropy when Py is directly in contact with Ir. This means there is some component of the Py magnetization that would point along the surface normal in zero field, i.e., the magnetization in zero field would not lie perfectly in the plane of the sample. It has been shown that the capping layer can influence the perpendicular anisotropy of permalloy films and in cobalt bilayers [3] [32]. Tunable magnetic anisotropy is of high interest due to promising technological

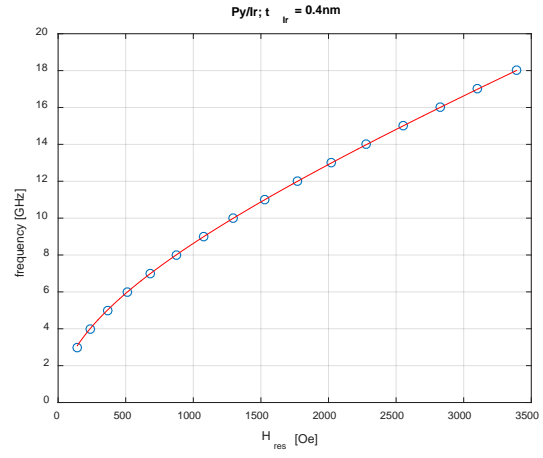
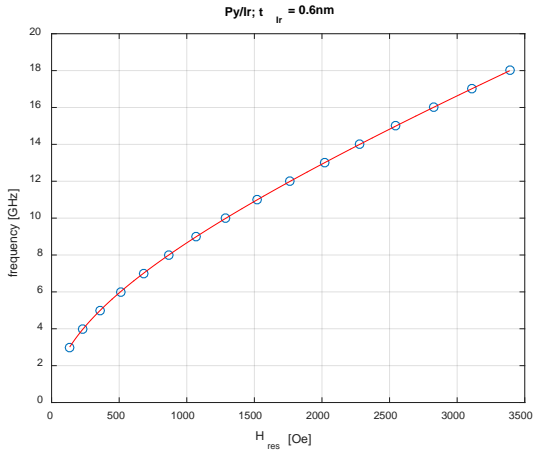
applications, because films with high-anisotropy can impart high thermal stability and low critical current for current induced magnetization and for current induced domain wall motion [33, 34]. The origin of the perpendicular anisotropy is induced from the anisotropy of the interfacial orbital angular momentum [3]. The non-magnetic heavy metal at the interface modifies the orbital angular momentum at the interface and increases the spin-orbit interaction [3]. For future work, the vibrating sample magnetometer will be excellent tool for investigating the perpendicular magnetic anisotropy [35]. It will be possible to orient the samples and obtain in-plane and out-of-plane effective magnetization.

Kittel Fits for all Py/Ir samples

Below are plots of the data and the Kittel fits for all Py/Ir samples. M_{eff} is the only fitting parameter. The error bars are not shown on the plots as the error bars are smaller than the data points. The standard deviations for H_{res} are shown on Table 5. The RF frequency, f , is accurate to $\pm 0.05\text{GHz}$.

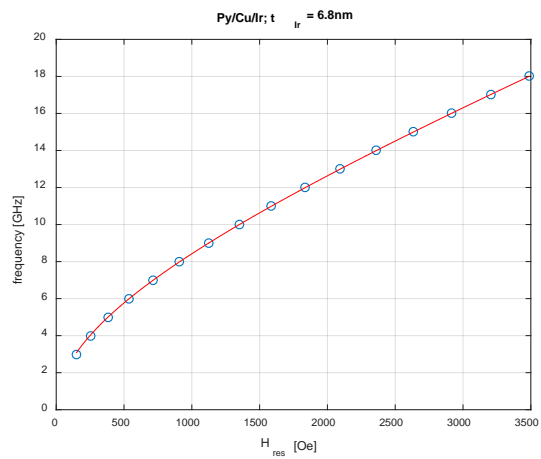
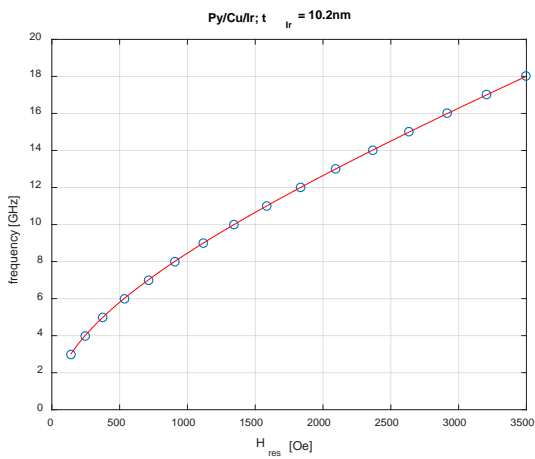
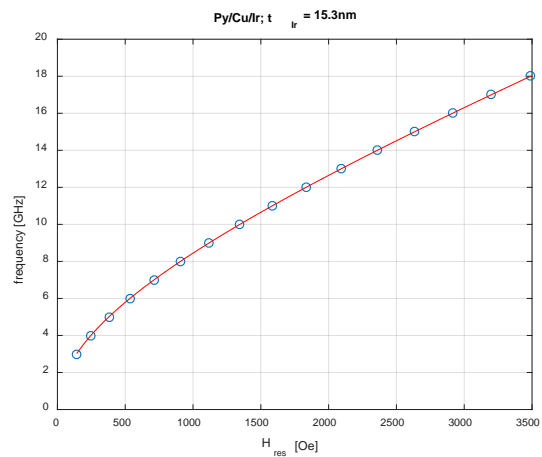
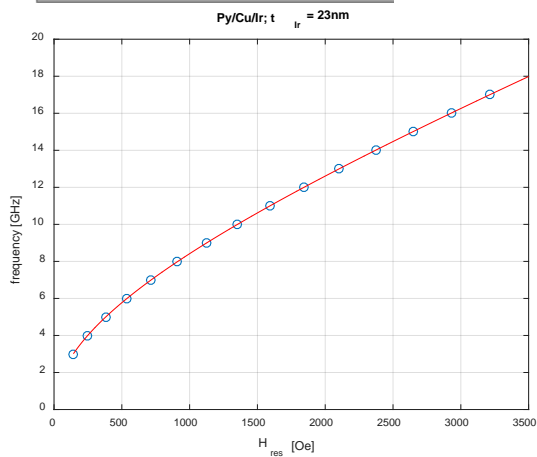
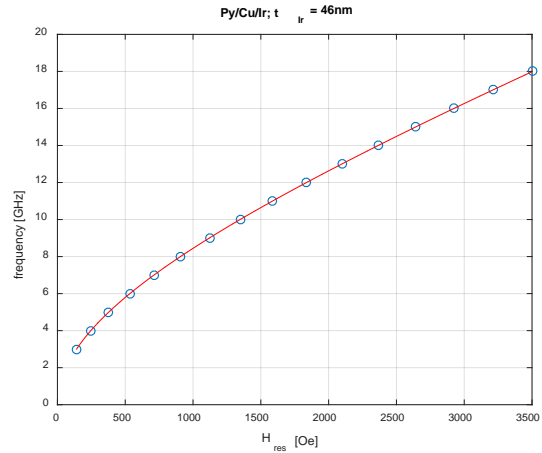
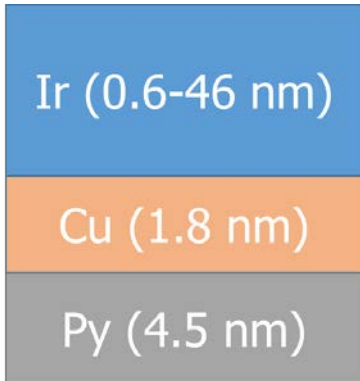


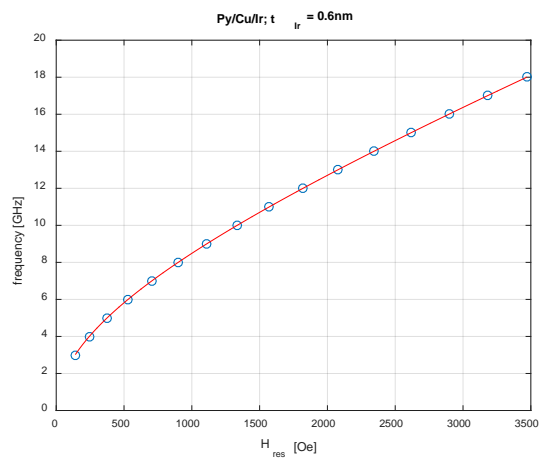
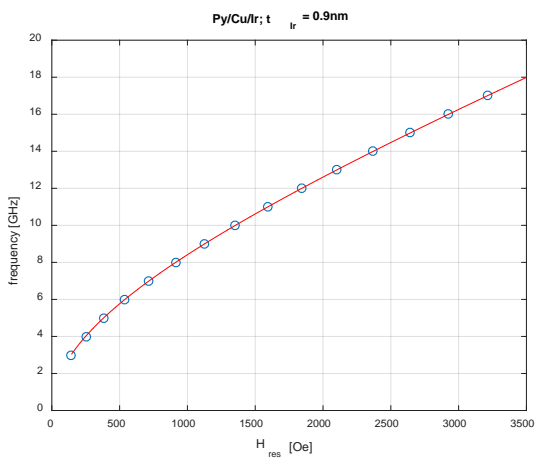
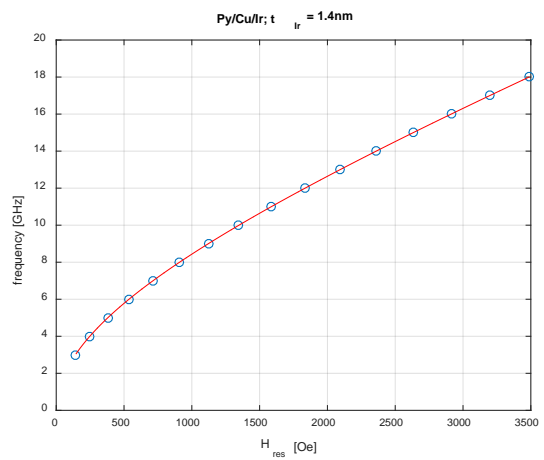
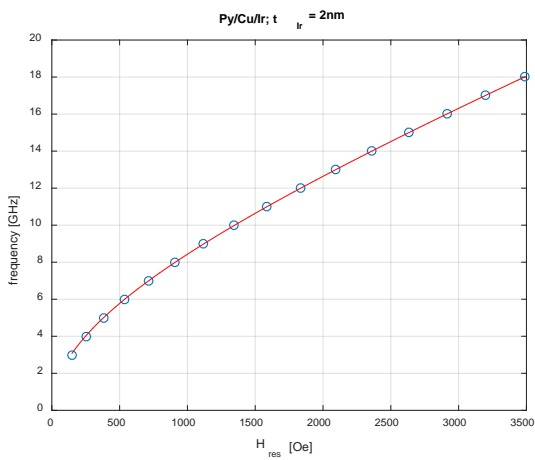
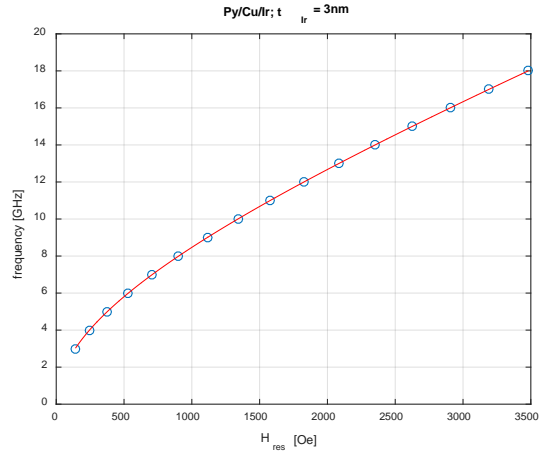
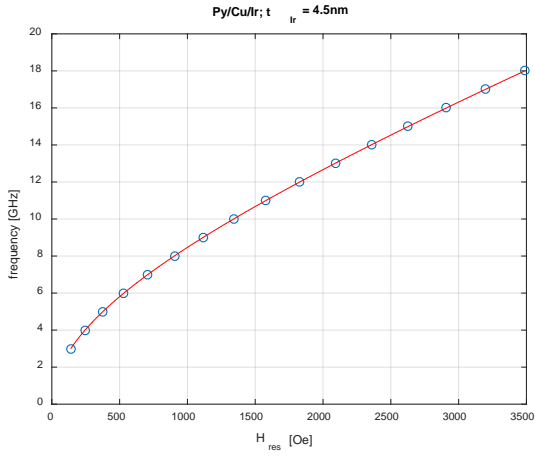




Kittel fits for all Py/Cu/Ir samples

Below are plots of the data and the Kittel fits for all Py/Cu/Ir samples. M_{eff} is the only fitting parameter. The error bars are not shown on the plots as the error bars are smaller than the data points. The standard deviations for H_{res} are shown on Table 5. The RF frequency, f , is accurate to $\pm 0.05\text{GHz}$.





Inhomogeneous Broadening

The inhomogeneous broadening, ΔH_0 , is the intercept parameter determined by fitting ΔH vs. f to a line [15, 22, 36]. As will be seen below, the Ir thickness had very little effect on the linewidth, and as a result, the data and fits shown in Figure 24 are representative of all the linewidth vs frequency results. The error bars shown are the standard deviation of 3-8 measurements per sample.

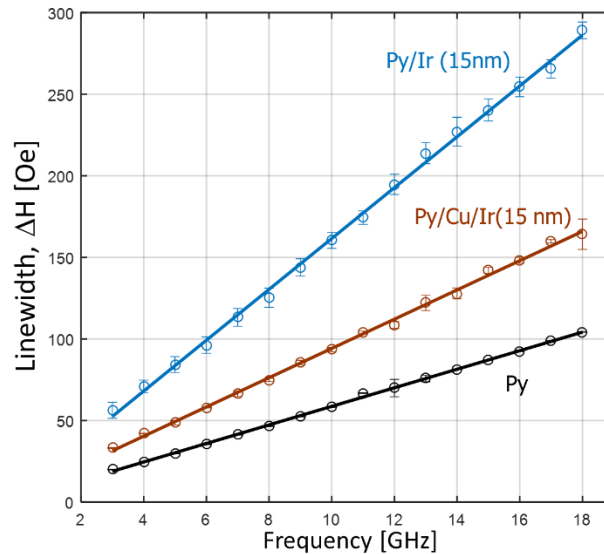


Figure 24: The ΔH vs. f for Py/Ir (blue), Py.Cu/Ir (copper), and the control (black); $t_{Ir}=15\text{nm}$ for both. A large increase in the slope for Py/Ir samples can be seen.

In our system, there may be a somewhat enhanced systematic inhomogeneous broadening because of geometrical factors (pole gap is about half the pole face diameter; samples were of the order 1 cm in a 3 cm gap). A fast study of measuring samples laterally along the CPW did not show any differences in the damping. The inhomogeneous broadening could be related to what is referred to as eddy-current damping and radiative damping. To minimize this effect, an insulating layer (Scotch® brand adhesive tape) is placed on top of the CPW [37]. Nevertheless, the control sample had a small but non-zero inhomogeneous broadening of 1.8 ± 0.6 Oe. It was found that the inhomogeneous broadening increased by nearly a factor of two when there is a direct Py-Ir interface. The average ΔH_0 for the Py/Cu/Ir samples was 3.7 ± 1.6 Oe compared to 6.9 ± 2.1 Oe for the Py/Ir samples; no Ir-thickness

dependence of ΔH_0 was observed for either sample type. Given that it was observed that different levels of broadening with and without the Py-Ir interface, the origin of the broadening is interfacial in nature, though the specific origin is not clear at this point. The larger ΔH_0 in Py/Ir could be structural in nature, given that the lattice mismatch between Py and Ir is 8.7% ($a_{\text{Py}} = 0.355 \text{ nm}$; $a_{\text{Ir}} = 0.389 \text{ nm}$), whereas it is only 1.7% for Py and Cu ($a_{\text{Cu}} = 0.361 \text{ nm}$). This could lead to different exchange strength distributions in the Py, e.g., through its thickness [38], which could affect broadening [39].

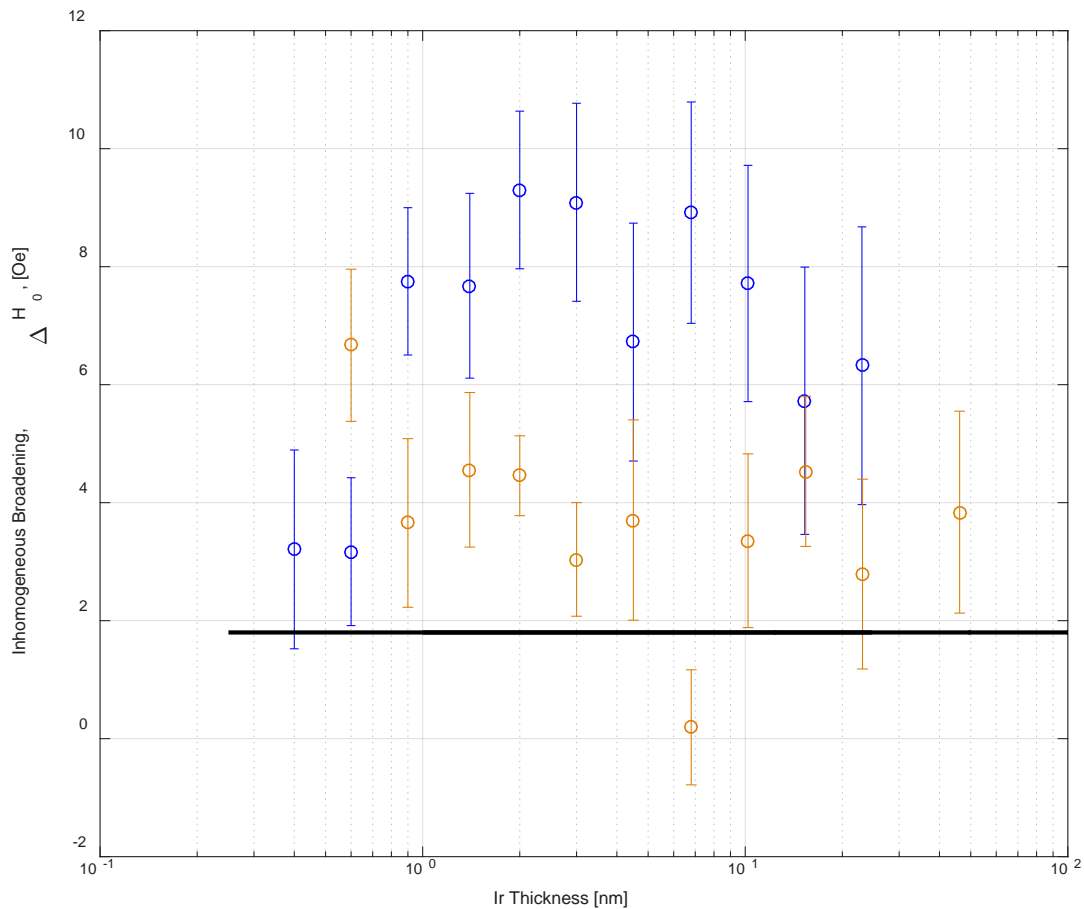


Figure 25: ΔH_0 vs. t_{Ir} , error bars come from the fit confidence. The ΔH_0 for Py/Cu/Ir is in orange and Py/Ir is in blue. The black line shows ΔH_0 for the Py standard. The x axis is on a log scale to make the data easier to see.

Gilbert Damping

The phenomenological Gilbert damping parameter, α , was determined by fitting ΔH vs. f [15, 22, 36]. The plots for ΔH vs. f with fits are shown. The error bars shown in the plots are the

standard deviation of 3-8 measurements per sample.

The linewidth of a resonance at a specific frequency gives information about the damping of the dynamic magnetic system. The linewidths observed for the control are comparable to Py of similar thicknesses in the literature. Relative to the control, adding Ir as a spin sink layer significantly increases the linewidth in Py/Cu/Ir and more drastically in Py/Ir. For a given frequency, the linewidths for Py/Cu/Ir and Py/Ir samples were larger than the control by factors of roughly 1.6 and 2.8, respectively. Relative to Py/Cu/Ir samples, the Py linewidth (and damping) is nearly twice as large when there is a direct Py-Ir interface. Similar behavior was seen in Py/Pt by Nan et al. [40], and Py/Pd and Py/Pt by Caminale et al. [24], both of which noted significant differences in linewidth when ultrathin Cu interlayers break the direct coupling between the Py and nominally nonmagnetic metals. Our results support those observations.

The damping parameter showed behavior commensurate with that of the linewidth. The Py standard had a damping parameter of 0.0084 ± 0.0001 . The asymptotic damping parameters, $\alpha(\infty)$, were measured to be $\alpha_{\text{Py/Cu/Ir}} = 0.0134 \pm 0.0006$ and $\alpha_{\text{Py/Ir}} = 0.0227 \pm 0.0004$. This indicates a spin-memory loss caused by the interface of Py and Ir. This observation of spin memory loss is consistent with observation made for other heavy metal interfaces [24, 25, 28, 22].

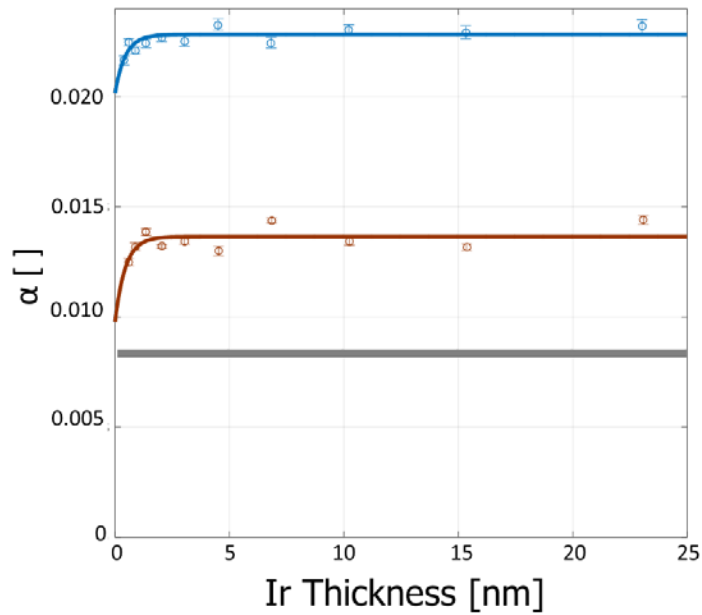
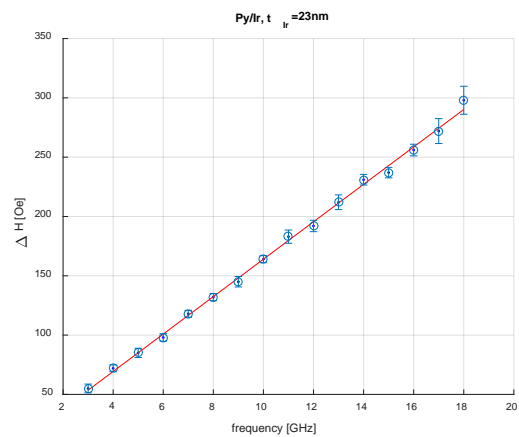
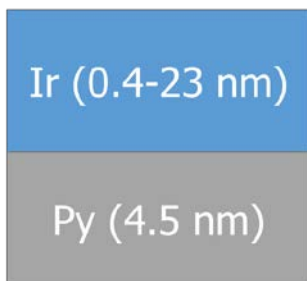
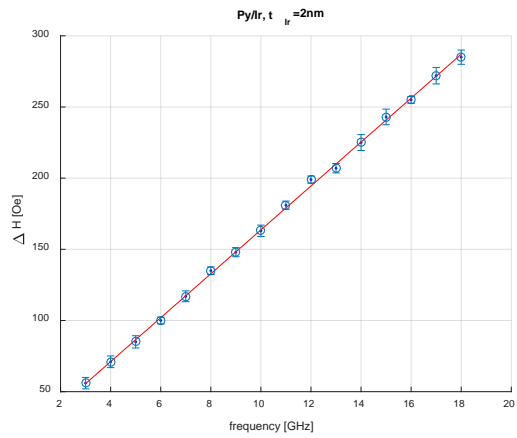
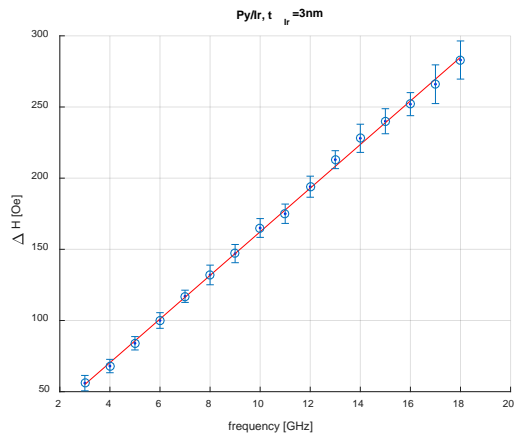
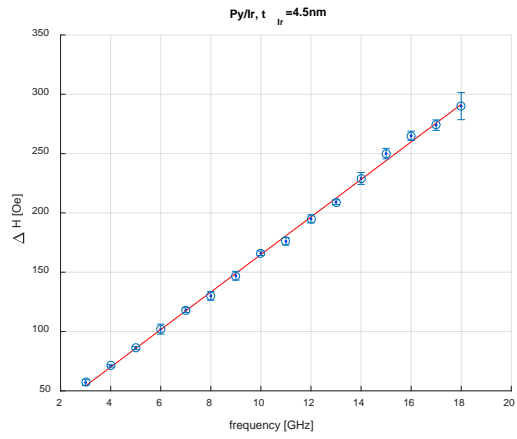
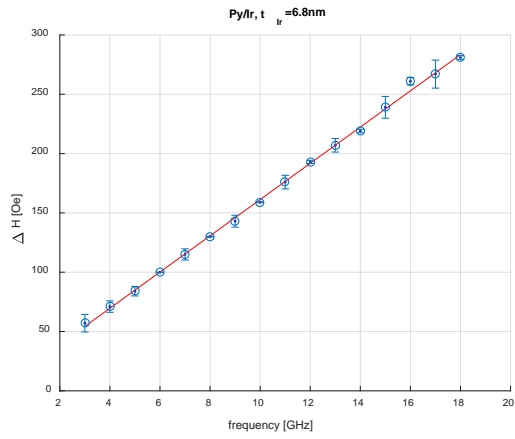
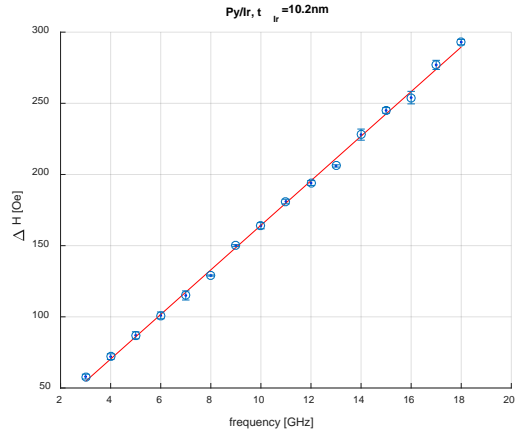
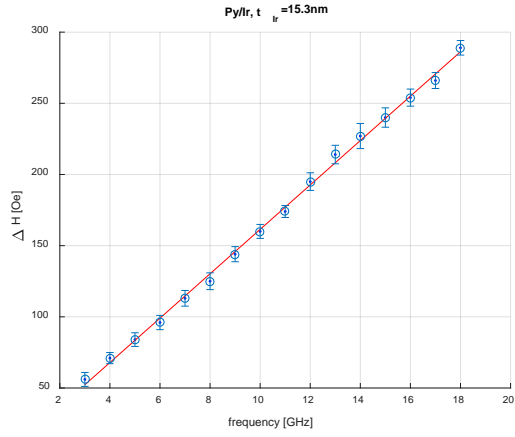


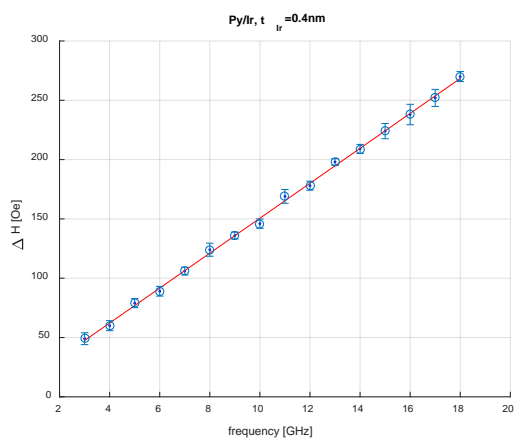
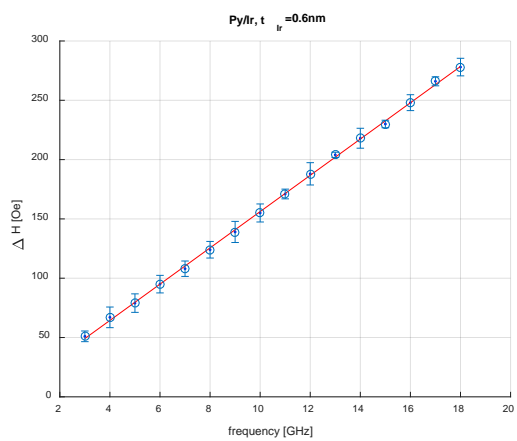
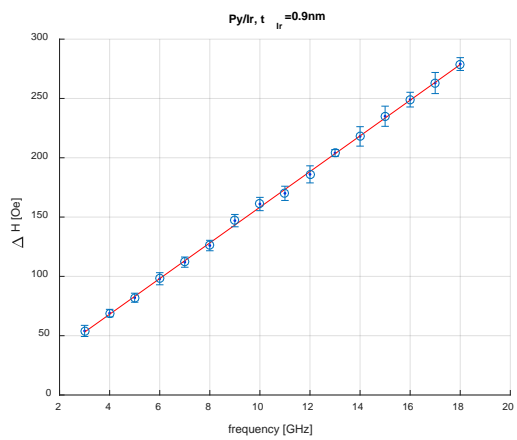
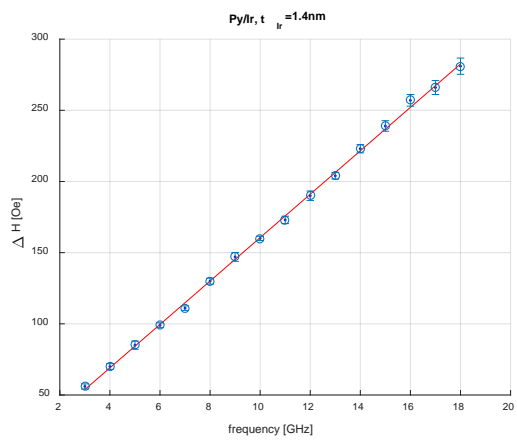
Figure 26: Gilbert damping parameter vs iridium thickness. As the iridium thickness increases alpha quickly saturates. The grey line is α for Py, 0.0084. The lines are fit using the characteristic length determined in the following section “Thickness Dependence of the Damping”.

Plots of ΔH vs. f for Py/Ir

Below are plots of the ΔH vs f data and the fits to Eqn. 3 for all Py/Ir samples. The error bars are from the standard deviation in averaging 3-8 measurements.

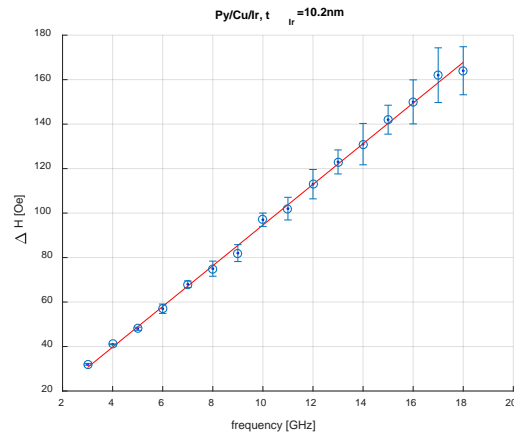
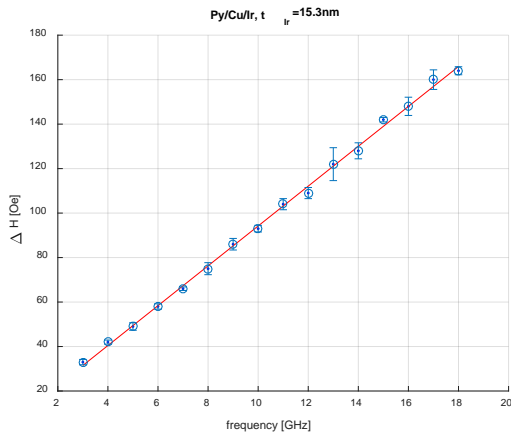
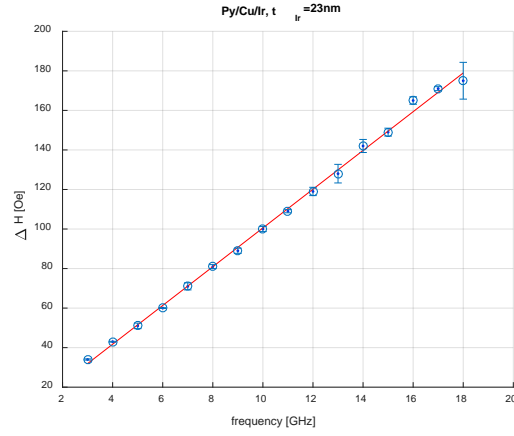
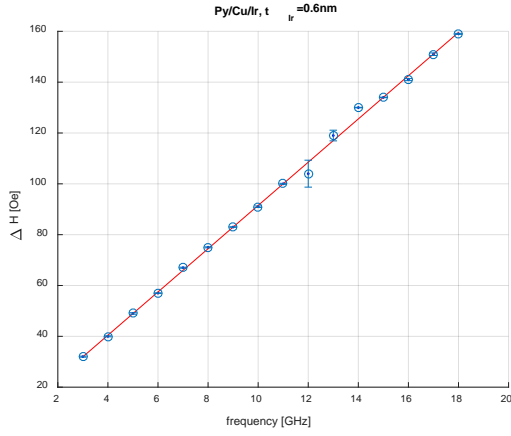
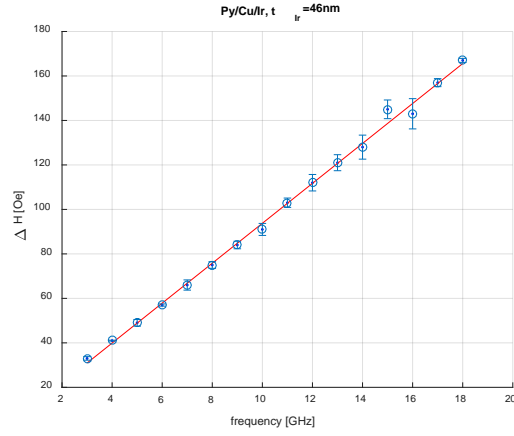
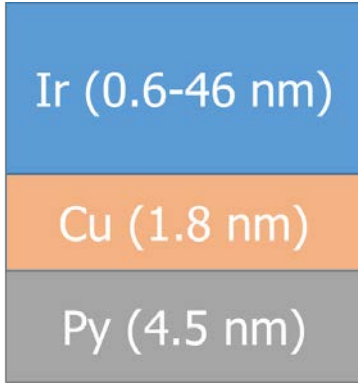


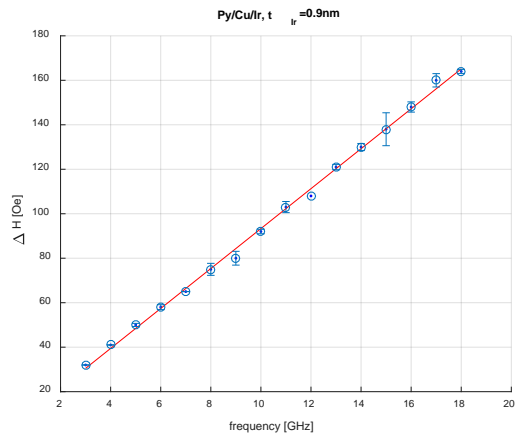
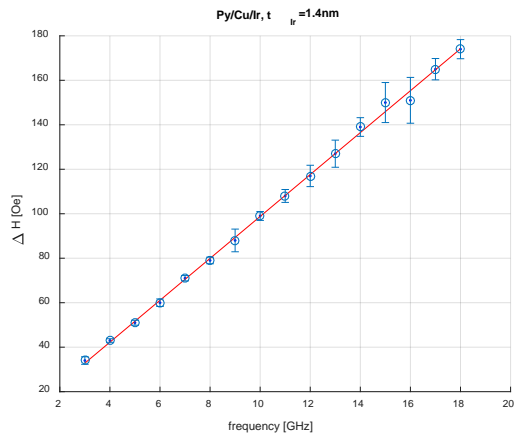
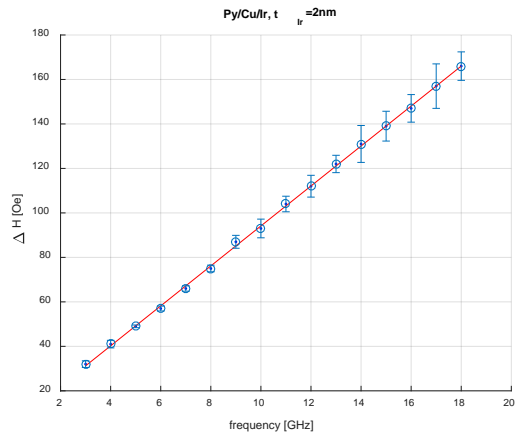
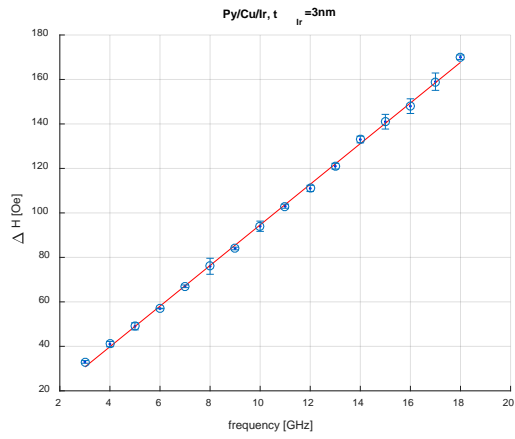
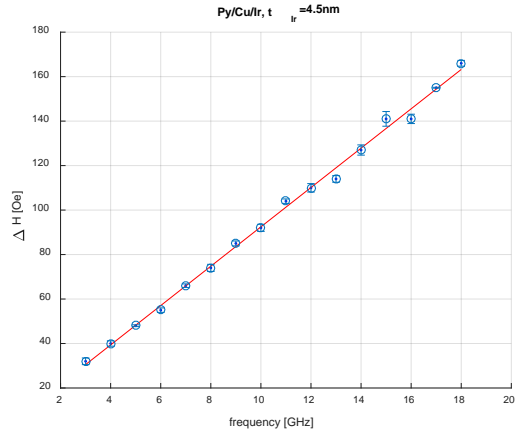
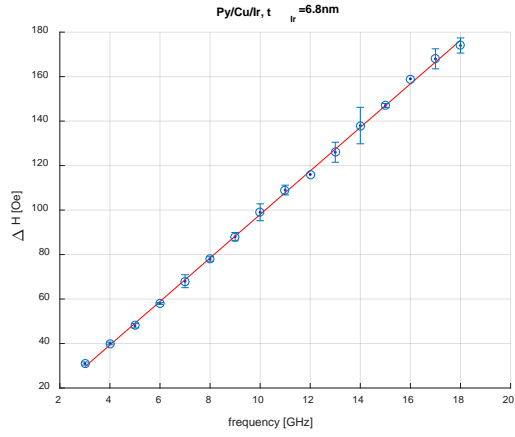




Plots of ΔH vs. f for Py/Cu/Ir

Below are plots of the ΔH vs f data and the fits to Eqn. 3 for all Py/Cu/Ir samples. The error bars are from the standard deviation of 3-8 measurements.





Thickness Dependence of the Damping

The standard procedure for evaluating the relationship between damping and thickness of a normal metal in a bilayer system is to fit an exponential decay function to α vs. t_{Ir} [23, 24]. When this was done with our data, the confidence in the fits was extremely low. In fact, statistical goodness of fit indicators, for example r-squared, are nearly the same for fitting to a constant value as to the exponential, meaning that it was unclear if there was a thickness dependence observed for the damping. Looking again at α vs. t_{Ir} in Figure 26, alpha quickly saturates as the iridium thickness increases. It appears there is a trend, but due to scatter in the data it was not possible to confidently obtain a characteristic length by fitting the data. To work around this, it was investigated if there was a thickness dependence observable in the linewidth, which is actually the more fundamental parameter because it is an input into the damping parameter calculation. Figure 27 shows ΔH vs. t_{Ir} for all frequencies measured. It appears that the linewidth decreases at very small iridium thickness consistently across frequencies.

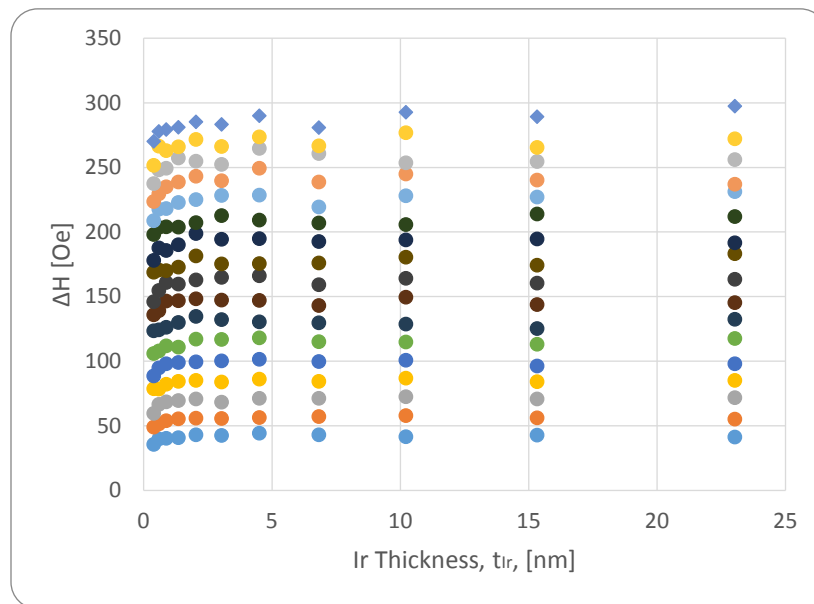


Figure 27: The ΔH vs. iridium thickness. Each color is a different frequency. The frequencies range from 18 (dark blue diamonds on top) down to 2 GHz (light blue, lowest points) in 1 GHz steps. A trend can be observed for all frequencies.

The fact that the trend is seen with linewidth makes sense; given the independence of the gyromagnetic ratio on Ir thickness, the linewidth is the fundamental parameter that can change in response to Ir thickness. As such, the fact that the linewidth is a function of the

frequency and the iridium thickness, $\Delta H = \Delta H(f, t_{Ir})$, was used to determine the impact of Ir thickness on the Py/Ir and Py/Cu/Ir sample sets. By fitting the thickness dependence of ΔH at constant frequency to

Eqn. 9

$$\Delta H(f, t_{Ir}) = \Delta H_f(\infty) - B_f e^{-(t_{Ir}/\lambda_f)}$$

$\Delta H_f(\infty)$ was obtained for each frequency, where $\Delta H_f(\infty)$ is the asymptotic linewidth at large thickness, t_{Ir} is the iridium thickness, and B_f and λ_f are fitting parameters. By dividing each frequency by its respective $\Delta H_f(\infty)$, a family of normalized constant-frequency curves were created that asymptotically approach unity. These data were then averaged across frequency (3-18 GHz) for each t_{Ir} to produce Figure 28 where the points are averages, error bars are standard deviations, and the line is a fit to:

Eqn. 10

$$\Delta H_{norm} = A - B e^{-(t_{Ir}/\lambda)}$$

where ΔH_{norm} is the average-normalized linewidth, A and B are fitting parameters, t_{Ir} is the iridium thickness, and λ is the characteristic length of iridium.

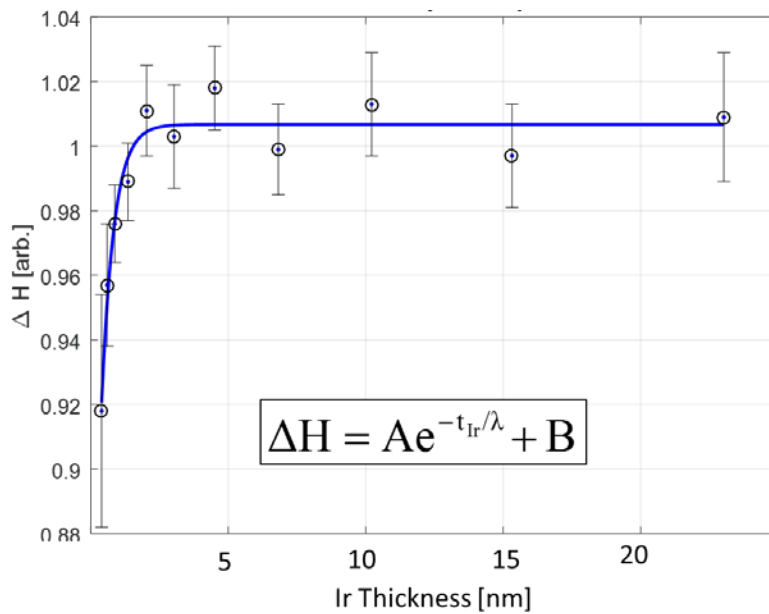


Figure 28: The ΔH were normalized and averaged across frequencies. A clear trend is now seen for ΔH vs. t_{Ir} .

While this approach is not fundamentally different from fitting the thickness dependence of the damping parameter, there is greater confidence in the resulting length scale because of the averaging across frequencies reduces fluctuations that affect the thickness dependence. The main parameter of interest is λ , which was found to be $0.5 \pm 0.1\text{nm}$ for the Py/Ir samples. Independent fits of $\alpha(t_{\text{Ir}})$ to $\alpha(\infty)\text{-Bexp}(t_{\text{Ir}}/\lambda)$ did not reveal a different length scale than the ΔH analysis above, but the fits yielded significantly lower confidence in the extracted parameters. Figure 26 shows that the 0.5nm length scale yields good fits for the thickness dependence of α .

The thickness dependence of the linewidth for Py/Cu/Ir was less clear as can be seen in Figure 29. This may be partly caused by the fact that the sample set for Py/Ir contains a sample with $t_{\text{Ir}}=0.4$ while the thinnest iridium layer for the Py/Cu/Ir samples is $t_{\text{Ir}}=0.6$ nm. Another possibility is that there is a relation to the proximity effect. The proximity effect refers to a phenomenon where the non-magnetic metal (Ir) becomes effectively ferromagnetic on the interfacial atoms. It is known that Pd and Pt when placed in contact with a ferromagnet (like Py) have a magnetic moment induced at the interface [24]. The role of the proximity effect on spin transport properties is still under debate.

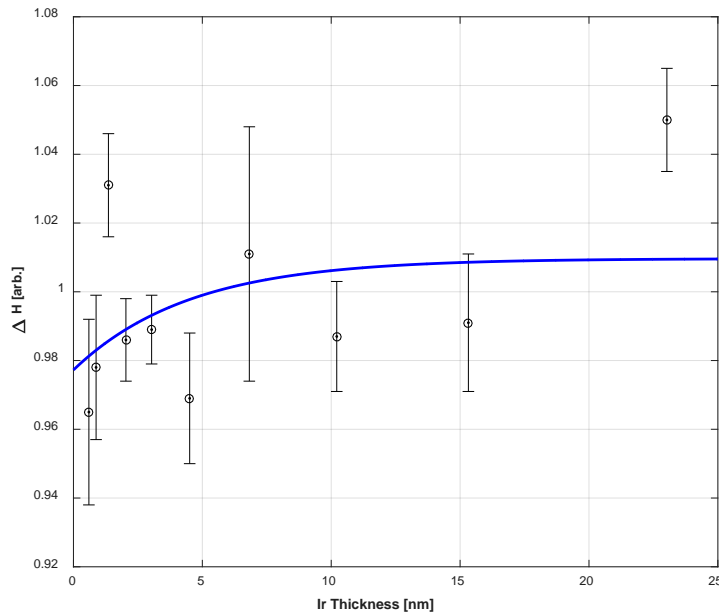


Figure 29: For ΔH vs. t_{Ir} for Py/Cu/Ir no thickness dependence is observed. This data were created by normalizing the linewidths as was done for Py/Ir in Figure 28.

Spin Mixing Conductance

The quantity g_{eff} describes the total spin current dissipated from the Py. g_{eff} is of interest in spintronics because it is an indicator at how efficiently a metal destroys a spin current. The enhancement of the Gilbert damping parameter relative to the control gives an estimate of the effective spin mixing conductance, g_{eff} , with the relation:

Eqn. 11

$$\Delta\alpha = \alpha_x - \alpha_{\text{Py}} = \frac{g \mu_B}{4\pi M_{\text{eff}} t_{\text{Py}} g_{\text{eff}}}$$

where α_x is the asymptotic damping parameter (α_{∞}) for Py/Ir or Py/Cu/Ir and α_{Py} is the measured alpha value of the Py control, $4\pi M_{\text{eff}}$ is the magnetization of Py, t_{Py} is the Py thickness, and g is the Landé g -factor [23, 24]. The values of g_{eff} were found to be $8.8 \pm 0.3 \text{ nm}^{-2}$ for Py/Cu/Ir, and $25.2 \pm 0.5 \text{ nm}^{-2}$ for the Py/Ir samples. These are comparable to the spin mixing conductance's with and without Cu spacers found for similar structures with Pd ($7.5, 14 \text{ nm}^{-2}$) and Pt ($8.3, 32 \text{ nm}^{-2}$) [24, 25]. Other measurements, namely the inverse spin hall effect voltage (ISHE), are needed to determine the efficiency with which the spin current is converted to a charge current (called Hall angle) [1, 23, 30].

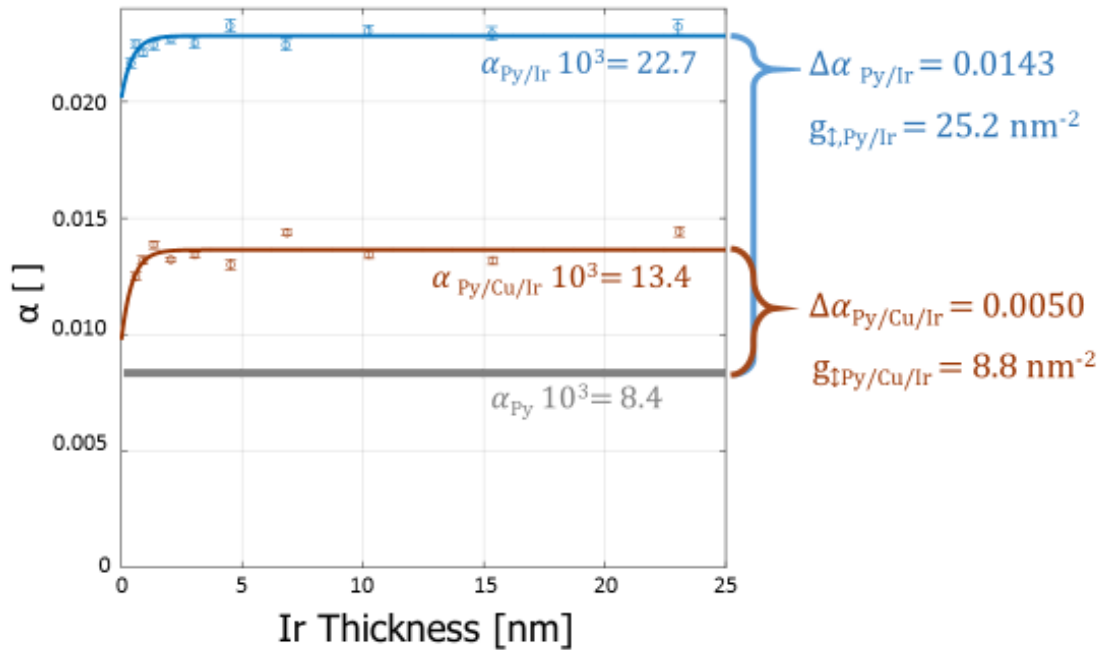


Figure 30: The damping enhancement is used to determine the effective spin mixing conductance, g_{eff} . Note that the fit lines are showing the characteristic length found for the linewidth dependency on thickness shown in Figure 28.

The ratio of g_{eff} for Py/Ir to Py/Cu/Ir falls between the values observed for similar structures of Pd and Pt.

The ratio of g_{eff} was found observed in our work (Py, Ir) to be 2.9; Caminale *et al.* observed the ratio using Py and Pd to be 1.9. Caminale *et al.* also observed the ratio using Py and Pt and found the ratio to be 3.9. Rojas-Sanchez *et al.* measured the ratio to be 2.0 in a Co-Pt system [23, 24].

The enhancement of g_{eff} may originate from at least two possible situations. First, the interface with Ir may be such a large spin sink itself that any spin current impinging upon it is destroyed. Second, we could be seeing a proximity effect in which the Ir is becoming polarized via direct exchange with the Py. In this situation, the thickness dependence is not related necessarily to the spin diffusion length of the Ir, but rather the $1/t$ dependence of any proximity effect. An X-ray magnetic circular dichroism (XMCD) study of the Ir at the Py/Ir interface should inform this debate, as it has with the Pt [41] and Pd [24].

Conclusion

A procedure was successfully developed to effectively evaluate spin pumping in the thin film multilayers Py/Ir and Py/Cu/Ir as a function of iridium thickness using ferromagnetic resonance spectroscopy (FMR). The gyromagnetic ratio, γ , was determined to be 29.4 ± 0.2 GHz/T, and no evidence was found that it is different for any samples. The effective magnetization, M_{eff} , showed a dependence on the thickness of the Ir layer for the Py/Ir samples. This is likely caused by induced perpendicular magnetic anisotropy. The damping showed a dependence on iridium thickness with a characteristic length of approximately 0.5 ± 0.1 nm for the Py/Ir samples. This thickness dependence was not observed for the Py/Cu/Ir. This leads us to believe that the cause is related to the proximity effect. The average inhomogeneous broadening ΔH_0 for the Py/Cu/Ir samples was 3.7 ± 1.6 Oe compared to 6.9 ± 2.1 Oe for the Py/Ir samples. The Py standard had a damping parameter of 0.0084 ± 0.0001 . For thick iridium layers, the Gilbert damping parameters were measured to be $\alpha = 0.0134 \pm 0.0006$ and $\alpha = 0.0227 \pm 0.0004$ for Py/Cu/Ir and Py/Ir respectively. This indicates the presence of spin memory loss at the Py-Ir interface. This also may be related to the proximity effect. The spin

mixing conductance, g_{eff} , was found to be $8.8 \pm 0.3 \text{ nm}^{-2}$ for Py/Cu/Ir, and $25.2 \pm 0.5 \text{ nm}^{-2}$ for the Py/Ir samples. This is comparable to observations made for permalloy multilayers of Pd and Pt.

Interpretation and Future Work

The original interpretation of the SML in the field was that spin currents destroyed by the interface are no longer available in the normal metal for conversion to a charge current. In our case, this rationale would imply that having a direct interface between Py and Ir would cause the conversion efficiency from spin current to charge current through the Inverse Spin Hall Effect to be significantly reduced; these measurements are future work. An observation made by Rojas-Sánchez et al. shows that this interpretation may be incorrect (though they did not state that in their publication). In addition to FMR measurements, they took measurements of the ISHE (the charge current generated from transverse to the spin-current) for Co/Pt vs. Co/Cu/Pt multilayers. They observed the same sort of increase in the damping for the direct interface samples as we did, but they measure an increase in the current generated for the direct interface samples compared to the FM/Cu/NM samples. This means there is higher conversion from spin current to charge current for the direct interface samples, contrary to the original logic. The interpretation that the interface destroys the spin current is still correct (otherwise there would be no difference in damping), but insufficient: it fails to explain why the absolute charge current in the Co/Pt samples exceeds that of the Co/Cu/Pt samples. A major potential explanation for this discrepancy could be that the Pt becomes magnetic via proximity effect with the ferromagnet (as in Caminale et al.), which means one really should not compare the two samples with respect to charge current generated. In our samples, where Ir is not likely to be affected by proximity effects, we would expect lower charge current for the Py/Ir samples than the Py/Cu/Ir. However, if the spins destroyed at the interface can actually participate in ISHE to create a charge current, it may be possible to increase the spin-to-charge current efficiency by adding additional interfaces. An experiment to test this would compare the damping of Py/Cu/Ir to Py/[Cu/Ir] n , where the subscript n indicates that the top is comprised of n Cu/Ir bilayers. A specific hypothesis is that damping and ISHE signal in Py/[Cu(2)/Ir(2)] 5 would be greater than those in Py/Cu(2)/Ir(10nm). This would be significant because the Cu spacers should be transparent to spin currents, so both heterostructures should have the same impact on damping and ISHE because they have the same total thickness of

iridium.

Rojas-Sánchez observed that the spin current is absorbed over a length scale that is almost double that observed for the enhancement of the damping, and that this length scale is the same for the Co/Pt and Co/Cu/Pt samples. The standard approach to bilayers predicted that damping should scale with the spin current absorption. If the spin pumping is viewed as an analogy to a water pump, (where whatever happens to the flow of the water downstream does not affect the operation of the pump) then it is easy to understand why the length scale of the damping is different than the length scale of the charge generation: the spins destroyed in the normal metal will not impact the damping. But the modern interpretation of spin pumping is compared to holding a jump rope (when rotating the jump rope, anything impacting the rope will be felt by the person rotating it). Therefore we should expect to see a direct correlation for the charge current to the damping: spins destroyed in the normal metal would increase the damping. The different length scales may be related to proximity effect. If this is true then metals that do not experience the proximity effect would show the same length scale dependence for the charge current generation and the damping. Gold is one of these metals. The length scale for Au layers have been observed to be the same for damping and for the spin current generation [42]. This does suggest that the different length scales are caused by the proximity effect. By including current measurements with Py/Ir bilayers and comparing the length scales of the damping and current generation, we could see if the proximity effect is playing a role in the damping.

X-ray magnetic circular dichroism (XMCD) measurements could be done To directly observe the proximity effect and see if it is occurring on the Py-Ir interface. XMCD is an element sensitive technique and allows quantification of proximity induced magnetization. From the observations in this study, it is predicted that the further measurements would be consistent with the proximity effects observed in Pt bilayers [24]. The magnitude of the induced magnetism in the proximity effect and the extent of its role in spin memory loss is a current debate [3]. Taking XMCD measurements could inform this debate. Also, investigating thin films with terbium as the normal metal could provide more interesting data on the role of the proximity effect, as Tb has substantially different magnetic properties than Ir, Pt, and Pd. XMCD

measurements would require measurement time at a national laboratory. A more immediately available option for future work is to directly observe the magnetic perpendicular anisotropy using the vibrating sample magnetometer. Another future work could be to include Spin Hall voltage measurements across the samples during the FMR measurements. Including spin Hall measurements in the laboratory's repertoire is very feasible and would be a great asset for more completely describing any multilayer thin film samples.

Section 4: Acknowledgments

I extend a sincere thank you to my advisor Dr. Casey Miller for all of his guidance and for the opportunity to be a part of this fascinating research.

Thank you Dr. Linda Barton, Dr. Joseph Hornak, and Dr. Steve Weinstein for being on my thesis committee.

Thank you Dr. Michael Pierce for your help with XRR and encouraging conversations. Jeffery Lonevill was extremely helpful for tricky soldering problems. Jan Maneti in the mechanical engineering shop was very efficient with his CNC work.

Most importantly, I thank my wife Kelly Hatton.

It has been a life goal to contribute to the common body of knowledge after reading the *Foundation Series* when I was 12. This research may be a minuscule contribution, but the challenge it has provided me has been extremely fulfilling. I have gained a tremendous amount from this experience, and I am filled with gratitude.

This research was supported by NSF Grant 1515677.

Section 5: Appendix

FMR Measurements: A Guide for Future Users

This section is intended as a guide to future users on the best practices for taking FMR measurements.

Prior to taking any measurements it is recommended to set up a measurement procedure that will allow efficiency and prevent errors. Planning the procedure should include creating a table of all samples to be made and a brief description of how measurements are to be completed. The description should be detailed enough that another person could complete your measurements by reading the description alone. By following a table, there should no need to make decisions about the experiment while taking measurements.

It is very important to have systems in place that prevent switching, misplacing, or mislabeling a sample. It is recommended to keep a designated spot next to the NanOsc Instrument where the case is placed when its respective sample is on the CPW.

The steps for measurements are:

1. Review the last measurement made. (This is to check there are no errors in the system or that the settings for the sweeps need to be adjusted)
2. Remove sample from CPW and immediately place in correct case and location using carbon tipped tweezers. (Critical: the NanOsc hardware is extremely sensitive to static electricity. Keep the tweezers attached to a grounding wire to prevent a discharge on the CPW that could damage the system (this has happened before).
3. Place the measured sample in its case and place where samples are stored.
4. Place new sample on CPW and place its case in the designated spot (A person walking into the lab needs to be able to identify what sample is sitting on the CPW. Do not leave any case near the FMR except for the current sample case).
5. Change file name in software.
6. Check the file directory.
7. Press start to initiate measurements.
8. Write the date, time, and initials into the checklist table.

Sample Preparation

Samples that are deposited on large “coupons” of oxidized Si(001) wafers or glass slides will need to be cleaved in order to fit on the CPW. The samples must be less than 2 cm along one dimension to fit on a portion of the CPW that is parallel to the applied field. To cut the samples, powder-free gloves and safety glasses are worn. In a designated hood, the samples

are placed on a chemwipe. A tungsten carbide blade (do not use iron or other ferromagnetic tool with any samples) is pressed on the far edges of the sample. A clean cut usually propagates (cleaves) a clean crack along the crystal's easy orientation. Be careful and take precautions against flying shards of the sample. It is recommended that a person practice on other films before trying to cleave samples. Another option is to use a diamond tip or other cutting tool to etch lines on the surface to guide fracturing. All the sections of the samples are returned to the same sample case. In the end, the samples should be about 1 cm in length; the width just needs to cover the entire CPW, which means about 1 mm is sufficient (the CPW center conductor is 0.2 mm wide).

Raw data files

Measurements made on the NanOsc FMR system are written to log files with time and date stamps appended to the sample name. The directory where these files are saved is an option on the sweep table set up page. It is recommended to save all measurements in a single directory, and religiously follow a checklist when taking measurements to prevent mislabeling measurements. The heading of the log files contain the sweep settings that were used for a measurement. If anomalies are observed in measurements or if settings that were used need to be retrieved, the log files can serve as a first reference.

Process Data

There are two Matlab functions to process the FMR measurements. The first is called `FMR_spectrum.m`. The input for `FMR_spectrum.m` is the folder that contains the measurement log files. The output is a table of the fitting parameters, most importantly, H_{res} and ΔH . The table output from `FMR_spectrum.m` can be opened with most any data handling software, including excel.

As discussed in the section on FMR Theory H_{res} and ΔH are fit vs. f to well-known equations in order to determine the parameters M_{eff} , γ , α , and ΔH_0 . The fitting of these parameters are done with the Matlab function `FMR_results.m`. The input of this function is simply the output of `FMR_spectrum.m`. Prior to calculating the parameters it is important to clean the H_{res} and ΔH data by removing outliers and mismeasurements. In addition to finding erroneous data, reviewing and finding trends in the H_{res} and ΔH can be very helpful in the analysis.

Matlab Tools for Processing FMR Data

Quick Start Guide

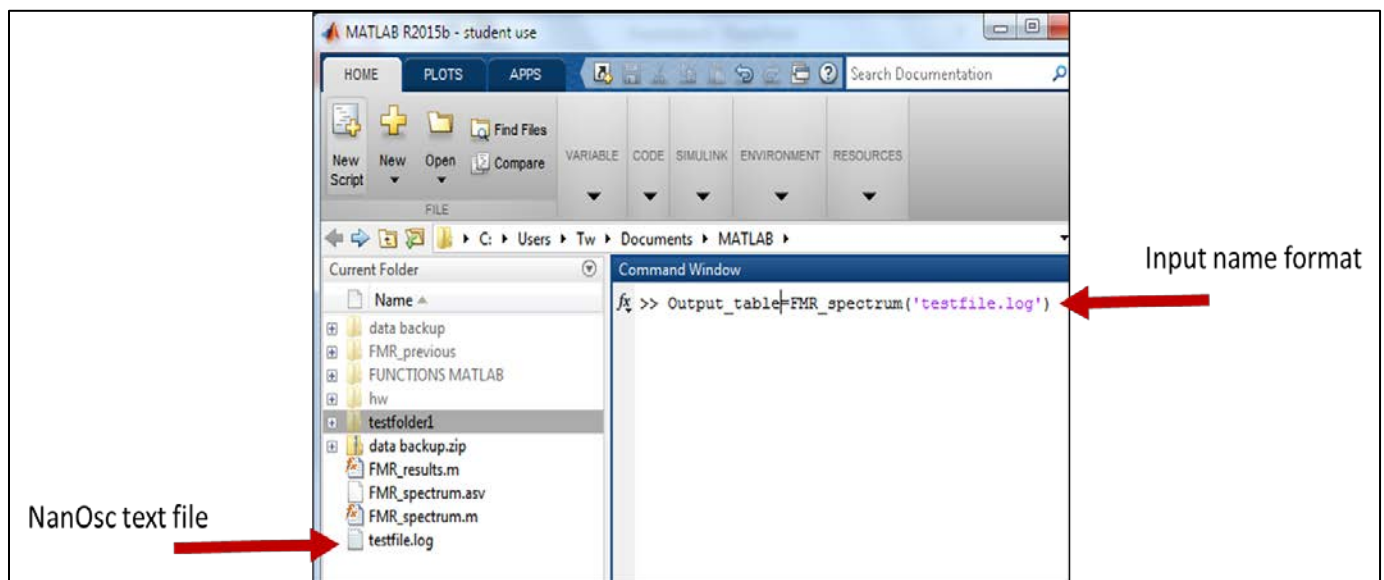
I have created Matlab code to process the text files that are created by NanOsc FMR software. There are two Matlab functions, **FMR_results.m** and **FMR_spectrum.m**.

FMR_spectrum reads the text files created by NanOsc and saves the resonance fields and linewidths into a table. The input can be an individual text file or a folder with any number of text files. Enter the input as the file name or folder name if it is in the current working directory. If the files are not in the current directory, you can enter the directory of the NanOsc files as the input. The output table is automatically saved as a text file in the current directory. The table is also saved in the Matlab workspace. The output table is saved as comma separated file and can easily be opened by excel or other software.

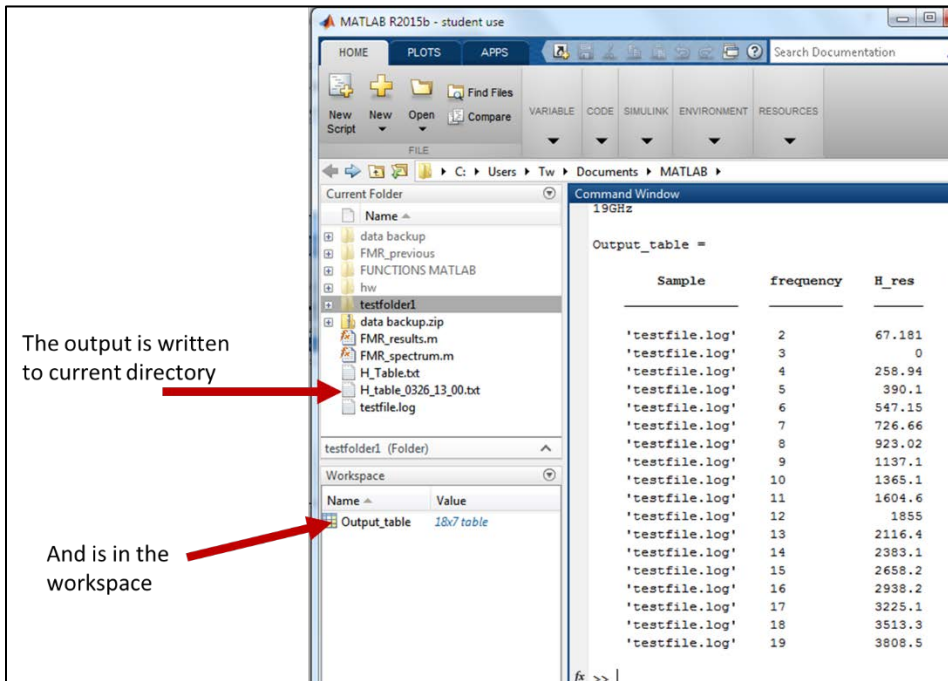
FMR_results uses the table from FMR_spectrum to calculate the sample properties like magnetization. The input is the table from FMR_spectrum. The input can be entered as the Matlab variable created by FMR_spectrum. Also, you can enter the text file name that was saved from FMR_spectrum but enclose it in single quotes. The output is a table. The output table lists the properties of all the samples. It is saved in a CSV text file and is automatically written to the working directory.

FMR spectrum Example 1: Single file input

Input:



Output:



The output is written to current directory

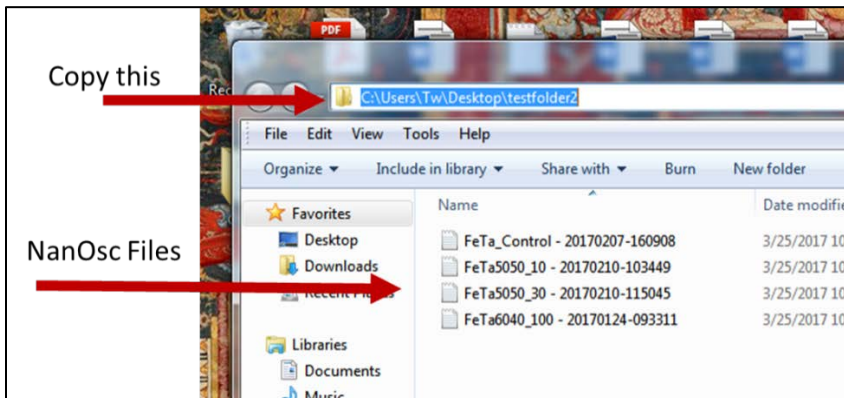
And is in the workspace

Sample	frequency	H_res
'testfile.log'	2	67.181
'testfile.log'	3	0
'testfile.log'	4	258.94
'testfile.log'	5	390.1
'testfile.log'	6	547.15
'testfile.log'	7	726.66
'testfile.log'	8	923.02
'testfile.log'	9	1137.1
'testfile.log'	10	1365.1
'testfile.log'	11	1604.6
'testfile.log'	12	1855
'testfile.log'	13	2116.4
'testfile.log'	14	2383.1
'testfile.log'	15	2658.2
'testfile.log'	16	2938.2
'testfile.log'	17	3225.1
'testfile.log'	18	3513.3
'testfile.log'	19	3808.5

FMR spectrum Example 2: Multiple files

Input:

To read multiple files and save into one output table, copy the directory of the folder that holds all the files:

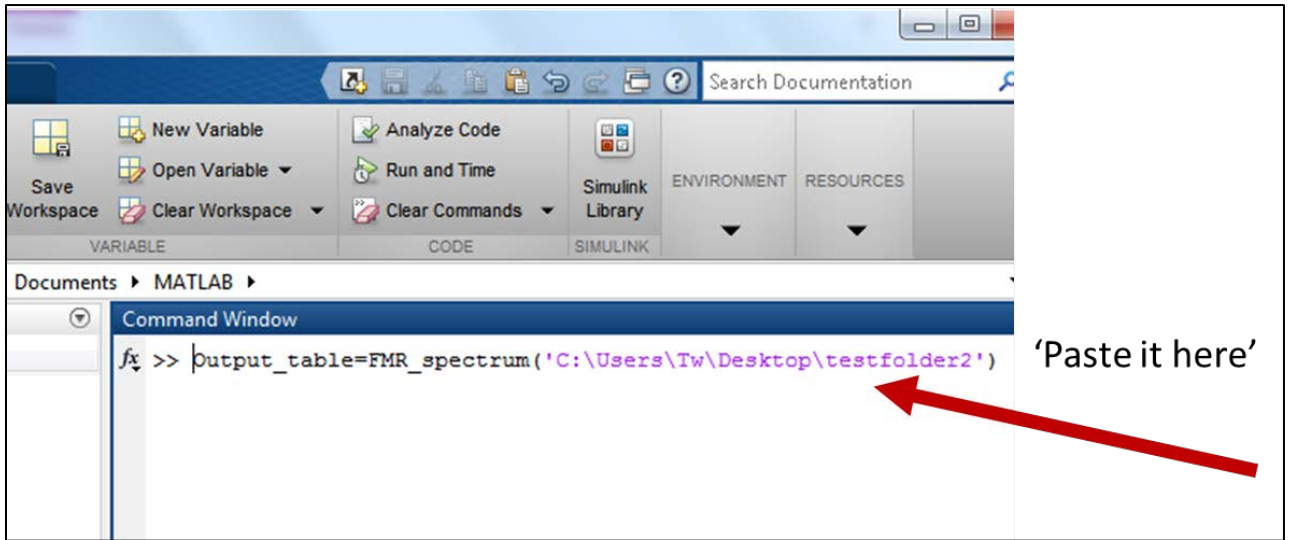


Copy this

NanOsc Files

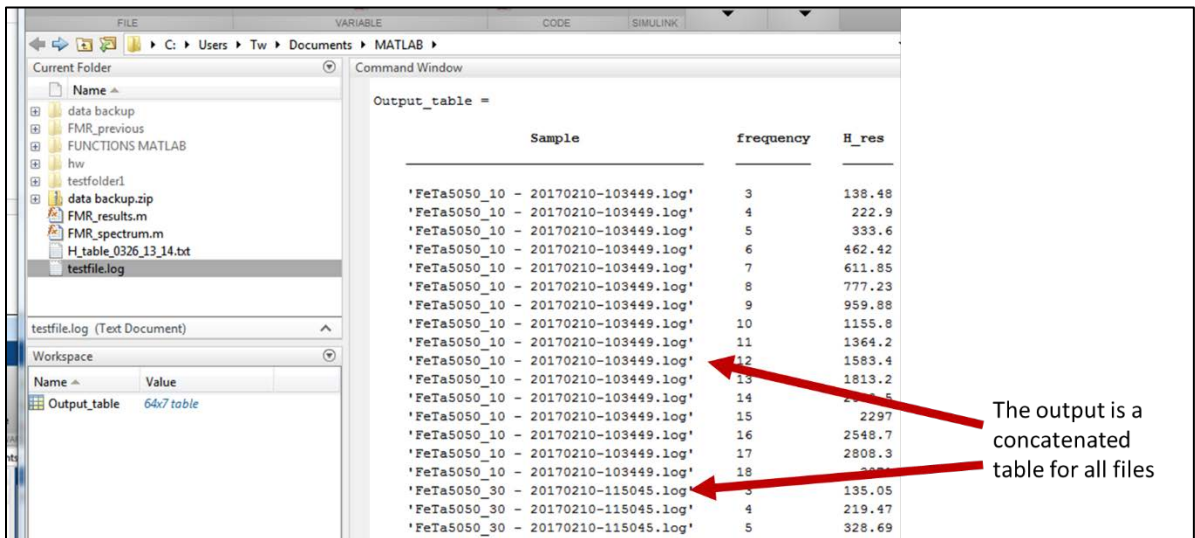
Paste this directory into the function input and enclose with single quotes (If the file is in the

current Matlab directory, you only need to enter the folder name):



Output:

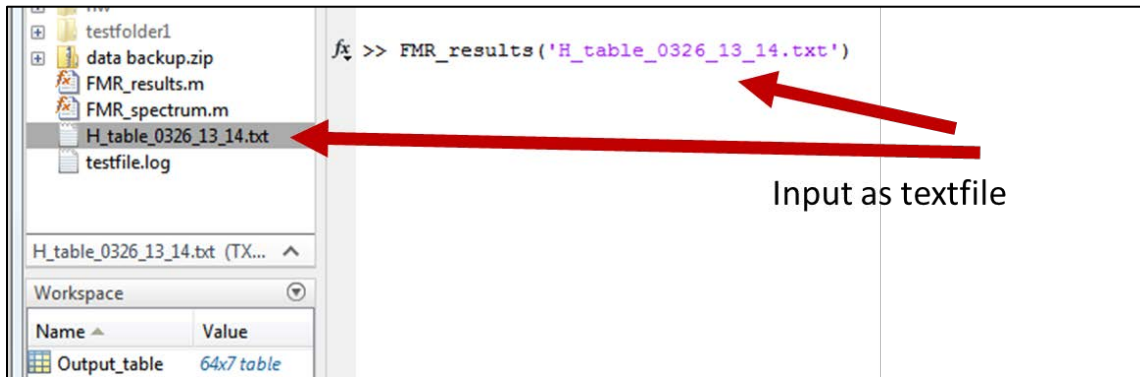
The output is the same as for a single file but now the table is a concatenated table for all files.



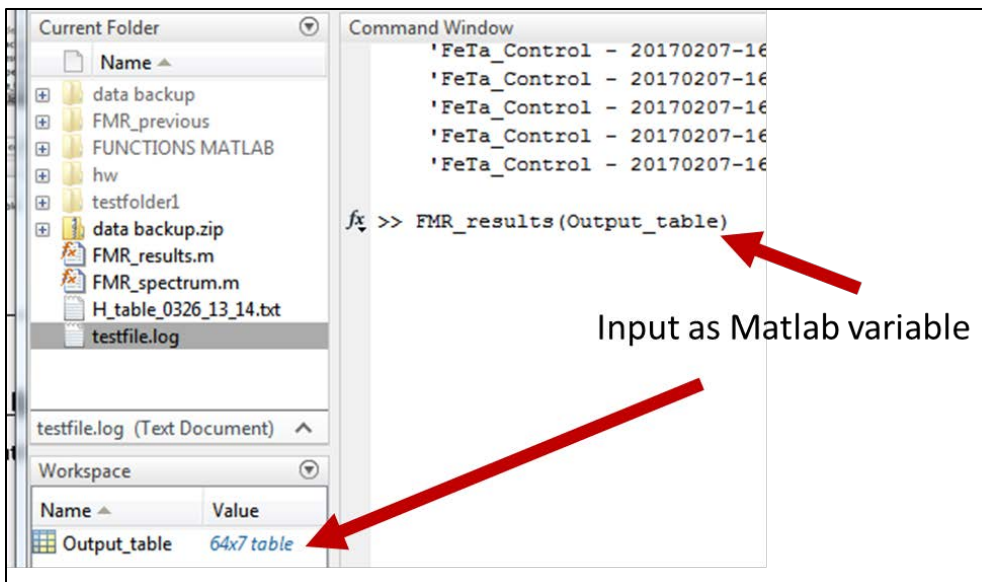
FMR results Example:

The input for `FMR_results` is the table from `FMR_spectrum`.

The input can be the textfile written by FMR_spectrum:

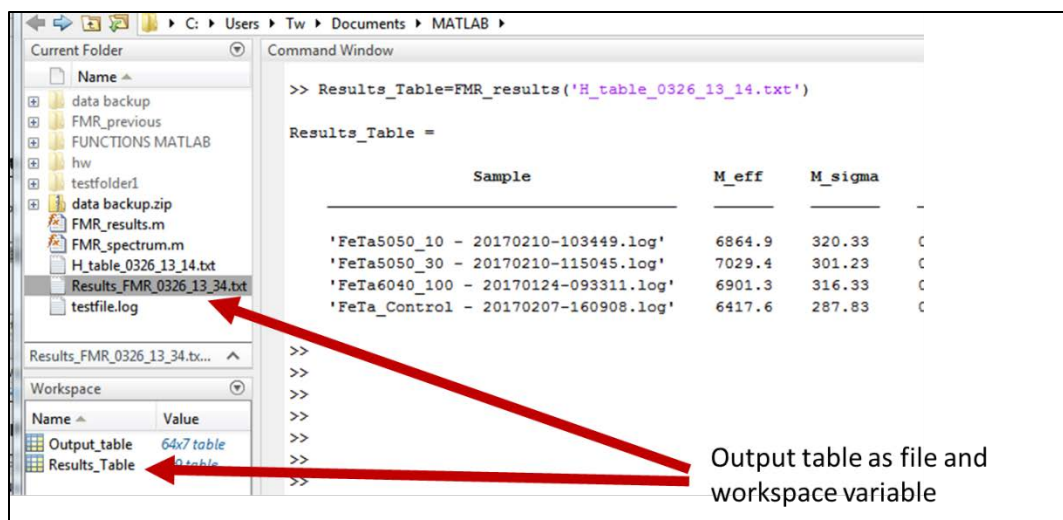


Or the input can also be the Matlab variable saved from FMR_spectrum:



Output :

An output file is saved in current directory. This file can be opened with any software that uses tables. It is a comma separated format (CSV).



Detailed Overview & Guide

Code Description

NanOsc provides a software to run the FMR. This NanOsc software has an interface where users select measurement settings. The results of a sweep table are saved in a log-file. The log-file contain a variable amount of heading information above the data that stored in columns. The pertinent information is frequency, field, and absorption. As mentioned in the paper I created a Matlab tool to process this data. The following is a detailed description of that tool that should serve future users who need to modify the functionality.

Overview

The tool was created in Matlabⁱ. There are two Matlab functions used to process the FMR data. The first function, called `FMR_spectrum.m`, takes as an input the raw log-files created by NanOsc to generate a

ⁱ Matlab is a play on the title "Matrix Laboratory." One advantage of Matlab is the ability to vectorize information. It can improve performance and make much less error prone to utilize this. If you rely on for-loops heavily or if the FMR code looks confusing, please take the time to learn this functionality. Start here: https://www.mathworks.com/help/matlab/matlab_prog/vectorization.html. It is frustrating using code too reliant on loops.

A note to any undergraduate or new graduate student working in this lab: take the time to get very proficient at Matlab and be able to modify this code. It will save you massive amounts of time in the future. I highly recommend the free course on Coursera.org, "Introduction to Programming with Matlab".

table of the resonance field H_{res} and linewidth ΔH . The table generated by `FMR_spectrum` is used as the input for the second function, `FMR_results.m`. `FMR_results.m` outputs a table that contains the properties and confidence intervals of the samples: effective magnetization, the gyromagnetic ratio, inhomogeneous broadening, and effective damping. The output tables for both functions use a format called Tidy Data [43]. Tidy data sets main concept is to arrange data in a way that each variable is a column and each observation is a rowⁱⁱ.

Next I will describe the framework of the two functions. This should serve as an introduction to any user wanting to gain an understanding of how the code works and where to go to make modifications or debug.

Overview of FMR spectrum

`FMR_spectrum` is spilt into the following sections:

- The parent function, **`FMR_spectrum`**: In order this contains the settings (see explanation in “Details of `FMR_spectrum`”), retrieves the directories to the log-files, then in a for-loop calls the sub-function `FMR_single_sample` on all the logfiles, and then writes the output as a table.
- The sub-function **`FMR_single_sample`**: This sub-function opens a logfile, finds the start of the data in the log-file, and temporarily saves all the data in a matrix. The field and absorption data are used as the input to the fitting function for each frequency. The fitting is done by the last sub-function, `fit_FMR_spectrum`. The output from `fit_FMR_spectrum` is the resonance field and linewidth that are saved into pre-allocated vectors.
- The sub-function **`fit_FMR_spectrum`**: This is the meat of the code. This uses a fitting function to extract the linewidth and the resonance field. It takes as an input the field and absorption data. This portion of the code looks complex but can be broken down simply if you understand what it is doing. Fitting the FMR spectrum requires iterative changing of the initial

ⁱⁱ Tidy-data is a common topic in statistics and data science that was relatively recently coined by Wadley Wickham. It is worth knowing the basics of tidy-data if you ever work with large data sets or if you find yourself spending a lot of time re-organizing your data. Wickham’s work is focused on R but I found the concept transfers directly to other languages and software, even Excel. Wickham’s paper can be found in *The Journal of Statistical Software*, vol. 59, 2014 or in pre-print form here: <http://vita.had.co.nz/papers/tidy-data.pdf>.

guesses of the fitting parameters K1 and K2 ⁱⁱⁱ. So there are two “for-loops”. Each iteration changes the initial guess of the respective coefficient. Within the loops there are logical tests. Once the coefficient of determination of the fit is greater than the setting `rsquare_min` (see “Details of `FMR_spectrum`”), the loop is aborted and the fitting parameters are the outputs.

Details of `FMR_spectrum`,

`Table_of_Hr_and_dH= FMR_spectrum('NanOsc_Output.log',plots_true_or_false)`

Inputs :

- `'NanOsc_Output.log'` : The required input is folder containing the files output by Nanosc’s PhaseFMR. A single file is also an allowed input. Other files could be input as long as the string “[Data]” appears two lines above the data and the data is organized in the same column order as the NanOsc files.
- `plots_true_or_false`: this is a true or false statement that turns making plots on or off. Allowed values are 1, 0 or t, f.

In this section I describe the code in order from the top lines to the bottom. This way a comprehensive review of the code is provided.

`FMR_spectrum` can use two formats as inputs: individual log-files or a folder that contains many of the log-files. There is an optional binary input, `plot_sweeps` that controls the plotting functionality of the code. If this is set to true the code will generate plots as the files are processed. The plots show the absorption vs. applied field strength and the fitting curve.

This section will describe the framework and detail of the function `FMR_spectrum`.

%%SETTINGS

The first section of `FMR_spectrum` contain the section `%%SETTINGS`. The settings are values that are used in the function that controls how it operates. These values were placed at the top of the code for ease of access. When processing data the values placed in settings can be modified to customize the code for different applications. For example, if the value for the constant “`rsquare_min`” is decreased,

ⁱⁱⁱ These are the symmetric and antisymmetric coefficients for the derivative Lorentzian function. These terms change according to the shape of the spectrum. An interesting further work would be to investigate the trends in these coefficient. I have noticed interesting patterns with these coefficients as a function of frequency for some samples. This would make an interesting further work.

the code will run faster but there will be less confidence in the fits. The %%SETTINGS section contains the following constants:

- `rsquare_min` : This refers to the coefficient of determination, also called the R-squared value^{iv}. This constant is used in the sub-function `fit_FMR_spectrum`.
- `Use_rigorous_fit`: 'Use_rigorous_fit' is a logical. If set to true, a preliminary fit is done to find an approximate linewidth and resonance field. The final fit is then done only using data that is near the resonance. The number of data used in final fit is controlled by 'fit_width'. **Set this to true if the sweeps are very broad and contain a large amount of background data not near the resonance.** The data that is used for the final fit is plotted as blue circles. In contrast, the data for the entire spectrum is plotted as black periods. Do not confuse this with Matlab's built in Robust fitting functionality.
- `fit_width`: this controls how many data are used for the final fit if `rigorous_fit` is set to true. The linewidth, ΔH from the preliminary fit is multiplied by `fit_width`. This value above and below the resonance field (found from the preliminary fit) contains all the data that is used for the final fit.
 - o Example: Pretend we have a sweep as a resonance near 100 Oe and a linewidth of 20 Oe (not realistic values), and `fit_width` is set =1. Then only data that lies from 80 Oe to 120 Oe will be used in the determination of the fit parameters.

%% DISTINGUISH FILE OR FOLDER; IF FOLDER PROCESS ALL FILES

This section determines if the input is an individual file or a directory with multiple files. It uses the function "isdir" that gives a binary output. If the input is a single file, loops are skipped and the sub-functions are called a single time with the line

```
H_Table=FMR_single_sample(...)
```

^{iv} The coefficient of determination is a statistical indicator of how close a fitted regression line is to the data. It ranges from 0 to 1 where 1 is a perfect fit. Matlab has many other statistical indicators that can be used for testing the goodness of fits (aside from costumed algorithms). Future users may investigate the advantages of using different statistical indicators. In addition there are different fitting algorithms that may be advantageous in the future. For example, Matlab's robust regression may be helpful for fitting data that contain outliers. I recommend reviewing Mathworks support page as a starting point.

If the input is a file, the number of directories are determined and a loop is set up. In each iteration, a file is used as the input for the sub-function `FMR_single_sample` and the outputs are vertically concatenated into `H_table`.

Source Code

FMR_spectrum.m

```
%% FMR_spectrum: reads '-.log' files created by NanOsc FMR software.
%The input can be a single text file or a folder with multiple files. The
%input is file name, folder name, or folder directory as string ('enclose
%with single quotes'). The output is a table that is automatically written
%to the current folder.

function H_Table=FMR_spectrum(input,plot_sweeps)
clc; close all; fclose all;
%% SETTINGS:
if nargin<2
    plot_sweeps=false;% 'plot_sweeps' is logical that controls if the data and
fits are plotted
end
rsquare_min=0.99;
Use_rigorous_fit=false;
rsquare_for_estimate=0.5;
fit_width=1;
%SETTINGS DESCRIPTIONS
%'rsquare_min' controls the minimum allowable quality of the fit before
%proceeding. Smaller values will make program run faster. Larger values
%improve reliability of the fits. Max value=1.

%'Use_rigorous_fit' is a logical if set to true, preliminary fit is done to
%find an approximate linewidth. The final fit is then done on
%data only near the spectrum. The number of data used in final fit is
%controlled by 'fit_width'. See below. Use this if there is a large
%amount of data not in the spectrum

%'rsquare_for_estimate' is used for the initial fit that is used to find
%linewidth and initial guesses.

%fit_width controls how much of the data will be fit from the spectrum.
%The number is a multiplier of the linewidth.
%For example if this =1 than and the linewidth is 20 Oe, Only data 20 Oe
%above and below the resonance field will be used for the final fitting.
%If all data must be included, you may use an arbitrarily large number(ex.
fit_width=10000)

if plot_sweeps
    mkdir('FMR_plots');
end

%% DISTINGUISH FILE OR FOLDER; IF FOLDER PROCESS ALL FILES
if isdir(input);
    file_structure=dir(input); %Outputs all files and folders in the input
directory as a structure. the first two entries are holders for parent
directories and use '.' and '..'
    file_list={file_structure(3:end).name}';%this saves just the file names
as strings
    addpath(input); %This places the input directory in Matlabs search path.
it cna now find the files
    %H_Matrix=zeros(4000,6); %!!!!!!I need to pre-allocate H_table to save
    %space.
```

```

    for j=1:length(file_list);
        display('Processing:')
        display(file_list(j))
        T=FMR_single_sample(file_structure(j+2).name,plot_sweeps,
rsquare_min, Use_rigorous_fit, rsquare_for_estimate, fit_width);
%Sample,frequency,H_res,deltaH,k_1,k_2,R_square_fit
        if j==1
            [r,~]=size(T);
            H_Table=T;
        else
            H_Table=vertcat(H_Table,T);
        end
    end
end
else
    H_Table=FMR_single_sample(input,plot_sweeps, rsquare_min,
Use_rigorous_fit, rsquare_for_estimate, fit_width);
end
writetable(H_Table, strcat('H_table_',datestr(now,'mddd_HH_MM')));
end
function SingleSampleTable=FMR_single_sample(input_file,plot_sweeps,
rsquare_min, Use_rigorous_fit, rsquare_for_estimate, fit_width);
% FIND DATA AND SAVE TO MATRIX
%the below for-loop finds the start of the data & bypasses heading
fileID=fopen(input_file); %opens text file written by NanOsc software
startline=0;
stop=0;
while stop~=1
    tline=fgetl(fileID);
    s1=tline;
    s2='[Data]';
    stop=strcmp(s1,s2);
    startline=startline+1;
end
fclose(fileID); %Closes file. 'fopen' is used for 'fgetl' to find start of
data. 'dlmread' is used to read data into Matlab.
startline=startline+2;

data_matrix=dlmread(input_file,'\t',startline,0); %reads in data and saves as
matrix.
rows=sortrows(data_matrix);% This sorts all rows in ascending order. This
does not distinguish separate sweeps using the same frequency.
f=rows(:,1); %frequency, 1st column
H=rows(:,2); %field data, 2nd column
R=rows(:,5); %Absorption data corrected phase and drift, 5th column
%I=row(:,3); %In-phase data, 3rd column
%Q=row(:,4); %Quadrature data, 4th column
%This code currently uses the phase and drift corrected data. I
% and Q are used in a version that corrects phase shift of quadrature data
% and also for the linear drift that is observed with some data.
%Contact Tom White for the additional code.

unique_f=unique(f);
%Below, all output variables are pre-allocated to matrices or cell;
frequency=unique_f;
H_res=zeros(length(unique_f),1);
H_r_stdv=zeros(length(unique_f),1);

```

```

deltaH=zeros(length(unique_f),1);
dH_stdv=zeros(length(unique_f),1);
k_1=zeros(length(unique_f),1);
k_2=zeros(length(unique_f),1);
R_square_fit=zeros(length(unique_f),1);
Sample=cell(length(unique_f),1);
Sample(:)={input_file};
% stop FIND DATA AND SAVE TO MATRIX
%% ISOLATE DATA BY FREQUENCY AND FIT
for i=1:length(unique_f);
    try
        current_rows=find(unique_f(i)==f);%creates an array of the indecies
where a frequency begins and starts- so this code will not work if frequency
data is not grouped.
        current_frequency=unique_f(i);
        display(strcat(num2str(unique_f(i)), 'GHz'))
        current_H_data=H(current_rows(1):current_rows(end));
        current_R_data=R(current_rows(1):current_rows(end));

        [~,index_min]=min(current_R_data);%finds the index for the minimum
absorption value
        [~,index_max]=max(current_R_data);%find index for the max value
        low_index=min(index_min,index_max);%finds which index is higher
value, i.e. higher field
        high_index=max(index_min,index_max);

        %Intitial Guesses for fits:
        if i==1
            Hr=((current_H_data(high_index)-
current_H_data(low_index))/2)+current_H_data(low_index);
            dH=(sqrt(3)/2).*(current_H_data(high_index)-
current_H_data(low_index));
            k1=-1.5.*(Hr./dH).^3;
            k2=(Hr./dH).^2;
        else
            Hr=fit2.Hr;
            dH=fit2.delta_H;
            k1=fit2.k1;
            k=fit2.k2;
        end
        if Use_rigorous_fit;
            %If 'Use_rigorous_fit' is set to 'true', does an initial fit to
%improve guesses and to focus fit only on data in the spectrum.
            %If set to false, skips to an initial fit and all data is fit
instead of
            %only data near the resonance field and the above initial guesses
are used.

[fit1,~]=fit_FMR_spectrum(current_H_data,current_R_data,Hr,dH,k1,k2,rsquare_f
or_estimate);
            %Initial fit to obtain initial guesses and to narrow the data so
that only
            %data near the resoance is fit to the function.

```

```

        Hr=fit1.Hr; %Overwrites initial guesses for parameters based on
initial fit.
        dH=fit1.delta_H;
        k1=fit1.k1;
        k2=fit1.k2;

        H_up=Hr+fit_width*dH; % magnitude of upper and lower fields that
will be chopped
        H_low=Hr-fit_width*dH;
        Upper_chop=abs(current_H_data-H_up);% subtract scalar field value
of chop locations so that it equals minimum absolute value
        Lower_chop=abs(current_H_data-H_low);
        [~, indexup]=min(Upper_chop);
        [~, indexlow]=min(Lower_chop);
        R_to_fit=current_R_data(indexup:indexlow);
        H_to_fit=current_H_data(indexup:indexlow);
    else
        R_to_fit=current_R_data;
        H_to_fit=current_H_data;
    end

[fit2,gof2]=fit_FMR_spectrum(H_to_fit,R_to_fit,Hr,dH,k1,k2,rsquare_min) ;

    fit2_bounds=confint(fit2,0.68);

    H_r_stdv(i)=fit2.Hr-fit2_bounds(1,1);
    H_res(i)=fit2.Hr;
    deltaH(i)=fit2.delta_H;
    dH_stdv(i)=fit2.delta_H-fit2_bounds(1,2);
    k_1(i)=fit2.k1;
    k_2(i)=fit2.k2;
    R_square_fit(i)=gof2;

%% PLOT DATA
if plot_sweeps
    figure('Name',[input_file(1:end-22), '_f_'
num2str(current_frequency)]);
    hold on;
    plot(current_H_data,current_R_data,'.k');
    plot(H_to_fit,R_to_fit,'ob')
    plot(fit2,'-g');
    ylabel 'Absorption [Arb.]';
    xlabel 'Field [Oe]';
    legend(['All data'],['Data for fit'] , ['Fit Line'])
    grid on;
    hold off ;
end %ends plot_sweeps if statment
% stop PLOT DATA

catch
    display('^^Fit failed for this frequency. Values stored as 0.')

```

```

    end % stop ISOLATE DATA BY FREQUENCY AND FIT
end %Ends loop when all sweeps have been processed

SingleSampleTable=table(Sample,frequency,H_res,H_r_stdv,deltaH,dH_stdv,k_1,k_
2,R_square_fit); %the output is a Table.

if plot_sweeps
    figs=get(0,'children');
for i=1:length(figs)
    saveas(figs(i),[pwd '/plots_FMR/' figs(i).Name])
end
close all %If you have a large number of sweeps and MAtlab crashes due to
memory issues- save and close each figure at each iteration. Just move this
saveas function into the primary for loop
end
end %End of Code
function
[best_fit,best_gof]=fit_FMR_spectrum(H_data,Absorption,Hr_guess,dH_guess,k1_g
uess,k2_guess,gof_setting)
%% FIT FUNCTION AND LOOP
%This function contains the fit equation and iteration loop

[H_prepared,Amplitude_prepared]=prepareCurveData(H_data,Absorption);

fit_equation=fittype('k1*(4*(x-Hr))/(delta_H^2+4*(x-Hr)^2)^2+k2*((delta_H^2-
4*(x-Hr)^2)/(delta_H^2+4*(x-Hr)^2)^2','independent','x','dependent','y'
);
%Lorentzian derivative fit equation. If a drift is seen in data add a slope
%and intercept term to the equation.

%Fit options: order of variables is (Hr,deltaH,k1,k2)
opts = fitoptions(fit_equation);
opts.Display = 'Off';
opts.Lower = [0 0 -Inf -Inf];
opts.StartPoint = [Hr_guess dH_guess k1_guess k2_guess];
opts.Upper = [20000 1500 Inf Inf];
opts.MaxIter=8000; %Controls maximum number of internal loops for Matlab's
fit function.
[fit_try,gof_current]=fit(H_prepared,Amplitude_prepared,fit_equation,opts);

%check Goodness of Fit
best_gof=gof_current.rsquare;
best_fit=fit_try;
if best_gof<gof_setting;
    k1_array = k1_guess.*[-1 10 -10];
    k2_array = k2_guess.*[1 -1 100 -100];

    for ii = 1: length(k1_array)

        for j=1:length(k2_array)
            % sprintf('Best GOF= %.3f \nCurrent GOF=
%.3f',best_gof,gof_current.rsquare)
            opts.StartPoint = [Hr_guess dH_guess k1_array(ii) k2_array(j)];

```

```

        [fit_try, gof_current] = fit(H_prepared,
Amplitude_prepared,fit_equation,opts);
        if gof_current.rsquare>best_gof
            best_gof=gof_current.rsquare;
            best_fit = fit_try;
        end
        if best_gof>=gof_setting
            break
        end
    end
    if best_gof>=gof_setting
        break
    end
end
end
end%end fit function

```

FMR_results.m

```

% Created by Tom White, 3/26/2017
% tomw9116@gmail.com
function Results_Table=FMR_results(Table,plots_true_false)
%% v.1.0 Fit H_res and Linewidth to calculate properties of samples.
% Calculates effective magnetization, gyromagnetic ratio, damping, and
% inhomogenous broadening by fitting resonance field and linewidth table.
% Input is the output from the function 'fit_spectrum.m' . Enter this
% either as the matlab variable directly or as the text file in the current
% directory enclosed with single quotes.

%% settings
if nargin<2;
    plots_true_false=false ;
end

%% FUNCTION CALCULATE PARAMETERS, PLOT, AND SAVE TO TABLE
if istable(Table);
else
    Table=readtable(Table);
end

Sample_list=unique(Table.Sample);
Results=zeros(length(Sample_list),8);
for i=1:length(Sample_list);
    index=ismember(Table.Sample,Sample_list(i));

    if nnz(index)>3
        f=Table.frequency(index);
        Hr=Table.H_res(index);
        dH=Table.deltaH(index);

        [kfit, kgof]=kittel_fit(Hr,f);
        [dHfit,dHgof]=dH_fit(dH,f);
    end
end

```

```

kfit_bounds=confint(kfit,0.68);
dHfit_bounds=confint(dHfit,0.68);

dHslope=dHfit.p1;
alpha=kfit.g*dHslope/2;

M_stdv=kfit.M-kfit_bounds(1,1);
g_stdv=kfit.g-kfit_bounds(1,2);
dH_0_stdv=dHfit.p2-dHfit_bounds(1,1);
slope_stdv=dHslope-dHfit_bounds(1,2);
alpha_stdv=alpha*.5*sqrt((g_stdv/kfit.g)^2+(slope_stdv/dHfit.p1)^2);

Results(i,:)=[kfit.M,M_stdv,kfit.g,g_stdv,dHfit.p2,dH_0_stdv,alpha,alpha_stdv
];

%% PLOTS
if plots_true_false
fighand=figure('Name', ['Kittel for ' Sample_list{i}]);
plot(kfit,Hr,f);
grid on; legend off; xlabel( 'Hr' ); ylabel( 'frequency' );

fighand=figure('Name',['Linewidth vs. Frequency for' Sample_list{i}]);
hold on
plot(dHfit,f,dH);
prediction = predint(dHfit,f);
plot(f,prediction,'m--');
grid on; legend off; xlabel( 'f, (GHZ)' ); ylabel( '\DeltaH' );
hold off
end %ends PLOTS
else
    sprintf('Too few sweeps to fit Kittel for %s.',Sample_list{i})
end %ends if statement requiring enough data points to do kittel or dH fits
end %ends for loop i
Results_Table=[Sample_list array2table(Results)];
Results_Table.Properties.VariableNames = {'Sample' 'M_eff' 'M_sigma' 'gamma'
'g_sigma' 'dH_0' 'dH_sigma' 'alpha' 'a_sigma'};
writetable(Results_Table, strcat('Results_FMR_',datestr(now,'mdd_HH_MM')));
end %ends the entire script
%% FIT: FREQUENCY VS. H_RES
function [kfit,kgof]=kittel_fit(Hres,freq);
[Hr2,f2]=prepareCurveData(Hres,freq);
kittel=fitype( 'g*sqrt(x*(x+M))', 'independent', 'x', 'dependent', 'y');
%order of outputs (M,g,x)
opts2 = fitoptions( kittel );
opts2.Display = 'Off';
opts2.Lower = [0 -Inf];
opts2.StartPoint = [0.0975 0.278];
[kfit,kgof]=fit(Hr2,f2,kittel,opts2);
end %ends kittel function

%% FIT: DELTA H VS. FREQUENCY
function [dH_fit,dHgof]=dH_fit(dH,freq);
[dH3,f3]=prepareCurveData(dH,freq);
[dH_fit,dHgof]=fit(f3,dH3,'poly1');
end %ends linewidth function

```

Bibliography

- [1] A. Hoffmann, "Spin hall effects in metals," *IEEE Transactions on Magnetics*, 2013.
- [2] Z. An, F. Q. Liu, Y. Lin and C. Liu, "The universal definition of spin current," *Scientific Reports*, vol. 2, May 2012.
- [3] F. Hellman, "Interface-induced phenomena in magnetism," *Reviews of Modern Physics*, pp. 1539-0756, 2017.
- [4] B. D. Cullity and C. D. Graham, *Introduction to Magnetic Materials*, John Wiley & Sons, 2011.
- [5] A. Fert, "Nobel Lecture: Origin, development, and future of spintronics," *Reviews of Modern Physics*, vol. 80, pp. 1517-1530, dec 2008.
- [6] S. Parkin, "The Spin on Electronics," in *UC Santa Barbara Kavli Institute for Theoretical Physics*, Santa Barbara, 2013.
- [7] G. Fernando, *Metallic multilayers and their applications: theory, experiments, and applications related to thin metallic multilayers*, Elsevier , 2008.
- [8] S. Bader, "Colloquium: Opportunities in nanomagnetism," *Reviews of Modern Physics*, vol. 78, no. 1, 2006.
- [9] O. Ozatay, "Spin Dependent Transport and Spin Transfer in Nanoconstrictions and Current Confined nanomagnets," Cornell University, Ithica, 2007.
- [10] P. Sharma, "Physics: How to Create a Spin Current," *Science*, vol. 307, pp. 531-533, jan 2005.
- [11] L. J. Cornelissen, J. Liu, R. A. Duine, J. B. Youssef and B. J. van Wees, "Long-distance Transport of Magnon Spin Information in a Magnetic Insulator at Room Temperature," *Nature Physics*, vol. 11, pp. 1022-1026, sep 2015.
- [12] E. Saitoh, M. Ueda, H. Miyajima and G. Tatara, "Conversion of Spin Current into Charge Current at Room Temperature: Inverse Spin-Hall Effect," *Applied Physics Letters*, vol. 88, p. 182509, may 2006.
- [13] A. Azevedo, L. H. Vilela-Leão, R. L. Rodríguez-Suárez, L. a. A. F. Santos and S. M. Rezende, "Spin pumping and anisotropic magnetoresistance voltages in magnetic bilayers: Theory and experiment," *Physical Review B - Condensed Matter and Materials Physics*, 2011.
- [14] Y. Tserkovnyak, A. Brataas, G. E. W. Bauer and B. I. Halperin, "Nonlocal magnetization dynamics in ferromagnetic heterostructures".
- [15] G. Woltersdorf, "Spin-Pumping and Two-Magnon Scattering in Magnetic Multilayers," 2004.

- [16] T. L. Gilbert, "Classics in Magnetism A Phenomenological Theory of Damping in Ferromagnetic Materials," *{IEEE} Transactions on Magnetism*, vol. 40, pp. 3443-3449, nov 2004.
- [17] S. Mankovsky, D. Ködderitzsch, G. Woltersdorf and H. Ebert, "First-principles calculation of the Gilbert damping parameter via the linear response formalism with application to magnetic transition metals and alloys," *Physical Review B*, vol. 87, jan 2013.
- [18] H. Chudo, K. Ando, K. Saito, R. Haruki, S. Okayasu, H. Yasuoka, K. Takanashi and E. Saitoh, "Spin pumping efficiency from half metallic Co₂MnSi," *Journal of Applied Physics*, vol. 109, no. 7, 2011.
- [19] R. F. L. Evans, W. J. Fan, P. Chureemart, T. A. Ostler, M. O. A. Ellis and R. W. Chantrell, "Atomistic spin model simulations of magnetic nanomaterials," *Journal of Physics: Condensed Matter*, vol. 26, p. 103202, 2014.
- [20] J. Fidler, T. Schrefl, V. D. Tsiantos, H. Forster, R. Dittrich and D. Suess, "FE-simulation of fast switching behavior of granular nanoelements," *{IEEE} Transactions on Magnetism*, vol. 38, pp. 2520-2522, sep 2002.
- [21] L. Bonneviot and D. Olivier, "Ferromagnetic Resonance," in *Catalyst Characterization: Physical Techniques for Solid Materials*, B. Imelik and J. C. Vedrine, Eds., Boston, MA: Springer US, 1994, pp. 181-214.
- [22] C. Kittel, "Interpretation of Anomalous Larmor Frequencies in Ferromagnetic Resonance Experiment," *Phys. Rev.*, vol. 71, no. 4, pp. 270-271, Feb 1947.
- [23] J.-C. Rojas-Sánchez, N. Reyren, P. Laczkowski, W. Savero, J.-P. Attané, C. Deranlot, M. Jamet, J.-M. George, L. Vila and H. Jaffrès, "Spin Pumping and Inverse Spin Hall Effect in Platinum: The Essential Role of Spin-Memory Loss at Metallic Interfaces".
- [24] M. Caminale, A. Ghosh, S. Auffret, U. Ebels, K. Ollefs, F. Wilhelm, A. Rogalev and W. E. Bailey, "Spin pumping damping and magnetic proximity effect in Pd and Pt spin-sink layers," *Physical Review B*, vol. 94, jul 2016.
- [25] J.-C. Rojas-Sánchez, N. Reyren, P. Laczkowski, W. Savero, J.-P. Attané, C. Deranlot, M. Jamet, J.-M. George, L. Vila and H. Jaff Es, "SUPPLEMENTAL MATERIAL Spin Pumping and Inverse Spin Hall Effect in Platinum: The Essential Role of Spin-Memory Loss at Metallic Interfaces".
- [26] T. C. Huang, R. Gilles and G. Will, "Thin-film thickness and density determination from x-ray reflectivity data using a conventional power diffractometer," *Thin Solid Films*, vol. 230, no. 2, pp. 99-101, 1993.
- [27] A. Richter, "In Situ X-ray Reflectivity Studies of Protein Adsorption onto Functionalized Surfaces," in *APS*, Denver, 2007.
- [28] Y. Zhao, Q. Song, S.-H. Yang, T. Su, W. Yuan, S. S. P. Parkin, J. Shi and W. Han, "Experimental Investigation of Temperature-Dependent Gilbert Damping in Permalloy Thin Films".

- [29] A. Ruiz Calaforra, T. Bracher, V. Lauer, P. Pirro, B. Heinz, M. Geilen, A. V. Chumak, A. Conca, B. Leven, B. Hillebrands, T. Br and Acher, "The role of the non-magnetic material in spin pumping and magnetization dynamics in NiFe and CoFeB multilayer systems," *J. Appl. Phys.*, vol. 117, 2015.
- [30] E. Papaioannou, P. Fuhrmann, J. Matthias, T. Brachler and P. Pirro, "Optimizing the spin-pumping induced inverse spin Hall voltage by crystal growth in Fe/Pt bilayers," *Applied Physics Letters*, vol. 103, no. 16, 2013.
- [31] J. M. Shaw, H. T. Nembach, T. J. Silva and C. T. Boone, "Precise determination of the spectroscopic g-factor by use of broadband ferromagnetic resonance spectroscopy," *Journal of Applied Physics*, vol. 114, no. 24, p. 243906, 2013.
- [32] F. J. A. den Broeder, W. Hoving and P. J. H. Bloemen, "Magnetic anisotropy of multilayers," *Journal of Magnetism and Magnetic Materials*, vol. 93, pp. 562-570, 1991.
- [33] L. Tryputen, F. Guo, F. Liu, T. N. A. Nguyen, M. S. Mohseni, S. Chung, Y. Fang, J. Åkerman, R. D. McMichael and C. A. Ross, "Magnetic structure and anisotropy of [Co/Pd]₅/NiFe multilayers," *Physical Review B*, vol. 91, jan 2015.
- [34] S. J. Gamble, H. M. Burkhardt, A. Kashuba, R. Allen, S. S. Parkin, H. C. Siegman and J. Stöhr, "Electric Field Induced Magnetic Anisotropy in a Ferromagnet," *Physical Review Letters*, vol. 102, no. 21, pp. 217201-2172014, 2009.
- [35] M. S. Gabor, T. Petrison Jr, T. Petrison and C. Tiusam, "Perpendicular magnetic anisotropy in Ta/Co₂FeAl/MgO multilayers," *Journal of Applied Physics*, vol. <http://dx.doi.org/10.1063/1.4818326>, 2013.
- [36] I. Harward, T. O'Keevan, A. Hutchison, V. Zagorodnii and Z. Celinsk, "A broadband ferromagnetic resonance spectrometer to measure thin films up to 70 GHz," *Review of Scientific Instruments*, vol. 82, p. 095115, 2011.
- [37] M. Schoen, J. M. Shaw, H. T. Nembach and T. J. Silva, "Radiative damping in wave guide based FMR measured via analysis of perpendicular standing spin waves in sputtered permalloy films," *Phys. Rev. B*, vol. 92, no. 18, 2015.
- [38] B. J. Kirby, F. H. Belliveau, D. D. Belyea, P. A. Kienzle, A. J. Grutter, P. Riego, A. Berger and C. W. Miller, "Spatial Evolution of the Ferromagnetic Phase Transition in an Exchange Graded Film," *Phys. Rev. Lett.*, vol. 116, no. 4, p. 047203, 2015.
- [39] D. J. Twisselmann and R. D. McMichael, "Intrinsic Damping and Intentional Ferromagnetic Resonance Broadening in Thin Permalloy Films," *Journal of Applied Physics*, vol. 93, no. 10, 2003.
- [40] T. Nan, S. Emori, C. T. Boone, X. Wang, T. M. Oxholm, J. G. Jones, B. M. Howe, G. J. Brown and N. X. Sun, "Comparison of spin-orbit torques and spin pumping across NiFe/Pt and NiFe/Cu/Pt interfaces," *Phys. Rev. B*, vol. 91, no. 21, p. 214416, Jun 2015.

- [41] Y. M. Lu, Y. Choi, C. M. Ortega, X. M. Cheng, J. W. Cai, S. Y. Huang, L. Sun and C. L. Chien, "Pt Magnetic Polarization on Y₃Fe₅O₁₂ and Magnetotransport Characteristics," *Phys. Rev. Lett.*, vol. 110, no. 14, p. 147207, Apr 2013.
- [42] J. T. Brangham, K.-Y. Meng, A. S. Yang, J. C. Gallagher, B. D. Esser, S. White, S. Yu, D. McComb, P. Hammel and F. Yang, "Thickness dependence of spin Hall angle of Au grown on Y₃Fe₅O₁₂ epitaxial films," *Phys. Rev. B*, vol. 94, pp. 054418-1, 2016.
- [43] H. Wickham, "Tidy Data," *The Journal of Statistical Software*, vol. 59, 2014.